AD_____

Award Number: DAMD17-03-1-0203

TITLE: Clinical and Molecular Consequences of NF1 Microdeletion

PRINCIPAL INVESTIGATOR: Karen Stephens, Ph.D.

CONTRACTING ORGANIZATION: University of Washington
Seattle, Washington 98105-6613

REPORT DATE: May 2007

TYPE OF REPORT: Final

PREPARED FOR: U.S. Army Medical Research and Materiel Command
Fort Detrick, Maryland 21702-5012

REPORT DOCUMENTATION PAGE

Form Approved
OMB No. 0704-0188

1. REPORT DATE *(DD-MM-YYYY)*	**2. REPORT TYPE**	**3. DATES COVERED** *(From - To)*
01-05-2007	Final	7 Apr 2003 – 6 Apr 2007

4. TITLE AND SUBTITLE

Clinical and Molecular Consequences of NF1 Microdeletion

5a. CONTRACT NUMBER

5b. GRANT NUMBER
DAMD17-03-1-0203

5c. PROGRAM ELEMENT NUMBER

6. AUTHOR(S)

Karen Stephens, Ph.D.

E-Mail: millie@u.washington.edu

5d. PROJECT NUMBER

5e. TASK NUMBER

5f. WORK UNIT NUMBER

7. PERFORMING ORGANIZATION NAME(S) AND ADDRESS(ES)

University of Washington
Seattle, Washington 98105-6613

8. PERFORMING ORGANIZATION REPORT NUMBER

9. SPONSORING / MONITORING AGENCY NAME(S) AND ADDRESS(ES)
U.S. Army Medical Research and Materiel Command
Fort Detrick, Maryland 21702-5012

10. SPONSOR/MONITOR'S ACRONYM(S)

11. SPONSOR/MONITOR'S REPORT NUMBER(S)

12. DISTRIBUTION / AVAILABILITY STATEMENT
Approved for Public Release; Distribution Unlimited

13. SUPPLEMENTARY NOTES

14. ABSTRACT

We have developed rapid and sensitive assays for the detection and mapping of both the common 1.4 Mb NF1 microdeletion and novel microdeletions; our subjects carrying microdeletions have contributed to diverse collaborations including development of a mouse model of plexiform neurofibroma tunorigenesis and the conservation of recombination hotspots . Our hypothesis that genome instability occurs during NF1-tumorigenesis continues to be supported by our findings. First, somatic instability leading to uniparental isodisomy and homozygous NF1 inactivation in NF1-related leukemias, which add to our understanding of leukemogenesis and identifies chromsomal regions were somatic recombination may be favored. Second, we localized neurofibromin to the centrosome in normal and malignant epithelial cells. Third, our preliminary observations show that centrosomes appear abnormal in NF1-derived neurofibromas, suggesting a potential new function for neurofibromin in normal centrosome function and in maintaining genome stability.

15. SUBJECT TERMS
Microdeletion, tumor initiation, modifying gene, genotype/phenotype, paralogs, duplication, neurofibromas

16. SECURITY CLASSIFICATION OF:			**17. LIMITATION OF ABSTRACT**	**18. NUMBER OF PAGES**	**19a. NAME OF RESPONSIBLE PERSON**
a. REPORT	**b. ABSTRACT**	**c. THIS PAGE**			USAMRMC
U	U	U	UU	43	**19b. TELEPHONE NUMBER** *(include area code)*

Standard Form 298 (Rev. 8-98)
Prescribed by ANSI Std. Z39.18

Table of Contents

Contents of appendices

Manuscripts attached:

1. Stephens K, Weaver M, Leppig KA, Maruyama K, Emanuel PD, Le Beau MM, Shannon KM. Interstitial uniparental isodisomy at clustered breakpoint intervals is a frequent mechanism of NF1 inactivation in myeloid malignancies. Blood 108:1684-1689, 2006.

In our last progress report, this paper was submitted as a preprint. The final publication is attached.

2. Stephens K. Neurofibromatosis. In Molecular Pathology in Clinical Practice. D.G.B. Leonard, Ed. New York: Springer –Verlag, 2007.

In our last progress report, this paper was submitted as a preprint. Electronic proofs of the final publication are attached; pdfs of chapters were not provided to the authors. The proofs have all the content of the final publication.

3. De Raedt T, Stephens M, Heyns I, Brems H, Thijs D, Messiaen L, Stephens K, Lazaro C, Wimmer K, Kehrer-Sawatzki H, Vidaud D, Kluwe L, Marynen P, Legius E. Conservation of hotspots for recombination in low-copy repeats associated with the NF1 microdeletion. Nature Genet 38:1419-1423, 2006.

4. Perrin GQ, Fishbein L, Thomson SA, Thomas SL, Stephens K, Garbern JY, Deries GH, Yachnis AT, Wallace MR, Muir D. Plexiform-like neurofibromas develop in the mouse by intraneural xenograft of an NF1 tumor-derived Schwann cell line. J Neurosci Res 85:1347-1357, 2007.

Introduction

About 5-10% of patients with neurofibromatosis type 1 (NF1) are heterozygous for a contiguous gene deletion that includes the entire *NF1* gene. Although limited in scope, previous studies provide compelling evidence that microdeletion patients show early onset and large numbers of cutaneous neurofibromas, and a higher frequency of plexiform neurofibromas, malignant peripheral nerve sheath tumors, and other solid tissue malignancies. We propose to perform systematic, comprehensive clinical and molecular studies of subjects with *NF1* microdeletion to examine the gene(s) responsible for the severe tumor phenotype of microdeletion patients. The specific aims of this research are 1) To determine the clinical spectrum, genotype/phenotype correlations associated with heterozygosity for an *NF1* microdeletion. Genomic DNA of NF1 subjects will be examined by a multi-step screening protocol to identify germline microdeletion carriers, to map the extent of each deletion. We will correlate molecular data with the results of a comprehensive clinical evaluation of deletion and nondeletional NF1 control subjects. 2) To determine if cutaneous neurofibromas of germline *NF1* microdeletion patients show evidence of genomic instability or homozygous *NF1* microdeletion that may contribute to the early onset of neurofibromagenesis. Primary neurofibroma tissue from microdeletion patients will be analyzed to determine the presence and nature of 2nd hit mutations and whether these cells exhibit characteristics of genomic instability. 3) To screen candidate modifier genes in the *NF1* microdeletion region for mutations in subjects with early onset cutaneous neurofibromas who are not carriers of an *NF1* microdeletion. 4) To employ the newly developed FLASH technology to interrogate the *NF1* microdeletion region and construct a physical map that will determine, the sequence of all of the genes, unique noncoding regions, and paralogs (including the putative *NF1* duplicated gene) of the *NF1* microdeletion region.

Body

The original STATEMENT OF WORK and progress to date described below.

Preface: This is a progress report for year 4 (rather than a final report) because a request for a no-cost extension is under consideration by Dr. Naba Bora and the staff of the CDMRP Neurofibromatosis Program. Earlier this year, I discussed with Dr. Bora imminent changes in my academic appointment at the University of Washington, which involved transfer to a new department and new responsibilities that are outside of the field of neurofibromatosis basic research. At Dr. Bora's request, and our mutual desire that the remaining funds in this grant be used to advance neurofibromatosis research, I submitted a a no-cost extension, along with a slightly modified SOW and subcontract of research activities to the University of Florida, laboratory of neurofibromatosis expert Dr. Margaret Wallace. This request is under consideration. Therefore, this progress report will summarize progress in my laboratory from April, 2006 until Jan, 2007 when my neurofibromatosis bench experiments ceased. Since that time data analysis and manuscript writing activities are on-going.

Year 1, Months 1-8: Statement of Work in original grant application (underlined) and progress to date:

- Develop a clinical database, train personnel to use.

Completed and described in previous progress reports.

- Design and test clinic evaluation forms for patient assessment.

Completed and described in previous progress reports.

- Design STS primers for interrogation of fosmid library.

Completed. Our analyses of 4 different data sources of genomic sequences (detailed in last year's progress report) did not support the presence of tandem *NF1* duplications at 17q11.2. Therefore, there is no valid scientific basis for further work on aim #4 (a project that was to be supported by the University of Washington Genome Center and performed at no cost to this grant).

Years 1-2 Statement of Work in original grant application (underlined) and progress to date:

- Enroll new patients in the study.

Completed. No new patients will be enrolled. Existing pathological specimens will be analyzed. Enrollment of patients was significantly delayed by the time required for the Army HSRRB to approve our application (submitted July 2003, approved February, 2004) and has remained a delaying factor in our research. We currently have enrolled about 50 subjects. These are in addition to existing DNAs from other previously ascertained patients and anonymous DNAs. If the no-cost extension and subcontract to the University of Florida is granted, the number of patients available for the study will increase significantly by the large cohort of NF1 patients ascertained by Dr. Wallace.

- Screen for *NF1* microdeletion patients, map extent of deletions, develop new deletion junction assays as needed.

Completed. In last year's progress report, I described 3 types of assays that were developed and validated.

1) PCR-based ssays to detect the recurrent 1.4 Mb deletions at PRS1 and PRS2 recombination hotspots.

These two assays rapidly detect the majority (~70%) of *NF1*-REP-mediated microdeletions. Therefore these data and the assays we developed can be used for rapid detection and diagnosis of *NF1* microdeletion carriers in either the research or clinical setting. A manuscript of these data is being revised by Dr. Stephens at this time. These data were originally submitted (to separate journals) for publication concurrently with the Forbes et al (6) manuscript. These manuscripts "crossed" in the mail, with one accepted and one rejected at their respective journals. Forbes et al. was accepted and published; however, because it summarized some of these, we must now re-package these data so they will complement, and not repeat the data described in Forbes et al (6).

New multi-center collaboration to study recombination hotspots in NF1 microdeletion subjects identified by the above assays.

DNAs of the subjects with recombination breakpoints at PRS1 and PRS2 were shared with the laboratory of Dr. Eric Legius (University Leuvin, Belgium) to contribute to a large study analyzing the conservation of hotspots in the REPs. This study found evidence for shared hotspots of recombination among the REPs. REP19, originally discovered by us on chromosome 19p (5),contained hotspots in the same place as the nonalllelic recombination hotspots in NF1-REP-:1 and NF1-REP-M that flank the NF1 gene. These data are detailed in De Raedt T, Stephens M, Heyns I, Brems H, Thijs D, Messiaen L, Stephens K, Lazaro C, Wimmer K, Kehrer-Sawatzki H, Vidaud D, Kluwe L, Marynen P, Legius E. Conservation of hotspots for recombination in low-copy repeats associated with the NF1 microdeletion. Nature Genet 38:1419-1423, 2006 (see Appendix for pdf of publication).

New application of assays: These assays facilitated collaboration between us and with Drs. Margaret Wallace and David Muir (University of Florida), which resulted in development of a model for the study of plexiform neurofibroma tumorigenesis. In this research an NF1 tumor-derived Schwann cell line was

chosen for xenografts into the peripheral nerve of scid mice. Our deletion specific assays were instrumental in screening NF1 tumor-derived cell lines in order to make a judicious choice on the one chosen for xenograft studies. The model facilitates testing of potential therapeutic interventions in a relevant cellular environment. This work is described in the recently published article Perrin GQ, Fishbein L, Thomson SA, Thomas SL, Stephens K, Garbern JY, Deries GH, Yachnis AT, Wallace MR, Muir D. Plexiform-like neurofibromas develop in the mouse by intraneural xenograft of an NF1 tumor-derived Schwann cell line. J Neurosci Res 85:1347-1357, 2007 (see Appendix for pdf of article).

2) Assays to detect microdeletions at unique regions, not at the recombination hotspots. These assays employed real-time competitive PCR to measure gene dosage.

Studies completed, with disappointing results. In last year's progress report we gave an extensive and detailed description of a series of new quantitative PCR (qPCR) assays at 5 loci that we developed to detect *NF1* regional deletions. As detailed last year, every aspect of these assays was sound: reproducibility and low intra- and inter-assay variation on bona fide disomic and monsomic NF1 patients. Importantly, the approximated 95% confidence limits (measured as ± 2 S.D.) for the range of normal and deleted values did not overlap. Inter-assay variations at each locus demonstrated distinct value ranges for normal and deleted (i.e., disomy and monosomy). These assays were used to screen >250 patients for novel deletions in/near NF1 and about 10 positives were identified. Surprisingly,the putative deletions were not confirmed by FISH and/or polymorphic marker analysis (including family members when available). We spent considerable time and energy last summer and fall trouble-shooting and trying to rescue the assays. After considerable work repeating assays, redesigning assays, repurifying template DNA, etc., we have come to the final, but difficult, conclusion that for reasons that cannot be determined, these assays are not reproducible nor reliable when applied on a large scale to unknown patient samples. In the interim, new techniques have been developed by others, such as multiplex ligation probe amplification that have been successfully applied to determine copy number at the *NF1* locus. Therefore, it is unreasonable to spend further resources on this assay. Failure of this assay was a major disappointment for the laboratory.

- Ascertain NF1 subjects that show early onset cutaneous neurofibromas that do not carry microdeletions.

To date we have identified 5 such patients, including one family that appears to have early onset cutaneous neurofibromas. I will no longer be enrolling patients at the University of Washington for these studies. However, if the no-cost extension and subcontract of research to the University of Washington is approved, Dr. Wallace will combine her subjects of similar phenotype with our 5 subjects and continue this work. Our combined subjects will make this a more robust study.

- Determine conditions for immunohistochemistry, test and choose optimal antibodies. *This work relates to Aim #2 - To determine if cutaneous neurofibromas of germline NF1 microdeletion patients show evidence of genomic instability.* There are several types of genomic instability that can be detected in cells, and an important type is centrosome abnormality, which leads to abnormal mitoses and consequent losses and gains of chromosomes. We propose that this might be a mechanism in NF1-related tumorigenesis because

  1) As are detailed in our progress report last year, we found that neurofibromin localizes to the centrosome in human primary keratinocytes, several simple epithelial cell lines, and mouse 3T3 fibroblasts. To examine more pathologically-relevant cells, we obtained normal cultured Schwann

cells (complements of Dr. David Muir, University of Florida) and found no nuclear localization of neurofibromin. A few months ago, we extended this study to examine primary cultured Schwann cells from a nonlesional, nontumor sciatic nerve site obtained at autopsy of a subject with neurofibromatosis, who was heterozygous for the 1.4 Mb NF1 microdeletion and died of an MPNST (complements of Dr. Margaret Wallace). These cultured cells also did not have centrosomal-neurofibromin.

- 2) Centrosome abnormalities in size, number, and structure are hallmarks of many solid and hematologic malignancies and pre-malignant neoplasms (10-13). In last years' progress report, we documented neurofibromin co-localization to the abnormally structured and clumped multi-centrosomes in squamous cell carcinoma cell lines. More importantly, we have documented and confirmed the presence of abnormally structured and clumped multi-centrosomes in one dermal neurofibroma from an NF1 patient with a ~1 kb microdeletion (see figure below). This observation poses several important questions, which will be addressed in experiments incollaboration with Dr. Margaret Wallace, if the no-cost extension and subcontract to the University of Florida is approved. The questions are whether other neurofibromas (from NF1 deletion and/or intragenic mutation patients) also show abnormal and multipolar mitoses and in particular, whether neurofibromin localizes to the abnormal centrosomes. The centrosome structure will be important to examine in MPNST tissues and cell lines, particularly because they show significant aneuploidy, which could be direct result of centrosome dysregulation. We will share our antibodies, and tumor blocks, with Dr. Wallace, who also has MPNST cells from NF1 patients and primary tumors that will extend our smll collection to make the study more robust. She has experience in immunofluorescence and neurofibrom antibodies and has published previously in this area. These studies will provide new insight into neurofibromagenesis and transition to malignancy and have the potential for identifying a tumorigenesis a marker for the transition from the benign to the malignant process.

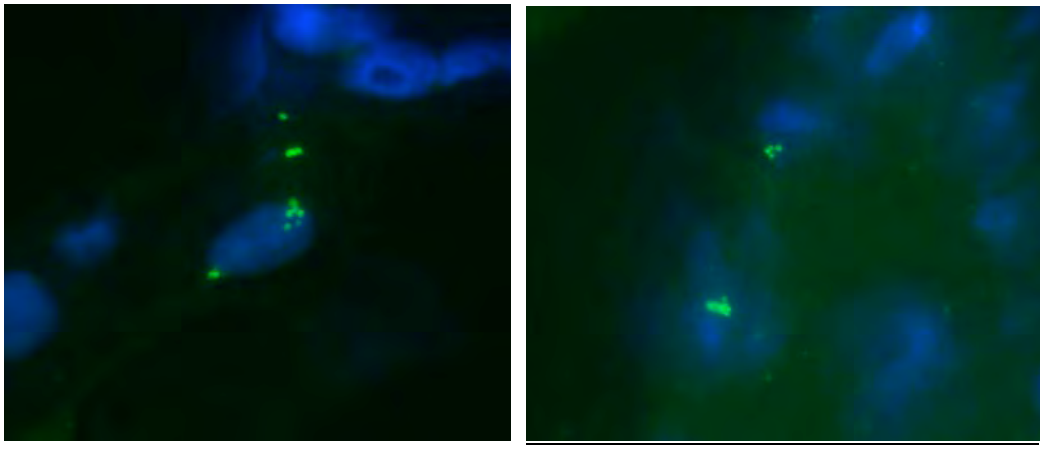

Immunofluorescence of an NF1-related neurofibroma showing a DAPI (blue) stained nucleus and FITC (green) stained centrosomes (anti-γ-tubulin), which are abnormal in number and arrangement. Note that the central cell in the left figure gives the appearance of being in early metaphase. If so, the centrosomes would be expected to lead to a multi-polar spindle and abnormal chromosome segregation.

- <u>Genomic instability during leukemogenesis in children with NF1.</u>

Completed. Related to our work on genomic instability in NF1 solid tumors, we recently published our discovery of interstitial uniparental disomy as a novel mechanism of genomic instability during

leukemogenesis in children with NF1. We submitted a preprint in our last year's progress report. See the Appendix for the final publication of Stephens K, Weaver M, Leppig KA, Maruyama K, Emanuel PD, Le Beau MM, Shannon KM. Interstitial uniparental isodisomy at clustered breakpoint intervals is a frequent mechanism of *NF1* inactivation in myeloid malignancies. Blood 108:1684-89, 2006.

In summary, these data suggest that the cases with interstitial uniparental isodisomy arose in a leukemia-initiating cell by double homologous recombination events at intervals of preferred mitotic recombination. Homozygous inactivation of *NF1* favored outgrowth of the leukemia-initiating cell. Our studies demonstrate that LOH analyses of loci distributed along the chromosomal length along with copy-number analysis can reveal novel mechanisms of LOH that may potentially identify regions harboring "cryptic" tumor suppressor or modifier genes whose inactivation contribute to tumorigenesis.

Year 2 Statement of Work in original grant application (underlined) and progress:

- Screen subjects with early onset cutaneous neurofibromas that are heterozygous at *NF1* for somatic mosaicism for an *NF1* microdeletion. The cells are ready and will be analyzed by FISH. These experiments were delayed due to the transition to my new academic appointment. Assuming the no-cost extension and subcontract are granted, Dr. Wallace and I will establish a collaboration with Dr. Karen Swisshelm, a cytogeneticist at the University of Colorado, to perform FISH analyses to rule out moscaicism for an *NF1* microdeletion.
- Construct STS-content maps, sequence fosmids, and construct haplotypes. This is part of Aim #4, which is not reasonable to pursue as described above..
- Obtain cutaneous neurofibromas from *NF1* microdeletion adults. To date we have obtained neurofibromas from two microdeletion patients, including multiple neurofibromas from on of the patients. In addition, we have obtained MPNST from one of these patients. Samples are frozen in OCT. These will be examined by immunofluorescence for centrosome abnormalities. These are the samples that Dr. Wallace will analyze. No more tumor speciments will be obtained from patients at the University of Washington for these studies.
- Perform immunohistochemistry and nucleic acid extraction of neurofibromas. Results of immunohistochemistry are described above. DNA has been purified from neurofibromas; our specimens will be combined with those of Dr. Wallace to increase robustness of the studies.
- Assemble data on clinical spectrum of *NF1* microdeletion patients; write manuscript.

We have not identified sufficient new deletion patients to date. Our collaborator, Dr. Mautner in Germany, has a large patient population and many NF1 deletion patients. I will share the phenotypic data and deletion data of the few newly-identified patients with Dr. Mautner (anonymously as approved by the IRB) to be combined with his data. Hopefully, our data will contribute to his study and conclusions. No further work will be done on this objective.

Year 3 Statement of Work in original grant application (underlined) and progress:

- Screen JJAZ1 gene for inactivating mutations in subjects with early onset cutaneous neurofibromas who are heterozygous at *NF1*

We developed PCR and sequencing primers and have completed sequencing of the JJAZ1 gene in 5 patients with early onset cutaneous neurofibromas who are heterozygous for the *NF1* gene. These data are currently being analyzed by Dr. Stephens. She has setup the reference files and other documentation necessary to employ the MutationSurveyor software program that rapidly detects mutations. We will share our primers and sequencing protocol with Dr. Wallace, who will extend this study by sequence anaysis of JJAZ1 in DNAs of subjects of similar phenotype in her cohort.

- Continue to obtain cutaneous neurofibromas from *NF1* microdeletion adults.

No more tumors will be collected. All patient recruitment and specimen collection will be terminated at the University of Washington. We have a pending modification to our IRB to continue analyzing existing pathological samples, but to terminate patient recruitment. Upon approval, appropriate similar documents will be filed with the Army IRB.

- Continue to perform immunohistochemistry of neurofibromas, MPNST, and tumor cells. Experiments will continue in the laboratory of Dr. Margaret Wallace, if the pending subcontract is granted.
- Perform microsatellite instability studies on neurofibromas tissue.

This study was not complete at the University of Washington. We will send the primers and protocols and DNA specimens to Dr. Wallace, who will extend the study by including appropriate specimens from her cohort.

- Identify 2nd hit *NF1* mutations in neurofibroma.

Dr. Wallace will complete this aim if time allows. However, it is not the most important of the objectives that remain.

- Continue fosmid analysis of *NF1* region; construct new libraries if needed.

This is part of Aim #4, which our data described above indicate is not necessary to pursue.

Year 4 Statement of Work in original grant application (underlined) and progress:

- Submit clinical information on *NF1* microdeletion patients to the National Neurofibromatosis Foundation International Database.

Dr. Stephens is assembling the phenotypic data in an appropriate format to submit to Dr. Friedman.

- Analyze data for phenotype/genotype correlations and prognostic utility.

Will not be completed. Phenotype/genotype data from our patients will be shared with Dr. Mautner to contribute to his continuation of these studies.

- Analyze the complete sequence of the *NF1* microdeletion region for new genes and paralogs.

This is part of Aim #4, which our data described above indicate is not necessary to pursue.

- Perform comparative mapping of final human sequence with that of the mouse.

This is part of Aim #4, which our data described above indicate is not necessary to pursue. Furthermore this work has been completed and published by us and our collaborators (15).

Key Research Accomplishments for this year

-
- Consistent with our hypothesis of genomic instability during NF1-related tumorigenesis, we have shown that loss of *NF1* heterozygosity in NF1-related leukemias occurs primarily by a novel mechanism of interstitial uniparental disomy with clustered breakpoints. This work has now been published, see reprint in Appendix. (. Stephens K, Weaver M, Leppig KA, Maruyama K, Emanuel PD, Le Beau MM, Shannon KM. Interstitial uniparental isodisomy at clustered breakpoint intervals is a frequent mechanism of NF1 inactivation in myeloid malignancies. Blood 108:1684-1689, 2006.
- Consistent with our hypothesis of genomic instability during NF1-related tumorigenesis, we have demonstrated that neurofibromin localizes with the centrosome in normal primary cells, cell lines, and malignant cell lines mostly of epithelial origin. We also demonstrated that Schwann cells from normal nerves, and from the nonlesional nerve of an NF1 patient with MPNST, do not have neurofibromin in the centrosomes. However, because of cellular interactions in the tumor microenvironment, this does not rule out a role for either centrosome dysregulation or neurofibromin/centrosome interactions in tumors of NF1 patients.

- Our preliminary data suggest that cells (of unknown type) in a neurofibroma from an NF1 microdeletion patient have abnormal centrosome regulation, as demonstrated by structurally abnormal and/or multipolar mitoses. This suggests a possible role for centrosome dysregulation in neurofibromagenesis. This discovery also poses the new and exicting possibility that neurofibromin haploinsufficiency or deficiency in some tumor cell types may be contributory to centrosome dysregulation and aneuploidy during tumorigenesis.

Reportable Outcomes

Manuscripts (see Appendices)

Stephens K. Neurofibromatosis. In *Molecular Pathology in Clinical Practice*. D.G.B. Leonard, Ed. New York: Springer –Verlag, 2007.

Stephens K, Weaver M, Leppig KA, Maruyama K, Emanuel PD, Le Beau MM, Shannon KM. Interstitial uniparental isodisomy at clustered breakpoint intervals is a frequent mechanism of NF1 inactivation in myeloid malignancies. Blood 108:1684-1689, 2006.

De Raedt T, Stephens M, Heyns I, Brems H, Thijs D, Messiaen L, Stephens K, Lazaro C, Wimmer K, Kehrer-Sawatzki H, Vidaud D, Kluwe L, Marynen P, Legius E. Conservation of hotspots for recombination in low-copy repeats associated with the *NF1* microdeletion. Nature Genet 38:1419-1423, 2006.

Perrin GQ, Fishbein L, Thomson SA, Thomas SL, Stephens K, Garbern JY, Deries GH, Yachnis AT, Wallace MR, Muir D. Plexiform-like neurofibromas develop in the mouse by intraneural xenograft of an NF1 tumor-derived Schwann cell line. J Neurosci Res 85:1347-1357, 2007.

Presentations

Virginia P. Sybert. Developmental Embryology of the Skin. David W. Smith Dysmorphology Meeting, Lake Arrowhead, CA September, 2006.

Virginia P. Sybert. Developmental Embryology of the Skin. Baylor University, Departments of Dermatology and Medical Genetics. March 16 & March 19th, 2007.

Virgina P Sybert. Molecular Mechanisms of Skin Development. University of Washington, Dept of Medicine, Division of Medical Genetics. April 27, 2007.

Conclusions

We have developed rapid and sensitive assays for the detection and mapping of both the common 1.4 Mb *NF1* microdeletion and novel microdeletions. These assays facilitated identification of patients of the same genotype for basic research on recombination hospots and clinical studies on genoypte/phenotype and genomic instability during tumor development. We have collected tumors from *NF1* microdeletion carriers, which are now being examined for mutations and genomic instability. We published a new mechanism of genomic instability for NF1-related leukemias that involves interstitial uniparental isodomy at clustered breakpoints in the ancestral leukemic cell. These data suggest somatic recombination is favored at specific chromosomal regions, which leads to neurofibromin-deficient tumor ancestral cells(s). We have extended our investigation on genomic instability of primary NF1-related neurofibromas, which suggest that centrosomes are abnormal in number and structure; although the type(s) of cells with these defects is unknown. These data, along with our data showing neurofibromin localizes to the centrosome in as least some primary cells and cell lines, suggests neurofibromin may have a normal function in centrosome regulation, which is disrupted during tumorigenesis. We are currently analyzing more data regarding genomic instability and plan to continue this work in collaboration with Dr. Margaret Wallace. So what? We have made significant contributions to our understanding of

germline and somatic rearrangements that contribute to NF1: Assays for detection of germline *NF1* microdeletions were developed. The novel mechanism of somatic *NF1* loss in NF1-related leukemias add to our understanding of leukemogenesis and identifies chromosomal regions were somatic recombination may be favored, which could have implications for tumorigenesis of solid neoplasms. The localization of neurofibromin to the centrosome in at least some cells, along with the observation that centrosomes appear abnormal in NF1-related neurofibromas, implicates neurofibromin in normal centrosome function and in maintaining genome stability. These observations will be critical to follow up in pathologically-relevant cells and in tumors.

REFERENCES

1. Gervasini, C., Bentivegna, A., Venturin, M., Corrado, L., Larizza, L. and Riva, P. (2002) Tandem duplication of the NF1 gene detected by high-resolution FISH in the 17q11.2 region. *Hum Genet,* **110,** 314-21.
2. Kehrer-Sawatzki, H., Assum, G. and Hameister, H. (2002) Molecular characterisation of t(17;22)(q11.2;q11.2) is not consistent with NF1 gene duplication. *Hum Genet,* **111,** 465-7; author reply 468-9.
3. Kehrer-Sawatzki, H. and Messiaen, L. (2003) Interphase FISH, the structure of reciprocal translocation chromosomes and physical mapping studies rule out the duplication of the NF1 gene at 17q11.2. A reply. *Hum Genet,* **113,** 188-90.
4. Venter, J.C. and Adams, M.D. and Myers, E.W. and Li, P.W. and Mural, R.J. and Sutton, G.G. and Smith, H.O. and Yandell, M. and Evans, C.A. and Holt, R.A. *et al.* (2001) The sequence of the human genome. *Science,* **291,** 1304-51.
5. Dorschner, M.O., Sybert, V.P., Weaver, M., Pletcher, B.A. and Stephens, K. (2000) NF1 microdeletion breakpoints are clustered at flanking repetitive sequences. *Hum Mol Genet,* **9,** 35-46.
6. Forbes, S.H., Dorschner, M.O., Le, R. and Stephens, K. (2004) Genomic context of paralogous recombination hotspots mediating recurrent NF1 region microdeletion. *Genes Chromosomes Cancer,* **41,** 12-25.
7. Lopez-Correa, C., Dorschner, M., Brems, H., Lazaro, C., Clementi, M., Upadhyaya, M., Dooijes, D., Moog, U., Kehrer-Sawatzki, H., Rutkowski, J.L. *et al.* (2001) Recombination hotspot in NF1 microdeletion patients. *Hum Mol Genet,* **10,** 1387-1392.
8. Dorschner, M.O., Brems, H., Le, R., De Raedt, T., Wallace, M.R., Curry, C.J., Aylsworth, A.S., Haan, E.A., Zackai, E.H., Lazaro, C. *et al.* (in revision) Tightly clustered breakpoints permit detection of the recurrent 1.4 Mb NF1 microdeletion by deletion-specific amplification.
9. Ruiz-Ponte, C., Loidi, L., Vega, A., Carracedo, A. and Barros, F. (2000) Rapid real-time fluorescent PCR gene dosage test for the diagnosis of DNA duplications and deletions. *Clin Chem,* **46,** 1574-82.
10. Duensing, S. (2005) A tentative classification of centrosome abnormalities in cancer. *Cell Biol Int,* **29,** 352-9.
11. Fukasawa, K. (2005) Centrosome amplification, chromosome instability and cancer development. *Cancer Lett,* **230,** 6-19.
12. Jefford, C.E. and Irminger-Finger, I. (2006) Mechanisms of chromosome instability in cancers. *Crit Rev Oncol Hematol.*
13. Kramer, A., Neben, K. and Ho, A.D. (2005) Centrosome aberrations in hematological malignancies. *Cell Biol Int,* **29,** 375-83.
14. James, C., Ugo, V., Le Couedic, J.P., Staerk, J., Delhommeau, F., Lacout, C., Garcon, L., Raslova, H., Berger, R., Bennaceur-Griscelli, A. *et al.* (2005) A unique clonal JAK2 mutation leading to constitutive signalling causes polycythaemia vera. *Nature,* **434,** 1144-8.
15. Jenne, D.E., Tinschert, S., Dorschner, M.O., Hameister, H., Stephens, K. and Kehrer-Sawatzki, H. (2003) Complete physical map and gene content of the human NF1 tumor suppressor region in human and mouse. *Genes Chromosomes Cancer,* **37,** 111-20.

Appendices

Interstitial uniparental isodisomy at clustered breakpoint intervals is a frequent mechanism of *NF1* inactivation in myeloid malignancies

Karen Stephens, Molly Weaver, Kathleen A. Leppig, Kyoko Maruyama, Peter D. Emanuel, Michelle M. Le Beau, and Kevin M. Shannon

To identify the mechanism of loss of heterozygosity (LOH) and potential modifier gene(s), we investigated the molecular basis of somatic *NF1* inactivation in myeloid malignancies from 10 children with neurofibromatosis type 1. Loci across a minimal 50-Mb region of primarily the long arm of chromosome 17 showed LOH in 8 cases, whereas a less than 9-Mb region of loci flanking *NF1* had LOH in the remaining 2 cases. Two complementary techniques, quantitative polymerase chain reaction (PCR) and fluorescence in situ hybridization (FISH), were used to determine whether the copy number at loci that showed LOH was 1 or 2 (ie, deleted or isodisomic). The 2 cases with LOH limited to less than 9 Mb were intrachromosomal deletions. Among the 8 leukemias with 50-Mb LOH segments, 4 had partial uniparental isodisomy and 4 had interstitial uniparental isodisomy. These isodisomic cases showed clustering of the centromeric and telomeric LOH breakpoints. This suggests that the cases with interstitial uniparental isodisomy arose in a leukemia-initiating cell by double-homologous recombination events at intervals of preferred mitotic recombination. Homozygous inactivation of *NF1* favored outgrowth of the leukemia-initiating cell. Our studies demonstrate that LOH analyses of loci distributed along the chromosomal length along with copy-number analysis can reveal novel mechanisms of LOH that may potentially identify regions harboring "cryptic" tumor suppressor or modifier genes whose inactivation contributes to tumorigenesis. (Blood. 2006;108:1684-1689)

Introduction

Tumor suppressor gene (TSG) inactivation commonly occurs by sequential somatic inactivation of both alleles or, in individuals who inherit a germline mutation, by a somatic mutation in the single normal homolog. In both groups of patients, somatic inactivation is frequently associated with loss of heterozygosity (LOH) at the TSG locus and at flanking loci.[1,2] Defining the minimal chromosomal region with LOH in a collection of tumors has been a successful strategy for mapping and cloning TSGs. LOH can occur by multiple mechanisms as demonstrated by the extensive analyses of retinoblastomas, which identified *RB1* intragenic deletions, segmental chromosomal deletions, loss of the entire chromosome, or mitotic recombination.[2-4] While hundreds of TSGs have been identified, LOH studies typically focus on the TSG and/or closely flanking loci. For most TSGs, remarkably little is known about the extent and underlying mechanism(s) of LOH in tumor tissues.

In this study, we sought to examine the extent and mechanism of LOH in myeloid leukemias from children affected with neurofibromatosis 1 (NF1). The gene responsible for this disorder, *NF1* at chromosome band 17q11.2, encodes neurofibromin, a GTPase-activating protein that negatively regulates the biochemical activation of $p21^{ras}$ (Ras) family members (reviewed in Boguski and McCormick[5] and Donovan et al[6]). Germline *NF1* mutations cause NF1, a dominant familial cancer syndrome that affects about 1 in 4000 people. Clinical features of NF1 include neurocutaneous abnormalities, learning disabilities, and a predisposition to specific benign and malignant tumors (reviewed in Friedman and Riccardi[7]). Children with NF1 are at a markedly increased risk of developing myeloid malignancies, particularly juvenile myelomonocytic leukemia (JMML).[8] JMML is an aggressive myeloproliferative disease (MPD) characterized by monocytosis, thrombocytopenia, splenomegaly, and by malignant infiltration of the skin, lymph nodes, lungs, liver, and other organs (reviewed in Arico et al[9] and Emanuel et al[10]). Together, the biochemical activity of neurofibromin and the dominant cancer predisposition seen in affected persons suggests that *NF1* functions as a TSG. Indeed, LOH at the *NF1* locus occurs in JMML and in other NF1-associated cancers (reviewed in Side and Shannon[11]). Similarly, tumorigenesis in heterozygous *Nf1* mutant mice is associated with loss of the wild-type *Nf1* allele.[12,13] Consistent with the Knudson model of

From the Departments of Medicine, Laboratory Medicine, Pathology, and Pediatrics, University of Washington, Seattle; the Division of Hematology/Oncology, Department of Medicine and Comprehensive Cancer Center, University of Alabama at Birmingham; the Department of Medicine, Section of Hematology/Oncology, University of Chicago, IL; and the Department of Pediatrics and Comprehensive Cancer Center, University of California, San Francisco.

Submitted November 22, 2005; accepted April 24, 2006. Prepublished online as *Blood* First Edition Paper, May 11, 2006; DOI 10.1182/blood-2005-11-011486.

Supported by U.S. Army Medical Research and Materiel Command grants DAMD17-97-1-7344 and DAMD17-03-1-0203 (K.S.), and National Institutes of Health grants PO1 CA40046 (M.M.L., K.M.S.), R01 CA72614 (K.M.S.), and K24 CA80916 (P.D.E.).

K.S. designed research, generated primary data and performed analyses in her laboratory, and wrote the paper; M.W. performed genotyping experiments in K.S.'s lab; K.A.L. generated and analyzed primary cytogenetic data; K.M. developed gene dosage assay and performed experiments in K.S.'s lab; P.D.E. contributed well-characterized patient samples; M.M.L.B. helped to design research, generated primary data on interphase FISH, and performed analysis in her laboratory; K.M.S. helped to design research, identified LOH in NF1-associated leukemias, and assisted in writing the paper.

The online version of this article contains a data supplement.

Reprints: Karen Stephens, University of Washington, Medical Genetics 357720, Seattle, WA 98195; e-mail: millie@u.washington.edu.

The publication costs of this article were defrayed in part by page charge payment. Therefore, and solely to indicate this fact, this article is hereby marked "advertisement" in accordance with 18 U.S.C. section 1734.

familial cancer genes, tumors from individuals with familial NF1 invariably show loss of the allele inherited from the unaffected parent (reviewed in Side and Shannon[11]). Somatic intragenic *NF1* mutations have been identified in primary neoplasms, (reviewed in Stephens[14]), providing compelling evidence that functional inactivation of *NF1* is central to tumorigenesis. Deregulated Ras signaling has been reported in tumors from NF1 patients and *Nf1* mutant mice. These data are consistent with the idea that the tumor suppressor function of *NF1* is related to the ability of neurofibromin to negatively regulate Ras output (reviewed in Side and Shannon,[11] Cichowski and Jacks,[15] and Dasgupta and Gutmann[16]).

In the course of investigating the extent and mechanism of LOH at the *NF1* locus in myeloid malignancies, we unexpectedly identified interstitial isodisomy for a large segment of chromosome 17 as a frequent underlying genetic mechanism. Remarkably, the LOH breakpoints clustered within centromeric and telomeric marker intervals in these leukemias. To our knowledge, this is the first report of interstitial isodisomy as a frequent mechanism of somatic TSG inactivation. These data have implications for uncovering novel TSGs and for understanding pathogenic mechanisms that contribute to the development of hematopoietic malignancies as well as solid tumors.

Patients, materials, and methods

Patients

Clinical descriptions, LOH, and mutation analyses of the *NF1* gene have been reported for most of the patients.[17-19] Selected demographic and laboratory data are summarized in Table 1. Additional patient characteristics from previous reports are in Table S1, available on the *Blood* website (see the Supplemental Materials link at the top of the online article). Study procedures involving human subjects were approved by the University of California at San Francisco (UCSF) Committee for Human Research. Informed consent was provided according to the Declaration of Helsinki.

NF1 gene dosage assay

This assay measures the copy number of *NF1* exon 32 by quantitating polymerase chain reaction (PCR) amplicons relative to those of a competitively amplified disomic control locus. Validation of the assay on nontumor DNA demonstrated that *NF1* disomy gave dosage values of 0.98 ± 0.08 SD, while monosomy gave values of 0.45 ± 0.04 SD (SD indicates 1 standard deviation). A range involving 2 SD was used to predict gene copy number (Table 1, ‡ footnote). Briefly, the assay is a quantitative, competitive PCR adapted from the method of Celi et al.[20] Assay conditions are available upon request.

FISH

Metaphase chromosome preparations of immortalized lymphoblastoid cells from patient 1 were prepared and hybridized as described previously.[21] The bacteriophage P1 probe P1-12 contains approximately 55 kb of sequence from *NF1* intron 27b.[21] Bacterial artificial chromosome (BAC) clone 1000G21 (17q25) was identified by hybridization of D17S928 amplicons to filter arrays of the RPCI-11 human male BAC library, segment 4 (Roswell Park Cancer Institute, Buffalo, NY). Hybridization signals were detected using a commercial system (Vector Laboratories, Burlingame, CA). Chromosomes were banded using Hoechst 33258–actinomycin D staining, counterstained with propidium iodide, and signals visualized by fluorescence microscopy using a dual-band pass filter (Omega, Brattleboro, VT). Images in Figure 2A-B were visualized using a Zeiss Axioskop 2 plus microscope (Carl Zeiss, Thornwood, NY) equipped with a 100×/1.2 numeric aperture (NA) oil objective. Images were acquired using Spot software version 3.5.9 (Diagnostic Instruments, Sterling Heights, MI) and were processed using Adobe Photoshop software (Adobe Systems, San Jose, CA).

Cryopreserved bone marrow samples were thawed and cultured at 1×10^6 cells/mL for 24 hours (90% RPMI 1640/10% fetal bovine serum, 100 U/mL penicillin, 100 μg/mL streptomycin, and 10 mM HEPES) at 37°C in 95% air/5% CO_2. Following incubation, the cells were exposed to hypotonic KCl (0.75 M for 8 minutes at 37°C), fixed in absolute methanol-glacial acetic acid (3:1), and air-dried on slides. *NF1* probes were P1 bacteriophage clone P1-9, which spans approximately 65 kb of the *NF1* gene, including exons 2-11, and clone P1-12.[21] Centromere-specific probes for chromosomes 7 and 17 (CEP7-Spectrum Green and CEP17-Spectrum Green; Abbott Molecular, Abbott Park, IL), and the P1-derived artificial chromosome (PAC) clone P263P1 (Genome Systems, St Louis, MO), were hybridized as controls. P263P1 was isolated by screening the PAC library using primers for *D5S479*, and contains an insert of 70 kb derived from 5q31. Labeled probes were prepared by nick-translation using Bio-11-dUTP (Enzo Diagnostics, New York, NY) or digoxigenin-11-dUTP (Boehringer Mannheim, Indianapolis, IN). Interphase fluorescence in situ hybridization (FISH) was performed as described previously.[22] Hybridization of

Table 1. *NF1* gene dosage in bone marrows of children with NF1 and malignant myeloid disorders

Patient no.	Sex	Age at onset, mo	Diagnosis	Parental origin		*NF1* gene dosage value*†	Predicted *NF1* gene copy no.‡
				NF1 mutation	LOH at *NF1* locus		
1	M	9	MPS	Paternal	Maternal	0.99	Disomy
2	M	10	AML	Paternal	Maternal	0.93	Disomy
3	M	24	Monosomy 7	Unknown	Maternal	0.96	Disomy
4	M	14	JMML	Maternal	Paternal	0.86	Disomy
5	F	30	JMML	Maternal	Paternal	0.94	Disomy
6	M	10	JMML	Maternal	Paternal	0.87	Disomy
7	M	5	Monosomy 7	Maternal	Paternal	0.90	Disomy
8	F	18	MPS	Paternal	Maternal*	0.85	Disomy
9	M	60	JMML	Maternal	Paternal	0.57	Monosomy
10	M	19	Monosomy 7	De novo	Maternal*	0.48	Monosomy

Clinical descriptions, LOH, and NF1 mutation analyses have been reported previously for most of the patients.[17-19]

*Data from this study employing quantitative PCR at *NF1* gene segment.

†Measured in unfractionated bone marrow cells except in patients 3 and 9, for whom leukemic cells in peripheral blood were used.

‡Predicted gene copy number based on *NF1* gene dosage values. Validation of the assay on nontumor DNA demonstrated that *NF1* disomy gave dosage values of 0.98 ± 0.08 SD, while monosomy gave values of 0.45 ± 0.04 SD. A range of 2 SD was used to approximate a 95% confidence interval. Therefore, values from 0.82 to 1.14 predicted disomy, and values from 0.37 to 0.53 predicted monosomy.

probes labeled with either biotin or digoxigenin was detected with fluorescein-conjugated avidin (Vector Laboratories) and rhodamine-conjugated antidigoxigenin antibodies (Boehringer Mannheim), respectively. Nuclei were counterstained with DAPI. The slides were randomized and examined by 2 observers in a blinded fashion, with 500 cells scored by each observer for each probe. We established control values by hydridizing the probes to cryopreserved bone marrow cells from patients in remission (C1, AML-M4) or with myeloid leukemias that retained heterozygosity at *NF1* (C2-C5 in Table S2). The cutoff value was set as the mean ± 3 SD.

The distribution of hybridization signals per nucleus for the CEP17 probe was determined in bone marrow cells from healthy control individuals (n = 10; Table S2).

Mapping the LOH region

Polymorphic loci were genotyped by PCR. LOH at the *NF1* locus was evaluated by PCR analysis of at least 1 informative intragenic site including exon 5, intron 27B *AluI*/*Alu*II, and intron 38. LOH was determined by comparing the genotype of the patient's tumor DNA to that of peripheral blood DNA of the patient's parents. For patients 1, 4, 5, 9, and 10, normal tissue or an Epstein-Barr virus (EBV)–transformed cell line was available to confirm a constitutional genotype with biparental inheritance of *NF1* alleles.[18,23] Segregation of alleles from parents to child for multiple informative loci on autosomes other than 17 was consistent with parentage as stated for each case (data not shown). Physical distances between chromosome 17 loci are based on the May 2004 assembly of the human genome (http://genome.ucsc.edu).

Results

Delineation of a large region of isodisomy in an NF1-associated MPD

Previous molecular analysis of bone marrow cells from children with NF1 revealed LOH at *NF1* in $CD34^+$ cells in 3 informative cases, whereas lymphoblasts immortalized by EBV retained heterozygosity in 2 of these patients.[18] The remaining child with LOH at *NF1* in EBV-transformed lymphoblasts was a 9-month-old boy with an unusual MPD and loss of the maternal *NF1* allele (Table 1, patient 1).[18] The retained paternal allele carried a de novo R1276X mutation (Table S1) that encoded a truncated protein lacking the GTPase-activating protein (GAP) domain.[19] We performed extended LOH analyses of chromosome 17, which demonstrated loss of maternally derived alleles from *D17S975* at 17q11.2 to *D17S1830* at 17q25.3, a segment of 50.3 Mb (Figure 1). Although a deletion of this size is readily detected by cytogenetic techniques, the bone marrow and lymphoblastoid cells of patient 1 had a normal 46, XY karyotype. These data suggested that the 50.3-Mb LOH region was not deleted, but present on both chromosome 17 homologs. To address this possibility, the lymphoblastoid cells were analyzed by FISH with an *NF1* intron 27b probe.[21] Hybridization signals were detected on both chromosome 17 homologs (Figure 2A). Together, these data suggest that a 50.3-Mb interstitial interval of the maternal chromosome had been replaced with a homologous paternal DNA segment, resulting in homozygosity for the mutant R1276X *NF1* allele (Figure 1). FISH with a BAC harboring the *D17S928* locus confirmed that the heterozygous 17qter segment had not translocated elsewhere in the genome of the leukemic clone (Figure 2B). Taken together, these data confirmed interstitial isodisomy.

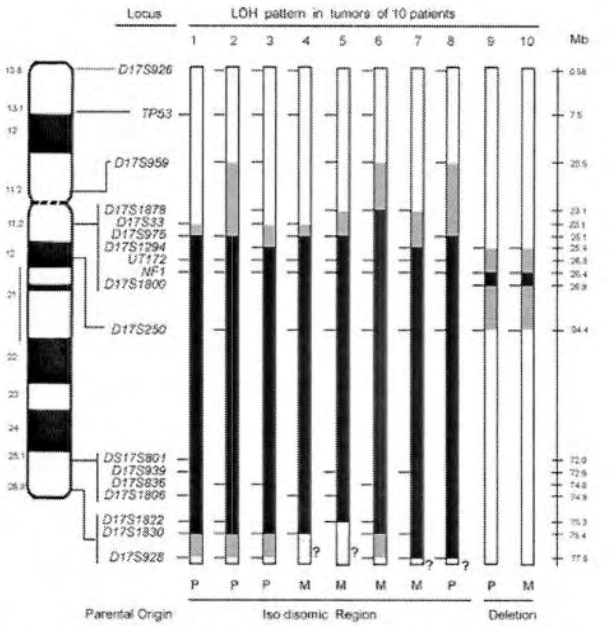

Figure 1. LOH at chromosome 17 loci in NF1-associated myeloid malignancies. Ideogram and schematic of chromosome 17 showing the loci that were screened for LOH. For each tumor, a bar shows the single chromosome 17 that underwent LOH with informative loci (tick marks), segments showing biparental inheritance (□), segments that underwent LOH (■), segments where a recombination event occurred (▨), and qter segments that lacked informative loci (?). Below the schematic, the parental origin is given for the isodisomic and deleted regions for each tumor. For patients 1, 2, 3, and 8, the maternal homolog is shown with the region of paternal isodisomy indicated in black. For patients 4 through 7, the paternal homolog is shown with the region of maternal isodisomy indicated in black. LOH in patients 9 and 10 occurred by intrachromosomal deletion indicated in black. Additional chromosome 17 loci that were tested, but not informative, are not shown. Physical distances (rounded to the nearest tenth of a megabase) are based on the May 2004 assembly of the human genome (http://genome.uscs.edu), in which the length of chromosome 17 is given as 78 774 742 bp.

Uniparental isodisomy is a frequent mechanism of LOH in NF1-associated leukemias

The unexpected findings in patient 1 prompted us to use a quantitative *NF1* gene dosage PCR assay to assess *NF1* copy numbers in 9 additional NF1-associated leukemia specimens with LOH at *NF1*.[17-19] Bone marrow DNA from patient 1 (Table 1) and from the normal tissues of his parents (data not shown) gave *NF1* gene dosage values ranging from 0.91 to 1.08, which are consistent with disomy. Surprisingly, the *NF1* dosage values for 7 of the 9 remaining NF1-associated myeloid malignancies were also consistent with disomy, whereas 2 cases had values consistent with monosomy (Table 1). Cryopreserved bone marrow specimens were available from 5 of these patients for copy number confirmation. FISH analyses using a chromosome 17 centromere-specific probe (Cep17) and 2 *NF1* probes (P1-9 and P1-12) provided physical confirmation that the leukemias of all 4 cases in which the dosage assay predicted disomy contained 2 *NF1* alleles (Figure 2D; patients 3-6 in Table S2). By contrast, the bone marrow of patient 10 demonstrated monosomy for *NF1* with 2 signals in 67% and 1 signal in 29% of cells (Figure 2D and Table S2), which was also consistent with the gene dosage assay (Table 1). To confirm that the cells being examined were from the malignant clone with LOH at *NF1*, a chromosome 7–specific probe (Cep7) was hybridized to bone marrow cells of patient 3, who had monosomy 7 and was disomic at *NF1* as measured by both gene dosage and FISH (Table 1, Figure 2D, Table S2). As expected, dual-color FISH

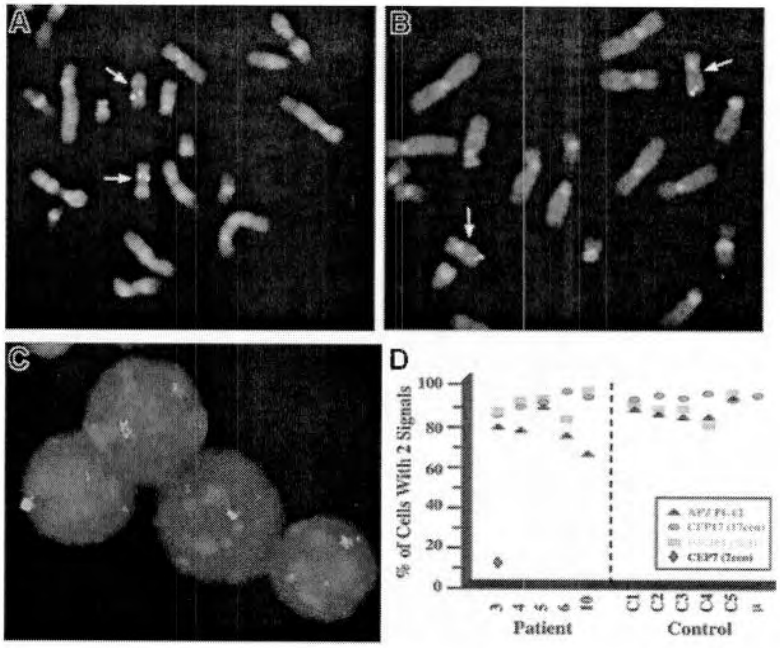

Figure 2. FISH analysis of NF1-associated myeloid malignancies. (A-B) Metaphase spreads of EBV-transformed cells from patient 1 that were hybridized with *NF1* probe P1-12 (A) and BAC clone 1000G21, which contains the *D17S928* locus at 17q25 (B). Each of 20 metaphase cells examined showed signals on both chromosome 17 homologs, consistent with disomy. The chromosome 17 homologs were identified by Hoechst–actinomycin D staining, which reveals a Q-banding–like pattern. (C) Dual-color FISH performed by cohybridizing a digoxigenin-labeled probe P1-12 (rhodamine signal) and an α-satellite probe specific for the centromere of chromosome 7 (CEP7, SpectrumGreen), which showed monosomy 7 and *NF1* disomy in bone marrow cells from patient 3. Interphase nuclei were counterstained with DAPI, and the slides mounted with PDD antifade solution. Images were visualized using a Zeiss Axioplan microscope equipped with a 63×/1.25 NA oil Plan Neofluar lens, Optivar setting 1.6. Images were acquired using a Photometrics cooled charge-coupled device (CCD) camera (Photometrics, Tucson, AZ) and NIH Image software (National Institutes of Health, Bethesda, MD), and were processed using Adobe Photoshop. (D) Graphic summary of interphase FISH analyses of myeloid leukemia cells with *NF1* (red triangle) and control probes. Probe 263P1 is a 70-kb PAC clone containing *D5S479* (chromosome band 5q31; yellow squares). CEP17 is a centromere-specific probe for chromosome 17 (green circles), and CEP7 is a centromere-specific probe for chromosome 7 (blue diamond). C1 is a cryopreserved bone marrow sample from a patient with AML-M4 in complete remission. Control samples C2 through C5 are cryopreserved bone marrow samples from 4 children with myeloid leukemias that retained heterozygosity at the *NF1* locus. The mean distribution of signals for the chromosome 17 centromere-specific probe was determined by the interphase analysis of bone marrow cells from 10 healthy individuals. This graph is a summary of data given in Table S2.

revealed monosomy 7 in cells that also had 2 structural *NF1* alleles (Figure 2C-D and Table S2). Together these studies demonstrate that LOH at *NF1* in myeloid malignancies is preferentially associated with isodisomy of a chromosomal segment carrying the mutant *NF1* allele.

Clustering and parental origin of chromosome 17 LOH breakpoints

Each of the 8 leukemias with isodisomy at *NF1* showed a large segment of LOH that minimally ranged from 50 to 52.7 Mb (Figure 1). Among these cases, both the proximal and distal LOH breakpoints were clustered. In all 8, the centromeric breakpoints mapped to a maximum interval of 4.9 Mb (6% of the chromosome 17 length of 78.77 Mb) between *D17S959* and *D17S1294*. In some leukemias, additional informative markers narrowed the breakpoint interval, as in patient 5 with a 2-Mb interval between *D17S1878* and *D17S975*. With the exception of case 6, the minimum common breakpoint region is 2 Mb and is delineated by *D17S33* and *D17S975*. The distal breakpoints in patients 1, 2, 3, and 6 were clustered between *D17S1830* and *D17S928*, an interval of 2.4 Mb (Figure 1). Lack of informativeness at *D17S928* and other 17qter loci tested precluded determining whether the large LOH segments in the tumors of patients 4, 5, 7, and 8 were isodisomic.

The bone marrows of patients 9 and 10 had LOH at loci flanking the *NF1* region. The leukemias of these 2 patients showed structural deletions that included the *NF1* locus as determined by gene dosage (Table 1) and FISH data (Figure 2D; Table S2). The centromeric breakpoints mapped to a 1.2-Mb interval between *D17S1294* and *NF1* intron 38 and the telomeric breakpoints were in a 7.5-Mb interval between *D17S1800* and *D17S250*. These data are consistent with an interstitial deletion ranging from 268 kb *(NF1* ex38 to *D17S1800)* to 9 Mb *(D17S1294* to *D17S250)*.

The bone marrows of patients 1, 2, 3, and 8 lost chromosome 17 maternal alleles and were isodisomic for a paternally derived DNA segment, whereas the cells of patients 4 through 7 lost paternal alleles and were isodisomic for a maternally derived interval of comparable length (Figure 1). In each patient with familial NF1, the isodisomic segment was derived from the parent with NF1 (Tables 1, S1). The bone marrow of patient 10, who had de novo NF1, showed loss of the maternal *NF1* allele (Table 1; Figure 1B). These data infer that patient 10 carried a germline mutation of the paternal *NF1* allele and underwent somatic deletion of the normal maternal *NF1* allele, which is consistent with the reported parental predisposition for *NF1* germline mutations.[24,25]

Discussion

Our analyses of myeloid malignancies from children with NF1 uncovered 2 distinct mechanisms underlying inactivation of the normal *NF1* allele: interstitial isodisomy and interstitial deletion (Figure 3A). The somatic interstitial deletions involving *NF1* are of interest as they may occur by a mechanism similar to that identified in constitutional and somatic mosaic *NF1* microdeletions in normal (nontumor) tissues. In these cases, the deletions are 1.2 to 1.4 Mb and occur by nonallelic homologous recombination between pairs of high-identity, low copy number repeat (LCR) elements that flank the *NF1* gene (reviewed in Stephens[26]). Microdeletions mediated by germline or somatic recombination between different LCR pairs[27,28] both involve the entire *NF1* gene and the D17S1800 locus, which are deleted in the tumors of patients 9 and 10. A mechanism of LCR-mediated recombination could be tested by precise mapping of the deletion breakpoints by single nucleotide polymorphism (SNP) mapping in the myeloid malignancies. Alternatively, the length of these somatic microdeletions in myeloid malignancies may be constrained if a 50% reduction in the expression of a critical flanking gene(s) inhibited outgrowth of the leukemic clone.

While segmental or interstitial uniparental isodisomy has been reported in constitutional rearrangements (reviewed in Vianna-Morgante[29]), we were surprised to find that interstitial isodisomy for 50 to 52.7 Mb of chromosome 17 is a common mechanism underlying LOH in NF1-associated myeloid malignancies. The leukemias of each of the 4 patients (1, 2, 3, and 6 in Figure 1) in whom *D17S928* was

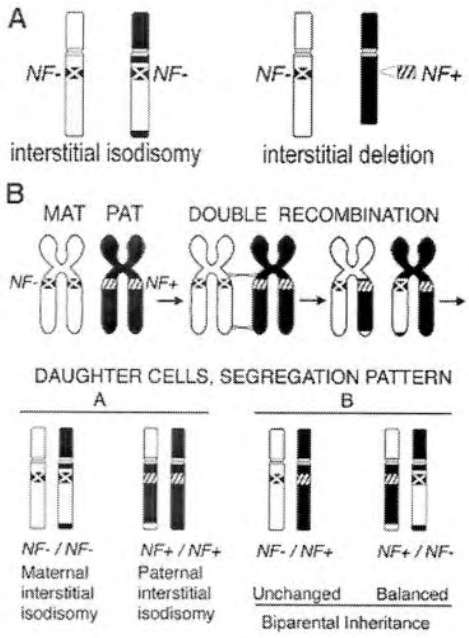

Figure 3. LOH in NF1-associated myeloid malignancies and proposed mechanism of interstitial isodisomy. (A) The schematic depicts the 2 different patterns of LOH observed in the tumors. The inactivated *NF1* allele (NF−) is marked with an X on the chromosome, while the normal *NF1* allele (NF+) is indicated by diagonal hashmarks (////). The interstitial isodisomic and deleted regions can be of maternal or paternal origin. (B) Proposed mechanism for double mitotic recombination during the S/G_2 phase of the cell cycle leading to interstitial uniparental isodisomy in a leukemic-initiating cell. The 4 possible daughter cells are depicted, along with their *NF1* genotypes and disomy patterns. Although this example depicts a cell with maternal interstitial isodisomy and *NF1* inactivation, paternal interstitial isodisomy was also observed in our study (Figure 1).

informative had interstitial isodisomy. The remaining 4 tumors (4, 5, 7, and 8 in Figure 1) may also be interstitial, but D17S928 or other regional markers were not informative. We propose that interstitial isodisomy results from a double mitotic recombination event between chromatids of the 2 chromosome 17 homologs during the S/G_2 phase of the cell cycle of a leukemia-initiating cell (Figure 3B). Depending upon the segregation pattern during mitosis, the daughter cells would have biparental inheritance at all chromosome 17 loci, or alternatively, would show interstitial isodisomy (Figure 3B). Only 1 of 4 possible daughter cells would have interstitial isodisomy along with homozygous inactivation of *NF1*, the latter of which is presumably essential for leukemic outgrowth.[30,31] The low frequency of double-mitotic recombination events, estimated at about 10^{-10} in normal lymphocytes,[32] infers that *NF1* inactivation confers a strong proliferative advantage in the leukemia-initiating cell. A possible mechanism may involve nonallelic mitotic homologous recombination between LCRs or Alu elements, which has been implicated in recurring translocations, isochromosomes, deletions, and amplifications in tumor tissues.[33-35] Other mechanisms that could give rise to 17q interstitial isodisomy are less likely. For example, 2 sequential single recombination events in different precursor cells are also possible, but would imply that each independent event conferred a proliferative advantage. A gene conversion–like event of a 50-Mb segment would be unprecedented as estimated conversion tracts in humans are typically less than 2 kb.[36,37] The clustered breakpoint intervals of the isodisomic segments suggest that mitotic recombination may be favored in these regions.

Our data are intriguing in light of recent reports showing *JAK2* point mutations in most patients with polycythemia vera (PV) and in some cases of essential thrombocythemia (ET) and chronic idiopathic myelofibrosis (CIMF).[38-41] An unexpected and intriguing result of these studies was the finding of biallelic mutations in approximately 30% of the PV specimens. The underlying genetic mechanism in these cases was a mitotic recombination that led to loss of the normal *JAK2* allele and resulted in isodisomy for a segment of the short arm of chromosome 9 estimated to span approximately 40 cM.[42] The most telomeric marker studied showed LOH in many cases, which is consistent with a single recombination event. We did not prove that the isodisomic regions were interstitial in patients 4, 5, 7, and 8 due to a lack of informative polymorphic markers near 17qter (Figure 1), and it is therefore possible that isodisomy resulted from a single recombination event in 1 or more of our cases. Similarly, it is possible that studies with additional markers near 9pter would uncover double-mitotic recombination events in some PV samples. Whereas biallelic *NF1* inactivation deregulates Ras signaling in response to hematopoietic growth factors, it is less obvious why loss of the normal *JAK2* allele and isodisomy of the mutant homolog would confer a growth advantage beyond that of a dominant heterozygous mutation. Since JAK2 molecules that are recruited to activated growth factor receptors transphosphorylate each other, it is possible that the normal protein has a dominant interfering activity that impairs the ability of mutant JAK2 to deregulate downstream effectors. Consistent with this idea, James et al[38] found that coexpressing wild-type and mutant JAK2 proteins restored erythropoietin-dependence in the Ba/F3 pro–B-cell line.

A broad implication of our work and of the recent studies of *JAK2* mutations in MPD is that segmental uniparental isodisomy may be a frequent but unrecognized mechanism in human cancers. Although isodisomy of a 25-cM interval was first described in children with Down syndrome who developed acute lymphoblastic leukemia by Rogan et al,[43] this genetic mechanism has received limited attention in hematologic malignancies until recently. The availability of automated allelotyping and the use of SNP and high-density arrays have been developed for high-resolution analysis of allelic losses and gains in tumors.[44-46] Interestingly, a number of investigators are now identifying regions of isodisomy in acute myeloid leukemia.[47-49] Our data extend these studies by showing that inactivation of a known myeloid TSG is frequently associated with acquired uniparental disomy. Importantly, DNA segments that are associated with partial or interstitial isodisomy will appear normal when examined by conventional cytogenetic analysis, FISH, or comparative genomic hybridization, making these approaches of limited use for cancers where LOH results in isodisomy. Together, LOH and copy-number analyses provide the opportunity to define new genetic mechanisms of somatic mutation, mitotic recombination sites, putative modifying or imprinted genes, and/or correlations between tumor genotype and neoplastic transformation. In addition, mono- or biallelic expression from a locus (loci), other than the TSG itself, could affect the efficacy of putative therapeutic agents.

Acknowledgments

We thank Virginia P. Sybert and Eric Sievers for referring patient 1, Melvin H. Freedman for bone marrow samples, Michael Dorschner for BAC1000G21, and Elizabeth M. Davis and Rafael Espinosa III for technical assistance.

References

1. Fearon ER. Human cancer syndromes: clues to the origin and nature of cancer. Science. 1997; 278:1043-1050.
2. Tischfield JA. Loss of heterozygosity or: how I learned to stop worrying and love mitotic recombination. Am J Hum Genet. 1997;61:995-999.
3. Qian F, Germino GG. "Mistakes happen": somatic mutation and disease. Am J Hum Genet. 1997; 61:1000-1005.
4. Cavenee WK, Dryja TP, Phillips RA, Benedict WF, et al. Expression of recessive alleles by chromosomal mechanisms in retinoblastoma. Nature. 1983;305:779-784.
5. Boguski MS, McCormick F. Proteins regulating Ras and its relatives. Nature. 1993;366:643-654.
6. Donovan S, Shannon KM, Bollag G. GTPase activating proteins: critical regulators of intracellular signaling. Biochim Biophys Acta. 2002;1602:23-45.
7. Friedman J, Riccardi VM. Clinical and epidemiological features. In: Friedman JM, Butmann DH, MacCollin M, Riccardi VM, eds. Neurofibromatosis Phenotype, Natural History, and Pathogenesis. 3rd ed. Baltimore, MD: The Johns Hopkins University Press; 1999:29-86.
8. Stiller CA, Chessells JM, Fitchett M. Neurofibromatosis and childhood leukemia/lymphoma: a population-based UKCCSG study. Br J Cancer. 1994;70:969-972.
9. Arico M, Biondi A, Pui CH. Juvenile myelomonocytic leukemia. Blood. 1997;90:479-488.
10. Emanuel PD, Shannon KM, Castleberry RP. Juvenile myelomonocytic leukemia: molecular understanding and prospects for therapy. Mol Med Today. 1996;2:468-475.
11. Side LD, Shannon KM. The NF1 gene as a tumor suppressor. In: Upadhyaya M, Cooper DN, eds. Neurofibromatosis type 1. Oxford, United Kingdom: Bios Scientific; 1998:133-152.
12. Mahgoub N, Taylor BR, Le Beau MM, et al. Myeloid malignancies induced by alkylating agents in Nf1 mice. Blood. 1999;93:3617-3623.
13. Jacks T, Shih TS, Schmitt EM, Bronson RT, Bernards A, Weinberg RA. Tumour predisposition in mice heterozygous for a targeted mutation in Nf1. Nat Genet. 1994;7:353-361.
14. Stephens K. Genetics of neurofibromatosis 1-associated peripheral nerve sheath tumors. Cancer Invest. 2003;21:901-918.
15. Cichowski K, Jacks T. NF1 tumor suppressor gene function: narrowing the GAP. Cell. 2001; 104:593-604.
16. Dasgupta B, Gutmann DH. Neurofibromatosis 1: closing the GAP between mice and men. Curr Opin Genet Dev. 2003;13:20-27.
17. Shannon KM, O'Connell P, Martin GA, et al. Loss of the normal NF1 allele from the bone marrow of children with type 1 neurofibromatosis and malignant myeloid disorders. N Engl J Med. 1994;330: 597-601.
18. Miles DK, Freedman MH, Stephens K, et al. Patterns of hematopoietic lineage involvement in children with neurofibromatosis type 1 and malignant myeloid disorders. Blood. 1996;88:4314-4320.
19. Side L, Taylor B, Cayouette M, et al. Homozygous inactivation of the NF1 gene in bone marrow cells from children with neurofibromatosis type 1 and malignant myeloid disorders. N Engl J Med. 1997;336:1713-1720.
20. Celi F, Cohen M, Antonarakis S, Wertheimer E, Roth J, Shuldiner A. Determination of gene dosage by a quantitative adaptation of the polymerase chain reaction (gd-PCR): rapid detection of deletions and duplications of gene sequences. Genomics. 1994;21:304-310.
21. Leppig KA, Viskochil D, Neil S, et al. The detection of contiguous gene deletions at the neurofibromatosis 1 locus with fluorescence in situ hybridization. Cytogenet Cell Genet. 1996;72:95-98.
22. Le Beau MM, Espinosa R III, Davis EM, Eisenbart JD, Larson RA, Green ED. Cytogenetic and molecular delineation of a region of chromosome 7 commonly deleted in malignant myeloid diseases. Blood. 1996;88:1930-1935.
23. Luna-Fineman S, Shannon KM, Lange BJ. Childhood monosomy 7: epidemiology, biology, and mechanistic implications. Blood. 1995;85: 1985-1999.
24. Jadayel D, Fain P, Upadhyaya M, et al. Paternal origin of new mutations in von Recklinghausen neurofibromatosis. Nature. 1990;343:558-559.
25. Stephens K, Kayes L, Riccardi VM, Rising M, Sybert VP, Pagon RA. Preferential mutation of the neurofibromatosis type 1 gene in paternally derived chromosomes. Hum Genet. 1992;88:279-282.
26. Stephens K. Neurofibromatosis 1. In: Lupski JR, Stankiewicz P, eds. Genomic Disorders: The Genomic Basis of Disease. 1st ed. Totowa, NJ: Humana Press; 2006:207-219.
27. Dorschner MO, Sybert VP, Weaver M, Pletcher BA, Stephens K. NF1 microdeletion breakpoints are clustered at flanking repetitive sequences. Hum Mol Genet. 2000;9:35-46.
28. Kehrer-Sawatzki H, Kluwe L, Sandig C, et al. High frequency of mosaicism among patients with neurofibromatosis type 1 (NF1) with microdeletions caused by somatic recombination of the JJAZ1 gene. Am J Hum Genet. 2004;75:410-423.
29. Vianna-Morgante AM. The ratio of maternal to paternal UPD associated with recessive diseases. Hum Genet. 2005;117:288-290.
30. Kalra R, Paderanga DC, Olson K, Shannon KM. Genetic analysis is consistent with the hypothesis that NF1 limits myeloid cell growth through p21ras. Blood. 1994;84:3435-3439.
31. Largaespada DA, Brannan CI, Shaughnessy JD, Jenkins NA, Copeland NG. The neurofibromatosis type 1 (NF1) tumor suppressor gene and myeloid leukemia. Curr Top Microbiol Immunol. 1996;211:233-239.
32. Morley AA, Grist SA, Turner DR, Kutlaca A, Bennett G. Molecular nature of in vivo mutations in human cells at the autosomal HLA-A locus. Cancer Res. 1990;50:4584-4587.
33. Bien-Willner GA, Stankiewicz P, Lupski JR, Northup JK, Velagaleti GV. Interphase FISH screening for the LCR-mediated common rearrangement of isochromosome 17q in primary myelofibrosis. Am J Hematol. 2005;79:309-313.
34. Saglio G, Storlazzi CT, Giugliano E, et al. A 76-kb duplicon maps close to the BCR gene on chromosome 22 and the ABL gene on chromosome 9: possible involvement in the genesis of the Philadelphia chromosome translocation. Proc Natl Acad Sci U S A. 2002;99:9882-9887.
35. van Dartel M, Hulsebos TJ. Amplification and overexpression of genes in 17p11.2 – p12 in osteosarcoma. Cancer Genet Cytogenet. 2004;153: 77-80.
36. Jeffreys AJ, May CA. Intense and highly localized gene conversion activity in human meiotic crossover hot spots. Nat Genet. 2004;36:151-156.
37. Padhukasahasram B, Marjoram P, Nordborg M. Estimating the rate of gene conversion on human chromosome 21. Am J Hum Genet. 2004;75: 386-397.
38. James C, Ugo V, Le Couedic JP, et al. A unique clonal JAK2 mutation leading to constitutive signalling causes polycythaemia vera. Nature. 2005; 434:1144-1148.
39. Levine RL, Wadleigh M, Cools J, et al. Activating mutation in the tyrosine kinase JAK2 in polycythemia vera, essential thrombocythemia, and myeloid metaplasia with myelofibrosis. Cancer Cell. 2005;7:387-397.
40. Baxter EJ, Scott LM, Campbell PJ, et al. Acquired mutation of the tyrosine kinase JAK2 in human myeloproliferative disorders. Lancet. 2005;365: 1054-1061.
41. Kralovics R, Passamonti F, Buser AS, et al. A gain-of-function mutation of JAK2 in myeloproliferative disorders. N Engl J Med. 2005;352: 1779-1790.
42. Kralovics R, Guan Y, Prchal JT. Acquired uniparental disomy of chromosome 9p is a frequent stem cell defect in polycythemia vera. Exp Hematol. 2002;30:229-236.
43. Rogan PK, Close P, Blouin JL, et al. Duplication and loss of chromosome 21 in two children with Down syndrome and acute leukemia. Am J Med Genet. 1995;59:174-181.
44. Huang J, Wei W, Zhang J, et al. Whole genome DNA copy number changes identified by high density oligonucleotide arrays. Hum Genomics. 2004;1:287-299.
45. Zhou X, Mok SC, Chen Z, Li Y, Wong DT. Concurrent analysis of loss of heterozygosity (LOH) and copy number abnormality (CNA) for oral premalignancy progression using the Affymetrix 10K SNP mapping array. Hum Genet. 2004;115: 327-330.
46. Zhou X, Rao NP, Cole SW, Mok SC, Chen Z, Wong DT. Progress in concurrent analysis of loss of heterozygosity and comparative genomic hybridization utilizing high density single nucleotide polymorphism arrays. Cancer Genet Cytogenet. 2005;159:53-57.
47. Fitzgibbon J, Smith LL, Raghavan M, et al. Association between acquired uniparental disomy and homozygous gene mutation in acute myeloid leukemias. Cancer Res. 2005;65:9152-9154.
48. Gorletta TA, Gasparini P, D'Elios MM, Trubia M, Pelicci PG, Di Fiore PP. Frequent loss of heterozygosity without loss of genetic material in acute myeloid leukemia with a normal karyotype. Genes Chromosomes Cancer. 2005;44:334-337.
49. Raghavan M, Lillington DM, Skoulakis S, et al. Genome-wide single nucleotide polymorphism analysis reveals frequent partial uniparental disomy due to somatic recombination in acute myeloid leukemias. Cancer Res. 2005;65:375-378.

Chapter 20

The Neurofibromatoses

Karen Stephens

Neurofibromatosis type 1 and neurofibromatosis type 2 are two distinct genetic disorders that predispose to the development of tumors primarily of the nervous system (Table 20-1).[1] A recently recognized third form of neurofibromatosis, known as schannomatosis,[2] is not included in this review, as molecular genetic testing is unavailable for this disorder.

NEUROFIBROMATOSIS TYPE 1

Molecular Basis of Disease

Neurofibromatosis type 1 (NF1) is an autosomal dominant progressive disorder with high penetrance but extremely variable expressivity (reviewed in References 1, 3, and 4). The cardinal features are café au lait macules, intertrigenous freckling, Lisch nodules, and multiple neurofibromas, although numerous other features and complications are common. Criteria for a diagnosis of NF1 were established in 1987 by a consensus meeting of the National Institutes of Health diagnostic criteria and are widely used.[5] Neurofibromas are benign nerve sheath tumors that arise on peripheral nerves. Cutaneous neurofibromas develop in virtually all cases of NF1, typically appear in the second decade of life, grow slowly, increase in number with age, and are considered at low risk for transformation to a malignant peripheral nerve sheath tumor (MPNST; previously known as neurofibrosarcoma). In contrast, diffuse plexiform neurofibromas and deep nodular plexiform neurofibromas are considered at increased risk for transformation to MPNST. Individuals affected with NF1 have a lifetime risk for MPNST of 8% to 13%.[6] Other neoplasms epidemiologically associated with NF1 include medulloblastoma, pheochromocytoma, astrocytoma, and adenocarcinoma of the ampulla of Vater. Primarily children affected with NF1 are at increased risk for optic pathway and brainstem gliomas, rhabdomyosarcomas, and malignant myeloid leukemias. NF1 patients are also at increased risk for a second malignancy, some of which may be treatment related.

NF1 is caused by inactivating mutations of 1 copy of the *NF1* gene resulting in haploinsufficiency for the gene product neurofibromin (Table 20-1). About 85% to 90% of constitutional mutations are nonsense, splicing, and missense; they are distributed throughout the gene, although some exons appear to be mutation rich (Figure 20-1). An estimated 5% of mutations are large contiguous gene deletions typically of 1.4 megabases (Mb) that delete 1 entire *NF1* allele (reviewed in Reference 7). About one half of cases are familial (inherited from an affected parent) and one half are sporadic, resulting from a de novo *NF1* mutation. An unknown fraction of sporadic cases are due to postzygotic mutation of the *NF1* gene, which complicates mutation detection and counseling issues. Neurofibromin functions as a negative regulator of the *RAS* oncogene by stimulating the conversion of active guanosine 5′-triphosphate (GTP)-bound RAS to the inactive guanosine 5′-diphosphate (GDP)-bound form by hydrolyzing GTP. Biochemical, cell culture, and genetic studies in both NF1 patients and mouse models are consistent with a model whereby a somatic mutation inactivates the remaining functional *NF1* gene (leading to increased activated RAS) in a progenitor Schwann cell as an early, probably initiating, event in the development of neurofibromas (reviewed in Reference 8). Biallelic inactivation of *NF1* also occurs in other types of progenitor cells that give rise to NF1-associated tumors such as glioma and myeloid malignancies.

Clinical Utility of Testing

A diagnosis of NF1 can almost always be made based on clinical findings, particularly after 8 years of age. Clinical DNA-based testing is available from many licensed clinical laboratories (see GeneTests, http://www.genetests.org/). Testing is not typically used for diagnostic purposes, but can be useful for confirming a clinical diagnosis, reproductive counseling, and prenatal or preimplantation diagnosis. Blanket recommendations for diagnostic testing for NF1 cannot be made because the sensitivity of clinical

Table 20-1. Comparison of Features of the NF1 and NF2 Disorders

Feature	Neurofibromatosis 1	Neurofibromatosis 2
Alternate name	Peripheral neurofibromatosis; von Recklinghausen neurofibromatosis	Central neurofibromatosis; bilateral acoustic neuroma
OMIM accession number*	162200	101000
Mode of inheritance	Autosomal dominant	Autosomal dominant
Frequency of disorder	1/3000–1/4000	1/25,000
Fraction of sporadic cases	30–50%	~50%
Gene symbol	*NF1*	*NF2*
Chromosomal location	17q11.2	22q12.2
Gene size; transcript size	~350 kb; ~11–13 kb†	~110 kb; 2 kb†
GenBank accession no. (gene; cDNA)‡	NT_010799; NM_000267	Y18000; NM••000268
Number of exons	60	17
Tissue expression pattern	Widely expressed	Widely expressed
Protein product (size; no. of residues)	Neurofibromin (>220 kDa; 2818)	Merlin; also known as schwannomin (65 kDa; 595)
Normal functions of protein	Tumor suppressor; negative regulator of ras oncogene	Tumor suppressor; associates with proteins of the cytoskeleton
Commonly associated tumors	Neurofibroma, MPNST, optic pathway and brainstem gliomas	Bilateral vestibular schwannomas, schwannomas of other central and peripheral nerves, meningiomas
Animal models	Mouse, fruit fly	Mouse, fruit fly

* Online Mendelian Inheritance in Man [database online] (http://www.ncbi.nlm.nih.gov:80/entrez/query.fcgi?db=OMIM).
† Alternative splicing produces transcripts of varying lengths.
‡ See Gene Lynx Human (http://www.genelynx.org/) for a compilation of, and hyperlinks to, gene, protein structure, and genomic resources.

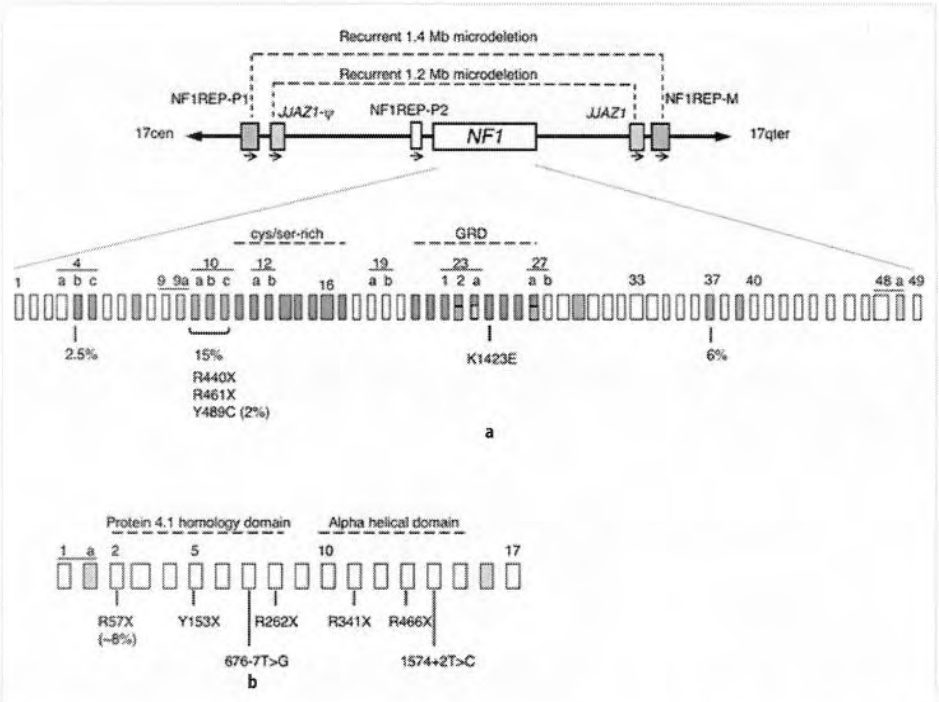

Figure 20-1. *NF1* and *NF2* genes: genomic structure and mutations. (a) At the top is a schematic of the *NF1* gene region at chromosome segment 17q11.2. The 350 kb *NF1* gene is flanked by 2 different sets of directly oriented paralogs. The 51 kb paralogs NF1REP-P1 (previously termed NF1REP-P) and NF1REP-M (orange boxes) and the 46 kb *JJAZ1* gene and pseudogene (−ψ) (yellow boxes) are shown. Homologous recombination between NF1REP elements results in a recurrent 1.4 megabase (Mb) microdeletion, while recombination between the *JJAZ1* paralogs results in a recurrent 1.2 Mb microdeletion.[11,16] NF1REP-P2 is a partial element with a limited role in mediating *NF1* microdeletions. The 60 exons of *NF1* are represented by boxes (not to scale), and exon numbering is sequential except as indicated. The GRD (exons 21-27a) and a cysteine/serine-rich domain with 3 cysteine pairs suggestive of ATP binding (exons 11-17) are indicated. Gray boxes indicate alternatively spliced exons that vary in abundance in different tissues. Mutations have been identified in virtually every exon. Exons where mutations are apparently in greater abundance than expected are indicated (green boxes).[21,22,25] In one study, exons 7, 10a, b, c, 23-2, 27a, 29, and 37 accounted for 30% of mutations, 15 of which were in exons 10a, b, and c, which harbor 3 recurrent mutations, including Y489C, which alone accounts for approximately 2% of mutations.[21] Blue boxes indicate exons that have clusters of missense or single base or codon deletion mutations, or both.[22] Some of the recurrent, although still infrequent, mutations are given below the exons. (b) The 17 exons of the *NF2* gene are represented by boxes (drawing not to scale), and the exon numbering is sequential. The protein 4.1-homology domain thought to mediate binding to cell surface glycoproteins (exons 2-8), the α-helical domain (exons 10-15), and the unique C-terminus (exons 16-17) are shown. Gray boxes indicate alternatively spliced exons; the inclusion of exon 16 creates an alternate termination codon resulting in a slightly truncated protein. Mutations have been identified involving each exon except for 16. Selected recurrent mutations found in a limited survey of references cited in the text are indicated. In several studies, R57X occurred in 8% of familial constitutional mutations.

diagnosis for NF1 is very high and the sensitivity of molecular testing is not 100%. Furthermore, benefits of diagnostic testing are subjective and may differ from family to family. Early planning is necessary for couples considering prenatal diagnosis using amniocytes or chorionic villus tissue or preimplantation diagnosis. These tests are available only when the pathogenic familial germline mutation (or the predisposing haplotype in the case of linkage testing) has been identified previously in an affected parent, a process that can require weeks or months.

The primary genetic counseling issue related to molecular testing of *NF1* is the inability to predict the severity or course of the disorder in a patient or fetus. Even among family members who carry the same *NF1* mutation, there can be considerable variation in clinical manifestations and complications. For the majority of cases, there is no correlation between genotype and phenotype. For the approximately 5% of individuals who carry a constitutional *NF1* deletion (most commonly 1.4 Mb), there is a 2-fold increased lifetime risk of MPNST,[9] a predisposition to childhood overgrowth,[10] an early age of onset with excessive numbers of cutaneous neurofibromas, numerous internal neurofibromas, learning disabilities, vascular anomalies, and astrocytomas (References 7 and 11 to 14 and references therein). A recommendation for routine testing for *NF1* microdeletion has been proposed, with follow-up for increased suspicion for MPNST.[9]

NF1 testing may be useful to confirm a diagnosis in a patient with equivocal findings, such as child who has a few café au lait macules and carries a presumptive diagnosis of NF1. In such cases, it is important to realize that the sensitivity and specificity of testing patients who do not fulfill the NIH diagnostic criteria for a diagnosis of *NF1* is unknown but is likely to be quite low.

For unaffected parents of a child with sporadic NF1, recurrence risk is a concern. Although thought to be rare, germline mosaicism has been reported in an asymptomatic parent of a child with sporadic NF1.[15] Therefore, there is a small, but unknown, increased risk of recurrence even if the child's pathogenic mutation is not detected in the genomic DNA from parental leukocytes. Although the frequency is unknown, sporadic NF1 cases with postzygotic mutations resulting in somatic mosaicism may not be as rare as once thought. One study suggests that among NF1 microdeletion cases, the frequency of somatic deletion may be very high (~40%).[16] Assuming that 10% of NF1 cases have microdeletions, a frequency of 4% mosaicism is expected in the general NF1 population. This is certainly an underestimate, as it does not consider mosaicism for intragenic *NF1* mutations. Mosaic individuals carry the *NF1* mutation in only a fraction of their cells, depending on the developmental interval and the cell type in which the mutation occurred. The phenotype of mosaic individuals ranges from localized (segmental) disease to mild or severe generalized disease.[16,17] The sensitivity of mutation detection may be lower due to an increased signal to noise ratio, that is, a low level of a mutant allele in a background of 2 normal *NF1* alleles. Offspring that inherit an NF1 mutation from a parent with mosaicism, however, will have a constitutional *NF1* mutation and may have more severe disease than their mosaic parent. Genetic counseling regarding the clinical and reproductive implications of NF1 mosaicism is highly recommended.[17]

Available Assays

Mutation of the *NF1* gene is the only known cause of the disorder. Molecular tests for diagnostic, prenatal, and preimplantation diagnosis are available. The choice of assay and testing laboratory depends upon the reason for referral and mutation types and detection rates of their assay(s).

Fluorescent in situ hybridization (FISH; see chapter 2) with *NF1* probes of either metaphase or interphase white blood cells is the optimal test to rule out or confirm the approximately 5% of cases due to a submicroscopic NF1 microdeletion (Figure 20-1).[18] In the future, a first-tier test may employ an *NF1* deletion junction-specific polymerase chain reaction (PCR) assay.[19] The recent availability of high-resolution genomic microarrays of the NF1 deletion region will facilitate clinical testing by array–comparative genomic hybridization (CGH),[20] which may become clinically important in the future if deletions involving a subset of genes predispose to certain manifestations. The sensitivity of deletion-specific PCR and array-CGH assays to detect low-level *NF1* deletion mosaicism will need to be determined. Routine cytogenetic analysis is of limited clinical utility, as the *NF1* microdeletions are submicroscopic, and translocation and rearrangement involving *NF1* are extremely rare.

Linkage analysis is an indirect test that tracks the inheritance of the mutant *NF1* allele in members of a family. This may be the quickest, most economical NF1 test for at-risk individuals and fetuses of families that fulfill the testing criteria. The primary requirement is the availability and cooperation of multiple family members whose NF1 status is known by detailed clinical evaluation. Multiple *NF1* intragenic polymorphic markers are available that facilitate identification and tracking of the predisposing haplotype in a family and provide the specificity for linkage testing.

Efficient detection of subtle intragenic *NF1* gene mutations, for purposes of diagnostic testing or mutation typing for prenatal or preimplantation diagnosis, is complicated by the large number of exons and large size of the gene (Table 20-1), variation in type and distribution of mutations, and large fraction of private mutations. About 70% to 80% of mutations result in a premature translation termination codon, with nonsense and splicing defects being

the most common.[21] These mutations can be detected by the protein truncation test (PTT; see chapter 2), which detects truncated neurofibromin polypeptides synthesized by in vitro translation of multiple overlapping *NF1* complementary DNA (cDNA) segments. A detection rate of about 80% can be attained with an optimized PTT testing
2 protocol (see below). The majority of such mutations are private to each individual or family, although there are recurrent mutations that may account for, at most, a few percent of cases (Figure 20-1).

About 10% of *NF1* mutations are missense or in-frame insertions or deletions of a few nucleotides,[21,22] some of which show clustering (Figure 20-1). Their identification requires direct sequence analysis of *NF1* exons and splice junctions in genomic DNA or cDNA segments. Prospective testing of NF1 subjects by direct genomic sequence analysis revealed a detection rate of 89%, which is more streamlined than PTT testing and allows for automation.[23] Various mutation scanning techniques of *NF1* genomic or cDNA are also employed by clinical laboratories, including denaturing high-performance liquid chromatography (DHPLC), temperature gradient gel electrophoresis (TGGE), single-strand conformation polymorphism (SSCP), and heteroduplex analysis (HA; see chapter 2). Although high detection rates are reported in the literature using DHPLC (72–95%),[24,25] it is important to realize that the detection rates for mutation scanning protocols will be laboratory specific due to the degree of optimization of the specific technique. A survey of clinical laboratories is recommended prior to sample submission. DHLPC has the advantages of using genomic DNA and high-throughput capability compared to the cDNA/gel-based PTT; however, a recently reported high-throughput PTT may be available for clinical testing in the future.[26]

Interpretation of Test Results

The detection of a truncated neurofibromin polypeptide by PTT can result in false positives.[21] High specificity requires identifying the underlying mutation at the genomic DNA or cDNA level, or both, since false positives can arise during
3 sample handling (see below). The interpretation of missense and subtle in-frame alterations as pathogenic mutations rather than neutral polymorphisms is complicated by the lack of a functional assay for neurofibromin. Apparent recurrence of a putative mutation requires careful study of the literature, since not all *NF1* mutational studies sequenced the entire gene. No comprehensive *NF1* mutation database is available; however, some mutations have been submitted to the Human Gene Mutation Database (http://archive.uwcm.ac.uk/uwcm/mg/hgmd0.html), and the largest NF1 database is actively managed and analyzed by Jan Friedman (http://www.medgen.ubc.ca/friedmanlab/). Although most likely rare, affected family members with different independent *NF1* inactivating mutations have been reported,[27] presumably a reflection of the high mutation rate of the gene ($\sim 10^{-5}$/gamete/generation). The interpretation of FISH with *NF1* probes can be complicated by mosaicism for an *NF1* microdeletion; therefore, an appropriate number of cells must be analyzed.[16] The frequency of mosaicism for an *NF1* mutation is not known; however, this is likely the underlying mechanism for patients with segmental or localized signs of the disorder.

Laboratory Issues

Optimal detection of mutations that predict a truncated neurofibromin polypeptide occurs when the nonsense-mediated decay pathway is at least partially inhibited, thereby increasing the ratio of mutant transcripts with a premature termination codon to normal transcripts. A protein synthesis inhibitor, such as puromycin, in the culture medium is effective for EBV-transformed lym- 4
phoblasts or phytohemaglutinin-stimulated primary lymphocytes.[21,28] Furthermore, blood handling and shipping protocols must be used to reduce false positives in PTT resulting from environmental effects such as cold shock[29] or delay in messenger RNA isolation.[21,28] There is no standardized proficiency program of interlaboratory comparison for *NF1* testing; performance assessment must be conducted by participation in ungraded proficiency survey programs, split sample analysis with other laboratories, or other suitable and documented proficiency-testing methods. No *NF1* testing kits, probes, or controls are approved or cleared by the Food and Drug Administration. Intronic primers for amplification of *NF1* exons and associated splice junctions that apparently do not coamplify the *NF1* pseudogene fragments have been reported.[23,30] Two other factors require consideration during test development and interpretation. Reports in support of,[31] and in opposition to,[32] an apparent tandem duplication of the *NF1* gene region have been published. In addition, transcriptional activity from *NF1* pseudogenes or pseudogene fragments has been reported.[33] Some issues related to *NF1* testing have been reviewed recently.[34]

NEUROFIBROMATOSIS TYPE 2

Molecular Basis of Disease

The development of bilateral vestibular schwannomas is a hallmark of neurofibromatosis type 2 (NF2). Other commonly associated tumors include schwannomas of other central, spinal, and peripheral nerves and meningiomas (reviewed in References 1 and 35 to 38). This is a life-threatening disorder due to the location of the tumors, along with the propensity for development of multiple

tumors. Most patients become completely deaf and can have poor balance and vision, and weakness. The mean age of onset is 18 to 24 years and the mean age of death is 36 years. The age at onset of symptoms and age at diagnosis are predictors of vestibular schwannoma growth rates and risk of death (Reference 39 and references therein). Ependymomas and astrocytomas occur less frequently and are usually indolent central nervous system tumors. Patients affected with NF2 are at minimal increased risk for malignancy. Juvenile posterior subcapsular cataract is a common nontumor manifestation. The disorder may be underdiagnosed in children who present with ocular and skin manifestations. Early diagnosis improves management, which is primarily surgical and radiological. Modifications to the criteria for a diagnosis of NF2, initially established by the 1987/1991 National Institute of Health Consensus Conference, have been proposed to increase the specificity.[40] A consensus statement on management of the NF2 patient and family was recently published.[41]

NF2 is caused by haploinsufficiency for the tumor suppressor merlin (also known as schwannomin), the protein product of the *NF2* gene (Table 20-1). About one half of patients are the first case of NF2 in the family. These sporadic cases result from de novo mutation of the *NF2* gene, a significant fraction of which are postzygotic mutations that result in mosaicism. The majority of constitutional mutations are private, predict the truncation of merlin, and are distributed throughout the gene (see below). In NF2 patients, a vestibular schwannoma develops from a progenitor Schwann cell that carries a somatic inactivating mutation in the single remaining *NF2* gene. Merlin is a protein of the cytoskeleton whose normal function remains to be determined, although it is known to associate with transmembrane proteins important in adhesion, proteins involved in signaling pathways, and cytoskeletal proteins (reviewed in Reference 42).

Clinical Utility of Testing

DNA-based clinical testing for NF2 is available (see GeneTests, http://www.genetests.org) and primarily is used for presymptomatic testing of at-risk individuals, typically young children of an affected parent. An early diagnosis of NF2 may improve outcome, and at-risk children who did not inherit the *NF2* mutation can be spared worry, costly brain imaging, and audiologic screening. Genetic counseling is recommended prior to testing presymptomatic at-risk children. Testing is also useful to confirm a clinical diagnosis, which may be most helpful in sporadic cases of NF2, particularly children who present with ocular or skin manifestations or adults with equivocal findings or mild disease. Some of these cases may be mosaic for an *NF2* mutation, as the estimated frequency of mosaicism is high (16.7–24.8% of sporadic cases).[43] Genetic counseling regarding the clinical and reproductive implications of *NF2* mosaicism is recommended.[17] Testing is also useful for reproductive counseling and prenatal or preimplantation diagnosis.[44] Prenatal diagnosis of NF2 using amniocytes or chorionic villus tissue is available only in cases where the pathogenic *NF2* germline familial mutation (or predisposing haplotype in the case of linkage testing) has been identified previously in an affected parent. For preimplantation genetic diagnosis, the specific parental *NF2* mutation must be known. Prepregnancy planning is important for couples considering prenatal diagnosis or preimplantation diagnosis. For sporadic NF2 patients undergoing surgery, it is advisable to freeze a portion of the tumor, which may be valuable at a later date for mutation identification if the patient is mosaic.

The primary genetic counseling issues regard predicting the course of the disorder and recurrence risks. There are genotype-phenotype correlations, but they cannot predict the age of onset or the course of disease for an individual patient. About 50% of *NF2* mutations are nonsense or frameshift, with about 24% splice site, 11% to 30% submicroscopic deletion, and 5% missense.[45] Typically, constitutional frameshift and nonsense mutations are associated with more severe NF2, defined by earlier age at onset and higher frequency and mean number of tumors.[46,47] Constitutional missense and small in-frame mutations are associated with mild disease,[47] and mutations in splice donor and acceptor sites result in variable clinical outcomes.[48] Interestingly, individuals with *NF2* splice-site mutations in exons 1 through 5 had an earlier age at onset and greater numbers of intracranial meningiomas compared to those with splice-site mutations in exons 11 through 15 (Figure 20-1b).[45] The type of constitutional *NF2* mutation is also correlated with the number of NF2-associated nonvestibular nervous system tumors including intracranial meningiomas, spinal tumors, and peripheral nerve tumors.[39] Individuals with constitutional nonsense or frameshift *NF2* mutations had significantly more of these tumors than individuals carrying missense, splice-site, or deletion mutations or somatic mosaicism.

Recurrence risks for asymptomatic parents of an affected child are unknown but are somewhat greater than the population risk, due to the possibility of germline mosaicism in a parent.[49] For mosaic patients, the risk of transmitting NF2 to offspring is ≤50%, depending on the proportion of gametes that carry the *NF2* mutation.[17] Offspring that do inherit the mutation, however, will have a constitutional *NF2* mutation and may have more severe disease than their mosaic parent. Testing asymptomatic parents of a child with NF2 has the potential to identify a mosaic mutation.

Available Assays

Mutation of the *NF2* gene is the only known cause of this disorder. Linkage analysis is clinically available for at-risk individuals and fetuses with multiple family members of

unambiguous clinical status regarding NF2 disease who are willing to participate in the testing process. The availability of highly informative intragenic *NF2* polymorphisms increases the specificity of this method. For certain families, linkage analysis will be the most cost- and time-effective test that gives a definitive diagnosis. It can sometimes be an option when mutation-scanning or sequencing test results are negative. See "Interpretation of Test Results," below, for cautions regarding linkage test interpretation.

Identifying an *NF2* mutation typically requires a multipronged testing protocol due to the high frequency of private constitutional mutations, the high frequency of postzygotic mutations, the different types of *NF2* mutations, and the distribution of mutations throughout the gene. Wallace et al.[50] (Figure 20-1b) describe a comprehensive testing service that includes 4 PCR reactions using a meta-PCR technique to link the amplicons into chimeric concatemers for direct sequencing, gene dosage PCR for deletions, loss of heterozygosity (LOH) studies, and subsequent sequencing of the gene in tumor tissue. In prospective studies, this approach yielded an 88% detection rate in familial NF2 cases and a 59% detection rate in sporadic NF2 cases. Direct sequencing or exon-scanning techniques (e.g., SSCP, TGGE, and HA; see chapter 2) of DNA from peripheral leukocytes, followed by direct sequencing to identify the underlying *NF2* mutation, generally have a lower detection rate.[46,47,51–53] The detection rate of either sequencing or exon scanning methods is significantly lower (34–51%) in sporadic cases in part due to the high frequency of postzygotic *NF2* mutations, which can be masked by the presence of normal alleles.[47,48,51,53] The mutation detection rate of mosaic cases can be increased 6 significantly by analysis of tumor tissue (see below).

Because schwannomas are clonal tumors with minimal cellular admixture, *NF2* mutations can be detected at high frequency in tumor tissue. Testing of tumor tissue is available clinically (see GeneTests, http://www.geneclinics.org/) and is most useful in cases where a mutation is not detected in primary lymphoblasts, where clinical manifestations are suggestive of somatic mosaicism, or where constitutional tissue is unavailable.[43,50,53] Moyhuddin et al.[53] nearly doubled the mutation detection rate among mosaic cases using vestibular schwannoma tissue rather than peripheral leukocytes. Mutations are likely to be germline (rather than somatic) if the identical mutation is detected in 2 or more pathologically or anatomically distinct tumors or if a tumor shows LOH for *NF2* intragenic or flanking loci, while constitutional tissue is heterozygous at these loci. Mutational analysis of tumor tissues is expected to have the greatest sensitivity for *NF2* somatic mosaic mutations[43] and sporadic cases with negative results from mutation scanning or sequencing tests.[54]

Efficient detection of the 11% to 30% of constitutional *NF2* deletions (typically multiexonic in nature) has been accomplished using numerous techniques, including FISH, various gene dosage PCR assays, multiplex ligation-dependent probe amplification (MPLA), and high-resolution genomic arrays.[53,55–57] 7

Note that for mutation scanning tests and deletion-detection assays, detection rates will be laboratory specific due to the varying degrees of optimization of the technique; therefore, a survey of testing laboratories is recommended prior to sample submission.

Interpretation of Test Results

Interpretation of the results of exon-scanning tests requires identifying the underlying *NF2* mutation at the genomic DNA or cDNA level, or both, to avoid false positives. Functional assays for merlin have been developed that can provide insight into the interpretation of missense and subtle in-frame alterations as pathogenic mutations rather than neutral polymorphisms;[58–60] however, such assays may not be part of a clinical testing protocol. An international *NF2* mutation database is available (Neurofibromatosis 2 (NF2) Mutation Databases, http://uwcmml1s.uwcm.ac.uk/uwcm/mg/nf2/), and this site also recognizes the United Kingdom population-based registry. Some mutations are also detailed in the Human Gene Mutation Database Cardiff (http://archive.uwcm.ac.uk/uwcm/mg/hgmd0.html). Somatic mosaicism or *NF2* gene deletions must be considered in patients who have a negative mutation test using DNA from peripheral leukocytes, regardless of the severity of their manifestations. The risk of recurrence from mosaic parent to offspring is considered very low if an *NF2* mutation cannot be identified in the parent.[53] NF2 linkage tests should consider excluding the first affected member in a family; if they are mosaic, the linkage results will be misleading in the next generation.[61] For similar reasons, linkage analysis for presymptomatic testing of subjects in this "next" generation should be performed with caution.

Laboratory Issues

There is no standardized proficiency program of interlaboratory comparison for *NF2* testing; performance assessment must be conducted by participation in ungraded proficiency survey programs, split sample analysis with other laboratories, or other suitable and documented proficiency-testing methods. No *NF2* testing kits, probes, or controls are approved or cleared by the Food and Drug Administration. Direct gene sequencing may not be the optimal test to detect *NF2* mosaic mutations in lymphoblasts, since reliable detection of a low-level point mutation will be difficult. Exon-scanning techniques that are semiquantitative, such as TGGE, will detect relative intensity differences between heteroduplexes and homoduplexes that suggest possible mosaicism.[51] Depending on age, fixation, and storage conditions, some tumors may not yield nucleic acid of sufficient quality for mutational analysis.

References

1. Friedman JM, Butmann DH, MacCollin M, Riccardi VM, eds. *Neurofibromatosis: Phenotype, Natural History, and Pathogenesis.* 3rd ed. Baltimore: Johns Hopkins University Press; 1999.
2. MacCollin M, Chiocca EA, Evans DG, et al. Diagnostic criteria for schwannomatosis. *Neurology.* 2005;64:1838–1845.
3. Friedman JM. Neurofibromatosis 1: clinical manifestations and diagnostic criteria. *J Child Neurol.* 2002;17:548–554.
4. Friedman JM. Neurofibromatosis 1. In: GeneReviews at GeneTests: Medical Genetics Information Resource [database online]. Seattle: University of Washington; 1997–2005. Available at: http://www.genetests.org. Accessed October 20, 2005. Updated October 5, 2004.
5. DeBella K, Szudek J, Friedman JM. Use of the national institutes of health criteria for diagnosis of neurofibromatosis 1 in children. *Pediatrics.* 2000;105(pt 1):608–614.
6. Evans DG, Baser ME, McGaughran J, Sharif S, Howard E, Moran A. Malignant peripheral nerve sheath tumours in neurofibromatosis 1. *J Med Genet.* 2002;39:311–314.
7. Stephens K. Neurofibromatosis 1. In: Lupski JR, Stankiewicz P, eds. *Genomic Disorders: The Genomic Basis of Genetic Disease.* Trenton, NJ: Humana Press; in press.
8. Dasgupta B, Gutmann DH. Neurofibromatosis 1: closing the GAP between mice and men. *Curr Opin Genet Dev.* 2003;13:20–27.
9. De Raedt T, Brems H, Wolkenstein P, et al. Elevated risk for MPNST in NF1 microdeletion patients. *Am J Hum Genet.* 2003;72:1288–1292.
10. Spiegel M, Oexle K, Horn D, et al. Childhood overgrowth in patients with common NF1 microdeletions. *Eur J Hum Genet.* 2005;13:883–888.
11. Dorschner MO, Sybert VP, Weaver M, Pletcher BA, Stephens K. NF1 microdeletion breakpoints are clustered at flanking repetitive sequences. *Hum Mol Genet.* 2000;9:35–46.
12. Gutmann DH, James CD, Poyhonen M, et al. Molecular analysis of astrocytomas presenting after age 10 in individuals with NF1. *Neurology.* 2003;61:1397–1400.
13. Venturin M, Guarnieri P, Natacci F, et al. Mental retardation and cardiovascular malformations in NF1 microdeleted patients point to candidate genes in 17q11.2. *J Med Genet.* 2004;41:35–41.
14. Kehrer-Sawatzki H, Kluwe L, Funsterer C, Mautner VF. Extensively high load of internal tumors determined by whole body MRI scanning in a patient with neurofibromatosis type 1 and a non-LCR-mediated 2-Mb deletion in 17q11.2. *Hum Genet.* 2005;116:466–475.
15. L'Azaro C, Gaona A, Lynch M, Kruyer H, Ravella A, Estivill X. Molecular characterization of the breakpoints of a 12-kb deletion in the NF1 gene in a family showing germ-line mosaicism. *Am J Hum Genet.* 1995;57:1044–1049.
16. Kehrer-Sawatzki H, Kluwe L, Sandig C, et al. High frequency of mosaicism among patients with neurofibromatosis type 1 (NF1) with microdeletions caused by somatic recombination of the JJAZ1 gene. *Am J Hum Genet.* 2004;75:410–423.
17. Ruggieri M, Huson SM. The clinical and diagnostic implications of mosaicism in the neurofibromatoses. *Neurology.* 2001;56:1433–1443.
18. Leppig KA, Viskochil D, Neil S, et al. The detection of contiguous gene deletions at the neurofibromatosis 1 locus with fluorescence in situ hybridization. *Cytogenet Cell Genet.* 1996;72:95–98.
19. Lopez-Correa C, Dorschner M, Brems H, et al. Recombination hotspot in NF1 microdeletion patients. *Hum Mol Genet.* 2001;10:1387–1392.
20. Mantripragada KK, Thuresson AC, Piotrowski A, et al. Identification of novel deletion breakpoints bordered by segmental duplications in the NF1 locus using high-resolution array-CGH. *J Med Genet.* 2005.
21. Messiaen LM, Callens T, Mortier G, et al. Exhaustive mutation analysis of the NF1 gene allows identification of 95% of mutations and reveals a high frequency of unusual splicing defects. *Hum Mutat.* 2000;15:541–555.
22. Fahsold R, Hoffmeyer S, Mischung C, et al. Minor lesion mutational spectrum of the entire NF1 gene does not explain its high mutability but points to a functional domain upstream of the GAP-related domain. *Am J Hum Genet.* 2000;66:790–818.
23. Mattocks C, Baralle D, Tarpey P, Ffrench-Constant C, Bobrow M, Whittaker J. Automated comparative sequence analysis identifies mutations in 89% of NF1 patients and confirms a mutation cluster in exons 11–17 distinct from the GAP related domain. *J Med Genet.* 2004;41:e48.
24. Han SS, Cooper DN, Upadhyaya MN. Evaluation of denaturing high performance liquid chromatography (DHPLC) for the mutational analysis of the neurofibromatosis type 1 (NF1) gene. *Hum Genet.* 2001;109:487–497.
25. De Luca A, Buccino A, Gianni D, et al. NF1 gene analysis based on DHPLC. *Hum Mutat.* 2003;21:171–172.
26. Gite S, Lim M, Carlson R, Olejnik J, Zehnbauer B, Rothschild K. A high-throughput nonisotopic protein truncation test. *Nat Biotechnol.* 2003;21:194–197.
27. Klose A, Peters H, Hoffmeyer S, et al. Two independent mutations in a family with neurofibromatosis type 1 (NF1). *Am J Med Genet.* 1999;83:6–12.
28. Wimmer K, Eckart M, Rehder H, Fonatsch C. Illegitimate splicing of the NF1 gene in healthy individuals mimics mutation-induced splicing alterations in NF1 patients. *Hum Genet.* 2000;106:311–313.
29. Ars E, Serra E, de la Luna S, Estivill X, Lazaro C. Cold shock induces the insertion of a cryptic exon in the neurofibromatosis type 1 (NF1) mRNA. *Nucleic Acids Res.* 2000;28:1307–1312.
30. Li Y, O'Connell P, Breidenbach HH, et al. Genomic organization of the neurofibromatosis 1 gene (NF1). *Genomics.* 1995;25:9–18.
31. Gervasini C, Bentivegna A, Venturin M, Corrado L, Larizza L, Riva P. Tandem duplication of the NF1 gene detected by high-resolution FISH in the 17q11.2 region. *Hum Genet.* 2002;110:314–321.
32. Kehrer-Sawatzki H, Messiaen L. Interphase FISH, the structure of reciprocal translocation chromosomes and physical mapping studies rule out the duplication of the NF1 gene at 17q11.2. A reply. *Hum Genet.* 2003;113:188–190.
33. Yu H, Zhao X, Su B, et al. Expression of NF1 pseudogenes. *Hum Mutat.* 2005;26:487–488.
34. Thomson SA, Fishbein L, Wallace MR. NF1 mutations and molecular testing. *J Child Neurol.* 2002;17:555–561; discussion 71–72, 646–651.
35. Ruggieri M, Iannetti P, Polizzi A, et al. Earliest clinical manifestations and natural history of neurofibromatosis type 2 (NF2) in childhood: a study of 24 patients. *Neuropediatrics.* 2005;36:21–34.
36. Baser ME, DG RE, Gutmann DH. Neurofibromatosis 2. *Curr Opin Neurol.* 2003;16:27–33.
37. Evans DG, Sainio M, Baser ME. Neurofibromatosis type 2. *J Med Genet.* 2000;37:897–904.
38. Evans DG. Neurofibromatosis 2. In: GeneReviews at GeneTests: Medical Genetics Information Resource [database online]. Seattle: University of Washington, 1997–2005. Available at: http://www.genetests.org. Accessed October 20, 2005. Updated April 6, 2004.
39. Baser ME, Kuramoto L, Joe H, et al. Genotype-phenotype correlations for nervous system tumors in neurofibromatosis 2: a population-based study. *Am J Hum Genet.* 2004;75:231–239.
40. Baser ME, Friedman JM, Wallace AJ, Ramsden RT, Joe H, Evans DG. Evaluation of clinical diagnostic criteria for neurofibromatosis 2. *Neurology.* 2002;59:1759–1765.
41. Evans DG, Baser ME, O'Reilly B, et al. Management of the patient and family with neurofibromatosis 2: a consensus conference statement. *Br J Neurosurg.* 2005;19:5–12.
42. McClatchey AI, Giovannini M. Membrane organization and tumorigenesis—the NF2 tumor suppressor, merlin. *Genes Dev.* 2005;19:2265–2277.
43. Kluwe L, Mautner V, Heinrich B, et al. Molecular study of frequency of mosaicism in neurofibromatosis 2 patients with bilateral vestibular schwannomas. *J Med Genet.* 2003;40:109–114.
44. Abou-Sleiman PM, Apessos A, Harper JC, Serhal P, Winston RM, Delhanty JD. First application of preimplantation genetic diagnosis to neurofibromatosis type 2 (NF2). *Prenat Diagn.* 2002;22:519–524.

45. Baser ME, Kuramoto L, Woods R, et al. The location of constitutional neurofibromatosis 2 (NF2) splice site mutations is associated with the severity of NF2. *J Med Genet.* 2005;42:540–546.
46. Parry DM, MacCollin MM, Kaiser-Kupfer MI, et al. Germ-line mutations in the neurofibromatosis 2 gene: correlations with disease severity and retinal abnormalities. *Am J Hum Genet.* 1996;59:529–539.
47. Evans DG, Trueman L, Wallace A, Collins S, Strachan T. Genotype/phenotype correlations in type 2 neurofibromatosis (NF2): evidence for more severe disease associated with truncating mutations. *J Med Genet.* 1998;35:450–455.
48. Kluwe L, MacCollin M, Tatagiba M, et al. Phenotypic variability associated with 14 splice-site mutations in the NF2 gene. *Am J Med Genet.* 1998;77:228–233.
49. Sestini R, Vivarelli R, Balestri P, Ammannati F, Montali E, Papi L. Neurofibromatosis type 2 attributable to gonosomal mosaicism in a clinically normal mother, and identification of seven novel mutations in the NF2 gene. *Hum Genet.* 2000;107:366–371.
50. Wallace AJ, Watson CJ, Oward E, Evans DG, Elles RG. Mutation scanning of the NF2 gene: an improved service based on meta-PCR/sequencing, dosage analysis, and loss of heterozygosity analysis. *Genet Test.* 2004;8:368–380.
51. Kluwe L, Mautner VF. Mosaicism in sporadic neurofibromatosis 2 patients. *Hum Mol Genet.* 1998;7:2051–2055.
52. Evans DG, Wallace AJ, Wu CL, Trueman L, Ramsden RT, Strachan T. Somatic mosaicism: a common cause of classic disease in tumor-prone syndromes? Lessons from type 2 neurofibromatosis. *Am J Hum Genet.* 1998;63:727–736.
53. Moyhuddin A, Baser ME, Watson C, et al. Somatic mosaicism in neurofibromatosis 2: prevalence and risk of disease transmission to offspring. *J Med Genet.* 2003;40:459–463.
54. Kluwe L, Friedrich RE, Tatagiba M, Mautner VF. Presymptomatic diagnosis for children of sporadic neurofibromatosis 2 patients: a method based on tumor analysis. *Genet Med.* 2002;4:27–30.
55. Kluwe L, Nygren AO, Errami A, et al. Screening for large mutations of the NF2 gene. *Genes Chromosomes Cancer.* 2005;42:384–391.
56. Diebold R, Bartelt-Kirbach B, Evans DG, Kaufmann D, Hanemann CO. Sensitive detection of deletions of one or more exons in the neurofibromatosis type 2 (NF2) gene by multiplexed gene dosage polymerase chain reaction. *J Mol Diagn.* 2005;7:97–104.
57. Buckley PG, Mantripragada KK, Benetkiewicz M, et al. A full-coverage, high-resolution human chromosome 22 genomic microarray for clinical and research applications. *Hum Mol Genet.* 2002;11:3221–3229.
58. Stokowski RP, Cox DR. Functional analysis of the neurofibromatosis type 2 protein by means of disease-causing point mutations. *Am J Hum Genet.* 2000;66:873–891.
59. Gutmann DH, Hirbe AC, Haipek CA. Functional analysis of neurofibromatosis 2 (NF2) missense mutations. *Hum Mol Genet.* 2001;10:1519–1529.
60. Ryu CH, Kim SW, Lee KH, et al. The merlin tumor suppressor interacts with Ral guanine nucleotide dissociation stimulator and inhibits its activity. *Oncogene.* 2005;24:5355–5364.
61. Bijlsma EK, Wallace AJ, Evans DG. Misleading linkage results in an NF2 presymptomatic test owing to mosaicism. *J Med Genet.* 1997;34:934–936.

QUERY FORM

During the preparation of your manuscript for publication, the questions listed below have arisen. Please attend to these matters and return this form with your proof.

Many thanks for your assistance.

Query References	Query	Remarks
1.	Au: I've spelled out CGH in the 3rd sentence, okay?	
2.	Au: In the penultimate sentence, can you reference a particular section rather than saying "below"?	
3.	Au: Can you point to a particular section rather than say "below" in the 2nd sentence?	
4.	Au: Please spell out EBV in the 2nd sentence.	
5.	Au: In the 4th sentence, refer to a section rather than "below"?	
6.	Au: In the last sentence, can you refer to a particular section instead of "below"?	
7.	Au: Can you confirm multiplex ligation-dependent probe amplification in the last sentence? In earlier chapters, MPLA is defined as multiplex ligation probe amplification.	
8.	Au: Can you update ref. 7?	
9.	Au: Please provide volume and page numbers for ref. 20.	
10.	Au: Please give full surname for 2nd author in ref. 36.	

nature genetics

Conservation of hotspots for recombination in low-copy repeats associated with the *NF1* microdeletion

Thomas De Raedt[1], Matthew Stephens[2], Ine Heyns[1], Hilde Brems[1], Daisy Thijs[1], Ludwine Messiaen[3], Karen Stephens[4], Conxi Lazaro[5], Katharina Wimmer[6], Hildegard Kehrer-Sawatzki[7], Dominique Vidaud[8], Lan Kluwe[9], Peter Marynen[1] & Eric Legius[1]

Several large-scale studies of human genetic variation have provided insights into processes such as recombination that have shaped human diversity. However, regions such as low-copy repeats (LCRs) have proven difficult to characterize, hindering efforts to understand the processes operating in these regions. We present a detailed study of genetic variation and underlying recombination processes in two copies of an LCR (NF1REPa and NF1REPc) on chromosome 17 involved in the generation of *NF1* microdeletions and in a third copy (REP19) on chromosome 19 from which the others originated over 6.7 million years ago. We find evidence for shared hotspots of recombination among the LCRs. REP19 seems to contain hotspots in the same place as the nonallelic recombination hotspots in NF1REPa and NF1REPc. This apparent conservation of patterns of recombination hotspots in moderately diverged paralogous regions contrasts with recent evidence that these patterns are not conserved in less-diverged orthologous regions of chimpanzees.

Recombination in LCRs is particularly interesting because crossovers that occur between two nearby copies of an LCR (generally referred to as nonallelic homologous recombination; NAHR) result in deletion or duplication of the region between the copies and are often associated with genomic disorders such as Charcot-Marie-Tooth type 1A, hereditary neuropathy with liability to pressure palsies, Williams-Beuren syndrome and neurofibromatosis type 1 (NF1). These NAHR events have sometimes been observed to cluster in relatively short hotspots[1–3], but otherwise, little is known about recombination in LCRs, including the extent to which patterns of recombination are shared across different copies of the same LCR and whether hotspots for NAHR also correspond to hotspots for nonallelic homologous gene conversion (NAHGC) and/or allelic homologous recombination (AHR). In principle, one can obtain considerable insight into these questions through studying patterns of genetic variation in LCRs. However, because of high sequence identity, accurate genotyping of SNPs in LCRs is not straightforward, and when such SNPs are typed in high-throughput genotyping projects, the obtained genotypes are often inaccurate and show nonmendelian inheritance or lack of Hardy-Weinberg equilibrium. As a result, virtually no reliable data are available on population genetic variation in LCRs.

We therefore undertook a detailed sequencing-based study of the patterns of genetic variation in three copies of an LCR, of which two are associated with the *NF1* microdeletion. **Supplementary Figure 1** online gives a schematic overview of the *NF1* microdeletion region and its LCRs, NF1REPa and NF1REPc (on chromosome 17) and REP19 (on chromosome 19). Two types of recurrent *NF1* microdeletions have been described. Type I *NF1* microdeletions are typically 1.4 Mb in length and of meiotic origin[4]. In individuals with type I *NF1* microdeletions, the deletion breakpoints tend to cluster in two regions called PRS1 (ref. 5) and PRS2 (ref. 1) (**Supplementary Fig. 1**). Regions paralogous to PRS1 and PRS2 are also present in REP19 (**Supplementary Fig. 1**) but with about 22 kb of extra sequence inserted between them compared with NF1REPa and NF1REPc. Type II *NF1* microdeletions are less frequent, have a length of 1.2 Mb and are mitotic in origin; their breakpoints tend to cluster in a different segment of the LCRs[6,7]. **Supplementary Figure 1** gives an overview of the repeat content of the different LCRs and the location of the typed SNPs.

To better characterize NAHR in NF1REPa and NF1REPc, we accurately mapped the location of the breakpoints in 60 individuals with type I *NF1* microdeletions ascertained in an unbiased manner. The results (**Fig. 1**) confirmed the presence of two clusters of breakpoints: a larger cluster in PRS2 (3.4 kb, containing 40/60 breakpoints) and a smaller cluster in PRS1 (1.8 kb, containing 13/60 breakpoints). This suggests the presence of hotspots for the initiation of NAHR in PRS1 and PRS2, in either one or both of NF1REPa and NF1REPc.

The effect of NAHGC will be to 'insert' a small segment of one LCR into another LCR. Thus, frequent NAHGC would tend to lead to

[1]Department of Human Genetics, Catholic University Leuven, Leuven, Belgium. [2]Department of Statistics, University of Washington, Seattle, Washington, USA. [3]Laboratory Medical Genetics, Department of Genetics, University of Alabama, Birmingham, Alabama, USA. [4]Department of Medicine, University of Washington, Seattle, Washington, USA. [5]Institut Catala d'Oncologia–Instituto de Investigación Biomédica de Bellvitge, L'Hospitalet de Llobregat, Barcelona, Spain. [6]Department of Human Genetics, Medical University of Vienna, Vienna, Austria. [7]Department of Human Genetics, University of Ulm, Ulm, Germany. [8]Laboratoire de Génétique Moléculaire, Institut National de la Santé et de la Recherche Médicale U745, Université Paris 5, Paris, France. [9]Laboratory for Tumor Biology and Development and Malformation, University Hospital Eppendorf, Hamburg, Germany. Correspondence should be addressed to E.L. (Eric.Legius@uz.kuleuven.ac.be).

Received 6 July; accepted 16 October; published online 19 November 2006; doi:10.1038/ng1920

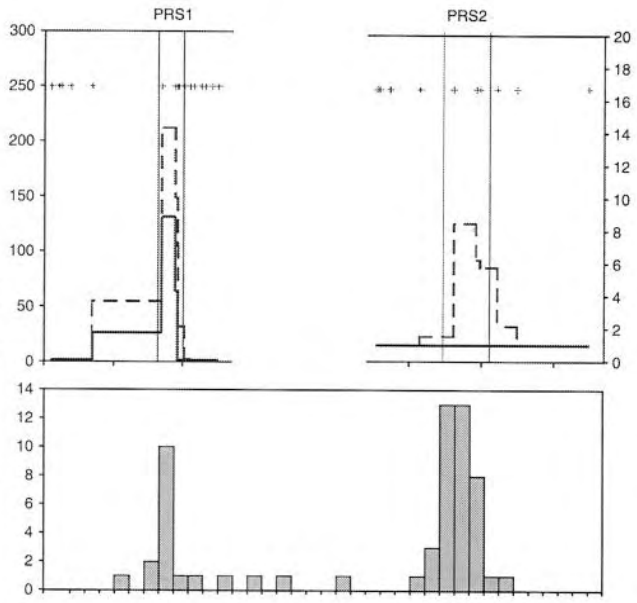

Figure 1 Comparison of hotspots of recombination inferred from haplotype and microdeletion data. Top: estimated rates of crossover across PRS1 and PRS2 in REP19 as calculated by PHASE. Lines show the posterior mean (dashed line) and median (full line) crossover rates from PHASE when both the location and intensity of any hotspot are estimated from the population haplotype data. The position of the SNPs (REP19) is represented by +. Vertical lines show locations of the NAHR breakpoint hotspots identified from the data in the bottom figure. Bottom: distribution of the NAHR breakpoints of 60 individuals with *NF1* microdeletions. The upper and lower panels are aligned: the estimated locations of AHR hotspots from the haplotype data on chromosome 19 agree closely with the locations of the NAHR breakpoint hotspots in the paralogous regions on chromosome 17. Note the very different scales of the *y* axes in the upper plot.

'shared' SNPs that are polymorphic in both LCRs. We therefore assessed relative rates of NAHGC in three regions (900 bp in PRS1, 1,500 bp in PRS2 and 800 bp in a region between PRS1 and PRS2) by sequencing these regions in both NF1REPa and NF1REPc (**Supplementary Table 1** online) and determining how many of the identified SNPs were 'shared' (that is, polymorphic in both NF1REPa and NF1REPc). In total, we identified 28 SNPs in NF1REPa and 26 in NF1REPc in the three specified regions. Of these, 12 were shared, providing strong evidence for NAHGC (the probability of 12 or more SNPs being shared if one draws 28 and 26 SNPs independently at random from 3,200 bp is $P = 2.2 \times 10^{-18}$). The region sequenced in PRS2 contained a higher proportion of shared SNPs (9/22) than the region sequenced in PRS1 (2/9), which contained a higher proportion than the intervening region (1/11; **Table 1**). Although only the difference between PRS2 and the intervening region approached statistical significance ($P = 0.066$), the results are consistent with the possibility that rates of NAHGC vary in a similar way to rates of NAHR; that is, the highest rate is found in PRS2, an intermediate rate in PRS1 and a lower rate in the intervening region, just as hotspots for allelic homologous gene conversion (AHGC) have been found to coincide with hotspots for AHR in the MHC and PAR1 regions[8]. This would be expected if NAHGC and NAHR were two alternative resolutions of a Holliday junction formed after a double-strand break, and if the hotspots for NAHR were due to an increased rate of double-strand break formation. Sequencing the same three regions in REP19, we did not find any SNPs shared with either NF1REPa or NF1REPc, and thus, as expected, there is no evidence for any ongoing genetic exchange between NF1REPa or NF1REPc and REP19.

In order to assess patterns of AHR, we first identified and typed SNPs in each of the three LCRs in 43 trios (parents plus child). We typed a total of 20 SNPs in the 33-kb region surrounding PRS1 and PRS2 in NF1REPa and NF1REPc. In REP19, where an additional 22 kb is found between PRS1 and PRS2, we typed 16 SNPs surrounding PRS1 and 12 SNPs surrounding PRS2 (**Supplementary Table 2** online; LD patterns are shown in **Supplementary Fig. 2** online). We then used a statistical approach[9–11] based on the observed haplotype data to assess the evidence for AHR hotspots at PRS1 and PRS2 in each of the LCRs. Specifically, as in ref. 11, we prespecified PRS1 and PRS2 as locations for potential hotspots and used the statistical method to estimate the background population-scaled recombination rate (ρ) and the relative intensity of recombination in the hotspot segments (λ). Thus, $\lambda = 1$ corresponds to no hotspot; we will refer to λ between 1 and 10 as a 'weak' hotspot and $\lambda > 10$ as a 'strong' hotspot. To summarize the strength of the evidence for either a strong or weak hotspot, we use the Bayes factor (BF), which is the probability of obtaining the data under the model that a weak or strong hotspot is present divided by the probability of obtaining the data under the model that no hotspot is present. Thus, a BF of >1 is evidence for a hotspot, and a BF of 10 means that the data are ten times more likely under a hotspot model than under a model without a hotspot, which might be considered strong evidence for a hotspot. The results are summarized in **Table 2**. One explanation for the different results for NF1REPa and NF1REPc (BFs ranging from 1.1–3.2) as compared with REP19 (BFs of 10.1 and 14,835) is that the polymorphism data for the former are comparatively uninformative about the presence or absence of a hotspot. This is suggested by results shown in **Supplementary Figure 3** online, which demonstrates little difference between the prior and posterior distribution of λ. In contrast, the polymorphism data in REP19 are substantially more informative and provide strong evidence for a hotspot of some kind in both PRS1 and PRS2 (BF $>$ 10,000 (strong hotspot) in PRS1, and BF = 10.1 (weak hotspot) in PRS2). Further, when we repeated these analyses for the REP19 data without prespecifying the location of the hotspot and allowing the statistical method to estimate the location, the estimated hotspot locations corresponded very closely to the regions paralogous to PRS1 and PRS2 (**Fig. 1**). (The estimated positions of the AHR and NAHR hotspots are, respectively, 6973–9059 and 7682–9525 for PRS1 and 5567–7316 and 4394–7564 for PRS2.)

Table 1 Number of SNPs across the different regions of the LCRs

	PRS1 (900 bp)	PRS2 (1,500 bp)	Region between hotspots (800 bp)	Total (3,200 bp)
NF1REPa only	4	5	7	16
NF1REPc only	3	8	3	14
Shared NF1REPa/c	2	9	1	12
REP19 only	6	11	2	19
Shared 17/19	0	0	0	0

'NF1REPa only': total number of nucleotide positions polymorphic only in NF1REPa and not at the paralogous position in NF1REPc. 'NF1REPc only': total number of nucleotide positions polymorphic only in NF1REPc and not at the paralogous position in NF1REPa. 'Shared NF1REPa/c': number of nucleotide positions polymorphic in NF1REPa and at the paralogous position in NF1REPc. 'REP19 only': total number of nucleotide positions polymorphic only in REP19 and not at the paralogous position in NF1REPa and/or NF1REPc. 'Shared 17/19': total number of nucleotide positions polymorphic in REP19 and at the paralogous position in NF1REPa or NF1REPc.

Table 2 Background recombination rates and λ values in the PRS1 and PRS2 regions of the LCRs

		NF1REPa	NF1REPc	REP19
PRS1	P(λ > 1)[a]	0.707	0.564	1.00
	P(λ > 10)[a]	0.393	0.296	0.989
	BF(weak)[b]	3.2	1.8	327[d]
	BF(strong)[c]	2.0	1.0	14,835[d]
	Median λ	5.47	1.78	152
PRS2	P(λ > 1)	0.719	0.532	0.865
	P(λ > 10)	0.429	0.327	0.412
	BF(weak)[b]	3.1	1.3	10.1[d]
	BF(strong)[c]	2.2	1.1	4.6
	Median λ	7.23	1.66	7.99
Background recombination rate (90% confidence interval)		1.31×10^{-4} (2.3×10^{-5} to 3.3×10^{-4})	6.41×10^{-5} (1.0×10^{-5} to 1.7×10^{-4})	PRS1: 1.48×10^{-4} (3.8×10^{-5} to 5.9×10^{-4}) PRS2: 5.09×10^{-4} (1.9×10^{-4} to 1.1×10^{-3})

[a]Proportion of the 50,000 iterations with λ > 1 or λ > 10. [b]BF comparing the model 'weak hotspot' versus the model 'no hotspot'. [c]BF comparing the model 'strong hotspot' versus the model 'no hotspot'. [d]BF values >10: strong indication in favor of a hotspot.

The high informativeness of the population data in REP19 compared with NF1REPa and NF1REPc could be due to several factors, including the greater number of SNPs available (28 in REP19 versus 20 in NF1REPa and NF1REPc) and the higher average minor allele frequency (average minor allele frequency of 29.8% in REP19 compared with 18.0% in NF1REPa and 14.7% in NF1REPc)[12,13]. It is also possible that differences in the background recombination rates[14] in the different regions could contribute to different power to detect hotspots, as the estimated background recombination rate (ρ) differs in the three LCRs. The estimate of ρ is about two times higher in NF1REPa (1.31×10^{-4}) compared with NF1REPc (6.41×10^{-5}). The background recombination rate for REP19 PRS1 is 1.48×10^{-4} (comparable to NF1REPa), whereas the background in REP19 PRS2 is higher (5.09×10^{-4}). It is possible that, due to the formation of deleterious microdeletions, a selective pressure against recombination exists in the LCRs of chromosome 17, reducing the historical recombination signature in the region.

Although it is notable that hotspots for AHR in REP19 identified from population data seem to occur in the same locations as the PRS1 and PRS2 hotspots for NAHR identified from individuals with *NF1* microdeletions, it is also worth noting that the estimated relative intensities of the hotspots identified from the two approaches differ appreciably. Intensities of the NAHR hotspots, computed by comparing the frequency of deletion breakpoints occurring inside each hotspot versus outside the hotspots, are 28.7 for PRS1 and 46.7 for PRS2. (Note that these estimates are likely biased slightly upward because the locations of the breakpoint hotspots were based on the observed NAHR events.) In contrast, estimated intensities of these hotspots from the REP19 population data are 152 and 8, respectively. In addition, in REP19, the population data suggest a lower average rate of AHR in the region surrounding PRS2 than in the region surrounding PRS1 (**Supplementary Fig. 3**), whereas the microdeletion data suggest the reverse for NAHR in chromosome 17. Although some of these discrepancies could be due to imprecision of the estimated intensities and deviations from modeling assumptions, other factors could also have a role. For example, the NAHR data measure the current recombination rate (microdeletions being formed), whereas population genetic data reflect the average historical recombination rate, and differences can exist between current and historical recombination rates[15]. Other factors that could influence the relative intensity of the recombination hotspots include the fact that REP19 contains 22 kb of additional sequence inserted between PRS1 and PRS2, or that differences in methylation pattern could result in a different DNA folding in each LCR (epigenetic effects).

In summary, the mapping of *NF1* microdeletion breakpoints (**Fig. 1**) and the presence of NAHGC give a clear view that sites of NAHR in (at least one of) NF1REPa and NF1REPc are not randomly distributed and are located in two distinct hotspots. Population genetic data in both NF1REPa and NF1REPc are not very informative for a hotspot of AHR but do not argue strongly against the presence of hotspots in either NF1REPa or NF1REPc. Population genetic data in the paralogous regions of REP19 provide strong evidence for hotspots of AHR. The initial duplication of the LCR from chromosome 19 to the *NF1* region took place before the human-gorilla split, about 6.7 million years ago[16]. Conservation of AHR hotspots in REP19 with NAHR hotspots in NF1REPa and NF1REPc in sequences that have been evolving separately for such a long time is notable, as hotspots for recombination in humans do not seem to be highly conserved in chimpanzee[11,17]. Others[18] have investigated the fine-scale recombination rate of three 500-kb regions both in humans and chimpanzees. Eighteen hotspots for recombination were found in humans, and of these, only one may correspond to a site of historical recombination in chimpanzees. Although it could be that we have simply found hotspots that happen to be conserved by chance, it is also possible that patterns of recombination in orthologous regions between humans and chimpanzees are less evolutionarily stable than patterns of recombination in paralogous regions. This could be due, for example, to differences in the recombination machinery or in epigenetic factors in the two species[17,18]. This potential role in hotspot evolution for distal regulators of recombination or epigenetic factors has been suggested before when looking at the presence or absence polymorphism of a human recombination hotspot[19]. Examining whether the AHR hotspots in PRS1 and PRS2 are present in the chimpanzee orthologs could help distinguish among these competing explanations.

METHODS

Samples. We collected DNA samples extracted from blood leukocytes from 43 nuclear families (trios). In addition, genomic DNA from 70 individuals was available for full sequencing of three regions in each LCR investigated. All individuals were of Flemish origin and gave their informed consent, and all experiments were approved by the ethical commission of the medical faculty of the Catholic University of Leuven.

Specific PCR amplification of sequences from the three different copies of the LCRs. Using the Expand Long Template PCR system (Roche), we amplified each copy of the LCR in fragments of a maximum of 5 kb. Primers were chosen to end on paralogous sequence variants (PSVs) in such a way that only one copy of the LCR would be amplified. Genotypes from some SNPs showed problems with mendelian inheritance and Hardy-Weinberg equilibrium. Primer positions of the relevant PCR fragments were sequenced in all individuals, and the PSV sites used for the LCR-specific amplification proved to be polymorphic and hence not LCR specific. In these cases, new primers were designed using other PSVs in the vicinity that were not polymorphic in

our set of 43 families. With the new primer sets, there were no longer problems with mendelian inheritance or Hardy-Weinberg Equilibrium. A complete list of primers is available in **Supplementary Table 3** online.

Detection of type I *NF1* microdeletion breakpoints. We amplified, nonspecifically, fragments from both NF1REPa and NF1REPc simultaneously during the same PCR reaction and sequenced PSVs at several sites throughout the LCR. In an individual with a microdeletion, one typically amplifies three different fragments, one derived from the normal NF1REPa, one derived from the normal NF1REPc and one derived from the hybrid NF1REPa/NF1REPc on the chromosome 17 with the microdeletion. By simply scoring the relative copy number of both nucleotides of the PSV, one can determine if the breakpoint is located centromeric of the PSV investigated (NF1REPc-specific nucleotide has a higher relative intensity on sequencing readout) or telomeric of the PSV (NF1REPa-specific nucleotide has a higher relative intensity) (**Supplementary Fig. 4** online). In this way, the interval where the breakpoint is located can be narrowed to an interval between two PSVs.

SNP discovery. In NF1REPa and NF1REPc, 31 kb of the 33 kb region investigated in the three LCRs were fully sequenced, and about 22 kb were sequenced in REP19 (BigDye Terminator Sequencing Kit v3.1, Applied Biosystems) in ten random individuals for SNP discovery. Regions left unsequenced in NF1REPa and NF1REPc had a high repetitive content. All SNPs typed in the 43 families were submitted to the dbSNP database. **Supplementary Table 2** gives an overview of all the SNPs typed in the different LCRs together with the minor allele frequency. In addition, three smaller regions in the different LCRs were fully sequenced in 70 unrelated individuals (900 bp in PRS1, 1,500 bp in PRS2 and 800 bp in a region between PRS1 and PRS2). The number of SNPs shared between the different copies of the LCRs was counted. **Supplementary Table 1** gives an overview of the total number of SNPs and the number of SNPs shared between LCRs.

SNP typing. A total of 68 SNPs (20 in NF1REPa and NF1REPc, 16 in the PRS1 region of REP19 and 12 in the PRS2 region of REP19) were typed in the 43 nuclear families and were submitted to the dbSNP database (**Supplementary Table 2**). The SNPs were typed by direct sequencing (BigDye Terminator Sequencing Kit v3.1, Applied Biosystems) or by SNaPshot analysis (Applied Biosystems) on the LCR-specific amplified PCR products. Because of the high sequence identity between the different copies of the LCR and the inherent problems of specific amplification of the LCRs, extensive precautions were taken to avoid mistyping. None of the SNPs in this report showed problems with mendelian inheritance, and all genotypes are in Hardy-Weinberg equilibrium. SNPs with a frequency lower than 4% were not included in the data analysis.

Haplotype analysis. For each copy of the LCR, the 172 parental haplotypes were estimated from the genotype data of the 43 trios using PHASE v2.1.1 (refs. 9,10,20–22). These estimated haplotypes were assumed to be known without error for subsequent analyses. We then used PHASE to assess the evidence for the presence of AHR hotspots in the three LCRs (NF1REPa, NF1REPc and REP19) at the location of the NAHR hotspots (PRS1 and PRS2) in NF1REPa and NF1REPc. The boundaries of PRS1 and PRS2 were chosen in such a way that they encompassed 90% of the breakpoints located in the PRS1 and PRS2 area, respectively. Based on the haplotype data, PHASE estimates the overall background recombination rate (ρ) and the relative intensity of any hotspots (λ). For example, $\lambda = 1$ corresponds to no hotspot, whereas $\lambda = 10$ corresponds to a hotspot where recombination occurs at a rate 10 times higher than in the surrounding sequence. The program makes a number of iterations (for example 10,000), and each iteration produces a sampled value of ρ and λ. We assumed the following prior distribution on λ: with probability 0.5, $\lambda = 1$ (that is, no hotspot); otherwise a hotspot is present ($\lambda > 1$) and $\log10(\lambda)$ is uniform in the range 0–3. The number of iterations that provide a sampled value of $\lambda > 1$ indicates the strength of the evidence for a hotspot. For our analysis, we used five different seeds, each time making 10,000 iterations, to provide a total of 50,000 samples. The numbers shown in **Table 2** reflect the proportion of iterations where $\lambda > 1$ or $\lambda > 10$, with $1 < \lambda < 10$ being considered a weak hotspot, and $\lambda > 10$ being considered a strong hotspot. For the prior on λ we assumed (see above) the prior probability of no hotspot is 0.5, the prior probability of a weak hotspot λ is 1/6 and the prior probability of a strong hotspot is 1/3. The evidence for a weak or strong hotspot is measured using the Bayes factor (BF). The BF is the probability of obtaining the data under the model that a weak or strong hotspot is present divided by the probability of obtaining the data under the model that no hotspot is present. A BF of 10 indicates that the data are ten times more likely to be obtained if there is a hotspot than if there is no hotspot. The BF is calculated as follows: $BF(\text{weak}) = (Pr(\text{weak hotspot}) \times 0.5)/(Pr(\lambda = 1) \times 1/6)$, and $BF(\text{strong}) = (Pr(\text{strong hotspot}) \times 0.5)/(Pr(\lambda = 1) \times 1/3)$, where $Pr(x)$ is the percentage of iterations observed under condition x, and 0.5, 1/6 and 1/3 are the prior probabilities of finding 'no hotspot', a 'weak hotspot' or a 'strong hotspot', respectively.

For the REP19PRS1 and REP19PRS2 regions, a second analysis with PHASE was performed, assuming that one AHR hotspot was present in each region without specifying the exact location of the AHR hotspot.

Statistical analysis. The number of observed shared SNPs between the different copies of the LCR was compared with the expected number by the binomial distribution. The *a priori* probability was calculated as the number of SNPs per bp present in the copy of the LCR to which the other LCR was compared. The α-level was Bonferroni corrected.

Statistical analysis software and URLs. PHASE can be found at http://www.stat.washington.edu/stephens/software.html. All input files for PHASE and all derived haplotypes are available in **Supplementary Table 4** online.

Note: Supplementary information is available on the Nature Genetics website.

ACKNOWLEDGMENTS

The authors thank T. de Ravel for critically reading the manuscript. T.D. is supported by the Emmanuel Vanderschueren Fonds. M.S. is supported by US National Institutes of Health grant 1RO1HG/LM02585-01. E.L. is a part-time clinical researcher of the Fonds voor Wetenschappelijk Onderzoek Vlaanderen (FWO). This work is also supported by research grants from the Fonds voor Wetenschappelijk Onderzoek Vlaanderen (G.0096.02, E.L.; G.0507.04, P.M.); the Interuniversity Attraction Poles (IAP) granted by the Federal Office for Scientific, Technical and Cultural Affairs, Belgium (2002-2006; P5/25) (P.M. and E.L.); by a Concerted Action Grant from the Catholic University of Leuven and by the Belgian Federation against Cancer (SCIE2003-33 to E.L.).

AUTHOR CONTRIBUTIONS

This study was coordinated by T.D., P.M. and E.L.; the manuscript was written by T.D., M.S. and E.L.; breakpoint detection was performed by T.D., I.H., H.B., L.M., K.S., C.L., K.W., H.K., D.V. and L.K.; SNP detection and typing was performed by T.D., I.H., H.B. and D.T. and computational analysis was performed by T.D. and M.S.

COMPETING INTERESTS STATEMENT

The authors declare that they have no competing financial interests.

Published online at http://www.nature.com/naturegenetics
Reprints and permissions information is available online at http://npg.nature.com/reprintsandpermissions/

1. Lopez-Correa, C. *et al.* Recombination hotspot in NF1 microdeletion patients. *Hum. Mol. Genet.* **10**, 1387–1392 (2001).
2. Repping, S. *et al.* Recombination between palindromes P5 and P1 on the human Y chromosome causes massive deletions and spermatogenic failure. *Am. J. Hum. Genet.* **71**, 906–922 (2002).
3. Reiter, L.T. *et al.* Human meiotic recombination products revealed by sequencing a hotspot for homologous strand exchange in multiple HNPP deletion patients. *Am. J. Hum. Genet.* **62**, 1023–1033 (1998).
4. Lopez Correa, C., Brems, H., Lazaro, C., Marynen, P. & Legius, E. Unequal meiotic crossover: a frequent cause of NF1 microdeletions. *Am. J. Hum. Genet.* **66**, 1969–1974 (2000).
5. Forbes, S.H., Dorschner, M.O., Le, R. & Stephens, K. Genomic context of paralogous recombination hotspots mediating recurrent NF1 region microdeletion. *Genes Chromosom. Cancer* **41**, 12–25 (2004).
6. Petek, E. *et al.* Mitotic recombination mediated by the JJAZF1 (KIAA0160) gene causing somatic mosaicism and a new type of constitutional NF1 microdeletion in two children of a mosaic female with only few manifestations. *J. Med. Genet.* **40**, 520–525 (2003).
7. Kehrer-Sawatzki, H. *et al.* High frequency of mosaicism among patients with neurofibromatosis type 1 (NF1) with microdeletions caused by somatic recombination of the JJAZ1 gene. *Am. J. Hum. Genet.* **75**, 410–423 (2004).

8. Jeffreys, A.J. & May, C.A. Intense and highly localized gene conversion activity in human meiotic crossover hot spots. *Nat. Genet.* **36**, 151–156 (2004).
9. Li, N. & Stephens, M. Modeling linkage disequilibrium and identifying recombination hotspots using single-nucleotide polymorphism data. *Genetics* **165**, 2213–2233 (2003).
10. Crawford, D.C. *et al.* Evidence for substantial fine-scale variation in recombination rates across the human genome. *Nat. Genet.* **36**, 700–706 (2004).
11. Ptak, S.E. *et al.* Absence of the TAP2 human recombination hotspot in chimpanzees. *PLoS Biol.* **2**, e155 (2004).
12. Fearnhead, P., Harding, R.M., Schneider, J.A., Myers, S. & Donnelly, P. Application of coalescent methods to reveal fine-scale rate variation and recombination hotspots. *Genetics* **167**, 2067–2081 (2004).
13. Fearnhead, P. & Smith, N.G. A novel method with improved power to detect recombination hotspots from polymorphism data reveals multiple hotspots in human genes. *Am. J. Hum. Genet.* **77**, 781–794 (2005).
14. Hudson, R.R. Two-locus sampling distributions and their application. *Genetics* **159**, 1805–1817 (2001).
15. Jeffreys, A.J., Neumann, R., Panayi, M., Myers, S. & Donnelly, P. Human recombination hot spots hidden in regions of strong marker association. *Nat. Genet.* **37**, 601–606 (2005).
16. De Raedt, T. *et al.* Genomic organization and evolution of the NF1 microdeletion region. *Genomics* **84**, 346–360 (2004).
17. Ptak, S.E. *et al.* Fine-scale recombination patterns differ between chimpanzees and humans. *Nat. Genet.* **37**, 429–434 (2005).
18. Winckler, W. *et al.* Comparison of fine-scale recombination rates in humans and chimpanzees. *Science* **308**, 107–111 (2005).
19. Neumann, R. & Jeffreys, A.J. Polymorphism in the activity of human crossover hotspots independent of local DNA sequence variation. *Hum. Mol. Genet.* **15**, 1401–1411 (2006).
20. Stephens, M., Smith, N.J. & Donnelly, P. A new statistical method for haplotype reconstruction from population data. *Am. J. Hum. Genet.* **68**, 978–989 (2001).
21. Stephens, M. & Donnelly, P. A comparison of bayesian methods for haplotype reconstruction from population genotype data. *Am. J. Hum. Genet.* **73**, 1162–1169 (2003).
22. Marchini, J. *et al.* A comparison of phasing algorithms for trios and unrelated individuals. *Am. J. Hum. Genet.* **78**, 437–450 (2006).

Journal of Neuroscience Research 85:1347–1357 (2007)

Plexiform-Like Neurofibromas Develop in the Mouse by Intraneural Xenograft of an NF1 Tumor-Derived Schwann Cell Line

George Q. Perrin,[1,2*] Lauren Fishbein,[3] Susanne A. Thomson,[3] Stacey L. Thomas,[7,8] Karen Stephens,[9] James Y. Garbern,[10] George H. DeVries,[8,11] Anthony T. Yachnis,[4] Margaret R. Wallace,[3,5] and David Muir[1,2,6]

[1]Department of Neuroscience, College of Medicine, University of Florida, Gainesville, Florida
[2]Shands Cancer Center, College of Medicine, University of Florida, Gainesville, Florida
[3]Department of Molecular Genetics and Microbiology, College of Medicine, University of Florida, Gainesville, Florida
[4]Department of Pathology and Laboratory Medicine, College of Medicine, University of Florida, Gainesville, Florida
[5]Department of Pediatrics, Genetics Division, College of Medicine, University of Florida, Gainesville, Florida
[6]Department of Pediatrics, Neurology Division, College of Medicine, University of Florida, Gainesville, Florida
[7]Neuroscience Program, Loyola University Medical Center, Maywood, Illinois
[8]Hines VA Hospital, Hines, Illinois
[9]Department of Medicine, University of Washington, Seattle, Washington
[10]Department of Neurology; Wayne State University, Detroit, Michigan
[11]Department of Anatomy and Cell Biology, University of Illinois, Chicago, Illinois

Plexiform neurofibromas are peripheral nerve sheath tumors that arise frequently in neurofibromatosis type 1 (NF1) and have a risk of malignant progression. Past efforts to establish xenograft models for neurofibroma involved the implantation of tumor fragments or heterogeneous primary cultures, which rarely achieved significant tumor growth. We report a practical and reproducible animal model of plexiform-like neurofibroma by xenograft of an immortal human NF1 tumor-derived Schwann cell line into the peripheral nerve of *scid* mice. The S100 and p75 positive sNF94.3 cell line was shown to possess a normal karyotype and have apparent full-length neurofibromin by Western blot. These cells were shown to have a constitutional *NF1* microdeletion and elevated Ras-GTP activity, however, suggesting loss of normal neurofibromin function. Localized intraneural injection of the cell line sNF94.3 produced consistent and slow growing tumors that infiltrated and disrupted the host nerve. The xenograft tumors resembled plexiform neurofibromas with a low rate of proliferation, abundant extracellular matrix (hypocellularity), basal laminae, high vascularity, and mast cell infiltration. The histologic features of the developed tumors were particularly consistent with those of human plexiform neurofibroma as well. Intraneural xenograft of sNF94.3 cells enables the precise initiation of intraneural, plexiform-like tumors and provides a highly reproducible model for the study of plexiform neurofibroma tumorigenesis. This model facilitates testing of potential therapeutic interventions, including angiogenesis inhibitors, in a relevant cellular environment.

Key words: neurofibromatosis; neurofibroma; angiogenesis; plexiform; xenograft

Neurofibromatosis type 1 (NF1) is a common autosomal dominant condition caused by disruptive mutations in the *NF1* gene, which encodes the GAP-related protein neurofibromin. These mutations result in absent or abnormal neurofibromin, which is associated with a high frequency of peripheral nerve sheath tumors called neurofibromas (Gutmann et al., 1991). Plexiform neurofibromas are often congenital, typically involve large nerves, can become very large, and when large, may cause serious functional impairment. Because they often occur on critical nerves and are not discrete masses, surgical removal is rarely complete. Recurrence is associated with increased morbidity and fatality, with progression to malignancy occurring in about 6% of NF1 patients. Although neurofibromas show marked cellular heterogeneity, Schwann cells (SCs) are the major

Contract grant sponsor: National Institutes of Health Training; Contract grant number: T32-CA09126-27; Contract grant sponsor: U.S. Department of Defense; Contract grant number: DAMD 17-01-10707, DAMD 17-03-1-0224.

*Correspondence to: George Q. Perrin, PhD, Dept. of Neuroscience, Box 100244, University of Florida College of Medicine, Gainesville, FL 32610-0244. E-mail: gperrin@ufl.edu

Received 13 July 2006; Revised 17 October 2006; Accepted 5 December 2006

Published online 4 March 2007 in Wiley InterScience (www.interscience.wiley.com). DOI: 10.1002/jnr.21226

cell type amplified and typically comprise 40–80% of the tumor cells (Hirose et al., 1986; Krone et al., 1986). Moreover, cumulative evidence indicates that neurofibromas contain a clonal population of Schwann cells that have disruptive mutations on the remaining *NF1* allele (Colman et al., 1995). Human plexiform neurofibromas have distinct characteristics (Scheithauer et al., 1997). They are hypocellular and composed of widely spaced, spindle-shaped cells with ovoid nuclei that variably stain positive for S-100. Most exhibit a low proliferative index (1–13% Ki67 positive cells), as compared to the high proliferative index (5–38% Ki67 positive cells) exhibited by malignant peripheral nerve sheath tumors (MPNST). They feature a prominent endoneurial mucopolysaccharide deposition, a variously collagenous matrix and basal laminae. Plexiform neurofibromas diffusely infiltrate the affected nerve and spread longitudinally as a fusiform enlargement rather than a globular mass. As with many other types of tumors, they can promote angiogenesis, are highly vascular and are infiltrated by numerous mast cells.

Several mouse models of NF1 engineered genetically have been developed to study tumorigenesis by neurofibromin-deficient mouse Schwann cells (Stemmer-Rachamimov et al., 2004). Past efforts to establish xenograft models of neurofibroma, however, have achieved limited success. Despite tumorigenic properties shown in vitro, neurofibroma cultures fail to form subcutaneous tumors in immunodeficient mice (Sheela et al., 1990; Muir et al., 2001). Inceptive studies showed limited growth by implanted human neurofibroma tissue or mixed cell preparations into the sciatic nerves of immunodeficient mice and advanced the potential of xenograft models for studying the tumorigenesis in NF1 (Appenzeller et al., 1986; Lee et al., 1992). Early xenografts of human neurofibromas relied on tissue explants and primary cultures of limited cell number with marked cellular heterogeneity and never were established as effective working models of NF1 tumors. Previously, we established highly enriched SC cultures from numerous benign and malignant NF1 peripheral nerve sheath tumors (Muir et al., 2001; Li et al., 2004). These cell lines were enriched for the somatically mutated SCs and most show no full-length neurofibromin. Schwann cell lines derived from benign NF1 tumors had low tumorigenic potential in classical in vitro assays yet several unique preneoplastic properties were observed frequently. In addition, several neurofibroma SC cultures when engrafted into the peripheral nerves of *scid* mice produced infiltrative and very slow-growing neurofibroma-like tumors. Although these xenografts provide an informative and useful model of neurofibroma, considerable time is required to achieve tumor growth representative of that seen in a clinical setting. Therefore, we developed more practical xenograft models of NF1 tumorigenesis by implantation of rapidly growing NF1 MPNST cell lines into the mouse nerve.

MATERIALS AND METHODS

Originative Tumor and NF1 Cell Line

The NF1 tumor cell line, sNF94.3, was derived from tumor tissue resected from a 43-year-old, female patient who met NF1 diagnostic criteria (Gutmann et al., 1997). Although there was no positive family history, the patient had definite features of NF1 including a mild learning disability, scoliosis, café-au-lait spots, Lisch nodules, hundreds of dermal neurofibromas, a congenital plexiform in the ankle and foot, and a MPNST in the thigh. The originative tumor tissue for the sNF94.3 cell line was obtained from a lung metastasis diagnosed by histopathology as an MPNST. The portion of the tumor specimen used for tissue culture was characterized independently by immuno histopathology as an MPNST. The tissue was acquired with patient consent and used according to IRB approved protocols.

DNA was extracted from blood leukocytes and tumor specimens as described previously by Colman et al. (1995). The sNF94.3 tumor cell line was established by methods described previously (Wallace et al., 2000; Muir et al., 2001). Briefly, tumor pieces were minced and dissociated for 3–5 hr with dispase (1.25 U/ml; Collaborative Research, Bedford, MA) and collagenase (300 U/ml; Type XI; Sigma, St. Louis, MO) in L15 medium containing 10% calf serum and antibiotics. The digested tissue was dispersed by trituration and strained through a 30-mesh nylon screen. Collected cells were seeded on laminin-coated dishes and grown in DMEM containing 10% fetal bovine serum, 5% calf serum, glial growth factor-2 (25 ng/ml), and antibiotics. Cultures were subsequently grown and expanded rapidly without laminin and glial growth factor-2. The sNF94.3 cell line showed a homogenous Schwann cell-like population and a clonal morphology, which was retained through protracted passages (19 thus far). The apparently immortal cell line has spindle-shape morphology and is immunopositive for S-100 and faintly for p75 (low-affinity neurotrophin receptor), indicating Schwann cell lineage. Nuclear S100 staining might indicate a dedifferentiated tumor cell line (Mirsky and Jessen, 1999). The sNF94.3 cell line was deposited in the American Type Culture Collection.

Clonality Analysis

Tumor clonality was analyzed by an X-chromosome inactivation assay. This PCR polymorphism-based assay allows for differential detection of the maternal and paternal chromosomes by methylation-sensitive enzymes (Singer-Sam et al., 1990). Both the androgen receptor gene locus (Allen et al., 1992) and the phosphoglycerate kinase gene (*PGK*) (Lee et al., 1994) were analyzed. On digestion of genomic DNA with HpaII followed by PCR amplification using primers flanking the HpaII sites, a clonal sample only shows amplification of one allele whereas a polyclonal sample shows amplification of both alleles (that can be distinguished in heterozygotes). For this study, 10 ng of genomic DNA was digested with 20 U of HpaII and 10 U of RsaI (New England Biolabs, Ipswich, MA) in a 20-μL reaction. Two microliters of the digest was used for PCR amplification. The following primers were used for the androgen receptor repeat polymorphism; A-Receptor 5′: 5′-GCT GTG AAG GTT GCT GTT CCT

CAT-3′, A-Receptor 3′: 5′-TCC AGA ATC TGT TCC AGA GCG TGC-3′ under the following standard PCR conditions: 94°C for 1 min, 65°C for 1 min, 72°C for 1 min for 35 cycles with a 30-min 72°C final extension step. The samples were electrophoretically separated on a 10% native polyacrylamide gel and stained with ethidium bromide for visualization. The *PGK* gene single nucleotide polymorphism was amplified under similar conditions, except with an annealing temperature of 58°C, with the following primers; PGK-5′: 5′-CTG TTC CTG CCC GCG CGG TGT TCC GCA TTC-3′, PGK-3′: 5′-ACG CCT GTT ACG TAA GCT CTG CAG GCC TCC-3′. In addition, 8 μL of amplified product was digested with 20 U of BstXI to detect the RFLP before separating fragments on a 10% PAGE. Densitometric analysis was carried out on all samples using NIH Image (freeware; National Institute of Health) and values were statistically analyzed by a *t*-test using Microsoft Excel.

NF1 Mutation Analysis

NF1 exons from tumor DNAs were analyzed by heteroduplex and SSCP analysis, as well as by direct sequencing (Abernathy et al., 1997). Samples were analyzed for loss of heterozygosity (LOH) using standard methods for genotyping *NF1* polymorphisms as described previously by Colman et al. (1995) and Rasmussen et al. (1998). Blood and tumor DNA results were compared when constitutional heterozygosity was seen at a given marker. In addition, standard cytogenetic analysis was carried out on the tumor derived Schwann cell cultures. Analysis for *NF1* region microdeletion used specific PCR assays.

Western Blot Analysis

Cell cultures were scraped from dishes and cell pellets were homogenized in ice-cold extraction buffer consisting of 50 mM Tris-HCl (pH 7.4), 250 mM NaCl, 1% Nonidet P-40, 0.25% sodium deoxycholate, and Complete protease inhibitor cocktail (Boehringer-Mannheim, Indianapolis, IN). The soluble fraction was collected by centrifugation (10,000 × *g*, 20 min) and reconstituted to be 2 M in urea. The extract was concentrated and fractionated by ultrafiltration using a 100-kDa cut-off membrane. Total protein content of the high molecular mass retentate was determined using Bradford Reagent (Bio-Rad, Hercules, CA). Samples were mixed with sodium dodecyl sulfate electrophoresis sample buffer containing 2 M urea and 5% 2-mercaptoethanol, normalized for total protein content and then heated at 80°C for 2 hr. Samples (50 μg of total protein) were electrophoresed into 4–15% polyacrylamide gradient gels and electroblotted to nitrocellulose sheets in transfer buffer containing 0.1% sodium dodecyl sulfate. Blots were rinsed in water and fixed in 25% isopropanol/10% acetic acid. Nitrocellulose sheets were washed with 50 mM Tris-HCl (pH 7.4) containing 1.5% NaCl and 0.1% Triton X-100 and then blocked in the same buffer with the addition of 5% dry milk (blocking buffer). The blots were incubated for 2 hr with anti-NF1GRP(N) antibody (1 μg/ml) (Santa Cruz Biotechnology, Inc., Santa Cruz, CA) in blocking buffer. Bound antibody was detected by peroxidase-conjugated swine anti-rabbit IgG (affinity purified; DAKO, Carpinteria, CA) diluted 1/2,000 in blocking buffer. Immunoreactive bands were developed by chemiluminescent methods (Pierce Chemical, Rockford, IL) according to the manufacturer's instructions. Relative molecular mass was determined using prestained markers including myosin (233 kDa) (Bio-Rad). Control samples were similarly processed from cell pellets obtained from normal human nerve Schwann cell cultures and Schwann cell cultures derived from embryonic homozygous *Nf1* knockout mice. In these studies, neurofibromin was detected using a number of antibodies. We used the antibody available from Santa Cruz Biotechnology raised against a peptide corresponding to residues 509–528 of the predicted *NF1* gene product. To further investigate the possible effects of truncated *NF1* gene products, we have developed monoclonal antibodies (McNFn27a, McNFn27b) raised against a peptide corresponding to the N-terminal residues 27–41 of the predicted *NF1* gene product. Similar results were obtained with all antibodies. Next, the blot was stripped with Restore Western Blot Stripping Buffer (Pierce Chemical), per manufacturers instructions, and blocked as described above. The blot was then re-immunoblotted with polyclonal anti-huGST (DAKO) (1/200) (that binds only human glutathione s-transferase) to check sample loading. This immunoblot was developed as described above.

Ras Activation Assay

Ras activation assay kit (Upstate Biotech, Lake Placid, NY) was used according to the manufacturer's protocol. The assay uses affinity precipitation to isolate Ras-GTP from cell lysate. Cells were lysed using RIPA buffer (1% Igepal, 0.5% NaDOC, 0.1% SDS in PBS) and the DC protein assay (Bio-Rad) was used to determine the protein concentration of the cell lysates. Cell lysate (500 μg) was incubated with an agarose-bound Raf-1 RBD fusion protein. Agarose beads were collected by pulsing with a microcentrifuge (5 sec at 14,000 × *g*), washed with lysis buffer, and resuspended in Laemmli sample buffer. The samples were then boiled for 5 min after which the supernatants were loaded onto a 4–20% gradient Novex Tris-Glycine gel (Invitrogen, Carlsbad, CA) along with SeeBlue Plus2 molecular weight standards (5 ul) (Invitrogen). The samples were electrophoresed (20 mA/gel) and then transferred (100 V) to a PVDF membrane (NEN, Boston, MA). The membrane was blocked with 5% nonfat dry milk and then incubated with primary antibody overnight at 4°C as follows: 1 μg/ml Anti-Ras clone RAS10 (Upstate Biotechnology, Lake Placid, NY); 1/250 Anti-N-Ras (F155), and Anti-K-Ras (F234) (Santa Cruz Biotechnology). This was followed by incubation with HRP-conjugated secondary antibody at room temperature for 1 hr. The blot was developed using Western Lightning Chemiluminescence Reagent (NEN).

Mouse Strains

Immunodeficient B6 *scid* mice were used as hosts to minimize immunologic rejection of the xenografted human cell line. The *scid* nonsense mutation in the DNA-PKCS gene, was described by Blunt et al. (1996). Based on genomic DNA sequence (GenBank AB005213) PCR primers were

designed flanking the mutation site in exon 85: scid 5 (GAGTTTTGAGCAGACAATGCTGA), and scid 3 (CTTTTGAACACACACTGATTCTGC). The resulting 180 bp PCR product was digested with Alu I to distinguish wild-type allele from mutant allele extra cut site via agarose gel electrophoresis, to genotype animals at the *scid* locus.

Intraneural Tumor Xenografting

Intraneural xenografts were initiated by injecting human NF1 tumor-derived, sNF94.3 cells (passage 5–8) into the sciatic nerves of adult *scid* mice. sNF94.3 cultures from cryopreserved stocks were grown in DMEM containing 10% FBS and antibiotics. Dissociated cells were collected, rinsed thoroughly, and resuspended at 1×10^8 cells/ml in calcium- and magnesium-free Hank's Balanced Salt Solution (HBSS). Young adult mouse hosts were anesthetized with isoflurane and the sciatic nerves exposed bilaterally at mid-thigh. A cell suspension (5×10^5 cells in 5 μl) was injected gradually into the sciatic nerve through a FlexiFil (0.2-mm OD) titanium needle syringe (World Precision Instruments, Sarasota, FL) driven by a UMII microinjector mounted on a motorized micromanipulator (World Precision Instruments). These techniques are for optimized tumor cell injection but successful xenografts can be accomplished by hand and with simple equipment, as they were in our initial studies. The surgical site was closed in layers. Muscles were sutured with 4-0 nylon monofilament. The skin opening was stapled with 9-mm stainless steel wound clips that were removed 7–10 days after surgery. The revived mouse was returned to specific pathogen-free housing. At 2–8 weeks after implantation, the animals were sacrificed under anesthesia and the nerves were removed and fixed by immersion in 4% paraformaldehyde. Xenograft success rate, based on the appearance of human glutathione s-transferase (huGST) immunopositive tumors, was approximately 95% (including initial studies). Nerve segments were embedded in paraffin and sectioned for staining. All animal use was carried out in accordance to the guidelines of the University of Florida Animal Care and Use Committee.

Immunohistochemistry

Cell Cultures. sNF94.3 monolayer cultures were examined for immunoreactivity with antibodies to the SC antigens S-100 (DAKO) (1/300) and the low-affinity neurotrophin receptor (p75) (4 μg/ml, hybridoma 200-3-G6-4; American Type Culture Collection, Rockville, MD). Cultures grown on laminin-coated chamber slides were fixed with 2% paraformaldehyde in 0.1 mM phosphate buffer (pH 7.2) for 20 min, then washed with PBS containing 0.5% Triton X-100. Nonspecific antibody binding was blocked with PBS containing 0.1% Triton X-100 and 10% normal swine serum (blocking buffer) for 1 hr. Primary antibodies were diluted in blocking buffer and applied to wells and allowed to incubate overnight at 4°C. Bound primary antibodies were labeled with swine anti-rabbit Igs (DAKO) (1/200) conjugated with fluorescein for 1 hr at 37°C diluted in blocking buffer in darkness and post-fixed with 2% paraformaldehyde in PBS for 10 min. After washing with PBS, slides were cover slipped and kept in the dark at 4°C until imaging. Imaging was carried out using an excitation wavelength of 450–490 nm and an emission wavelength of 515–565 nm.

Tissue Specimens. Portions of the primary human tumor specimen used for cell culture and xenografted mouse nerves were fixed by immersion in 4% paraformaldehyde in 0.1 mM phosphate buffer (pH 7.2) overnight at 4°C, embedded in paraffin, sectioned on the longitudinal nerve axis, and stained with hematoxylin and eosin (H&E) for routine light microscopic examination. Deparaffinized sections were pretreated with methanol containing 1% hydrogen peroxide for 30 min to quench endogenous peroxidase activity. Nonspecific antibody binding was blocked with 10% normal serum in PBS for 60 min at 37°C. Primary antibodies were diluted in blocking buffer and applied to sections overnight at 4°C. Bound antibody was labeled with a biotinylated secondary antibody for 4 hr at 37°C followed by the avidin-biotin-peroxidase reagent (DAKO) for 2 hr. Chromogenic development was accomplished with diaminobenzidine-$(HC1)_4$ (0.05%) and hydrogen peroxide (0.03%) in PBS. Immunostained sections were lightly counter-stained with hematoxylin. Primary tumor tissue sections were immunolabeled for neurofibromin using polyclonal NF1GRP(N) antibody (1 μg/ml) (Santa Cruz Biotechnology) and monoclonal NFn27b (5 μg/ml) (Novus Biologicals, Littleton, CO). Human sNF94.3 tumor cells were identified in mouse nerve xenografts by immunostaining with polyclonal anti-huGST (DAKO) (1/100). sNF94.3 xenografts were examined for immunoreactivity with antibodies to the SC antigens S100 (DAKO) (1/300) and the low-affinity neurotrophin receptor (p75) (5 μg/ml, Promega, Madison, WI). Cellular proliferation in vivo was assessed by immunostaining with a monoclonal antibody to Ki67 (DAKO) (1/100) (a nuclear antigen present in proliferating human cells). Blood vessels were immunolabeled with polyclonal anti-von Willebrand Factor (DAKO) (1/500) (that binds endothelial cells). Basal laminae produced by the xenografted sNF94.3 cells was immunolabeled with monoclonal anti-laminin (3 μg/ml) (2E8) with pepsin antigen retrieval (Engvall et al., 1986; Graham et al., 2007). This antibody recognizes only human laminin and not laminin of mouse origin. Negative controls used no primary antibody. Mast cells were visualized using acidic toluidine blue as described by Enerback et al. (1986) on sections immunostained for huGST previously. Mucopolysaccharide was stained with 1% Alcian blue (Scott and Mowry, 1970) in combination with H&E staining.

RESULTS

Phenotypic and Genetic Characterization of the sNF94.3 Cell Line

Samples of the sNF94.3 tumor showed ultrastructural features and focal S100 immunopositivity indicative of a neurofibrosarcoma (data not shown). The Schwann cell cultures derived from the originative sNF94.3 sample immunostained for the Schwann cell marker S-100 (Fig. 1A) and the low-affinity nerve growth factor receptor p75 (Fig. 1B), indicating a Schwann cell-like phenotype.

The spindle-shaped monolayer cultures of sNF94.3 cells showed apparent full-length neurofibromin (*Mr*

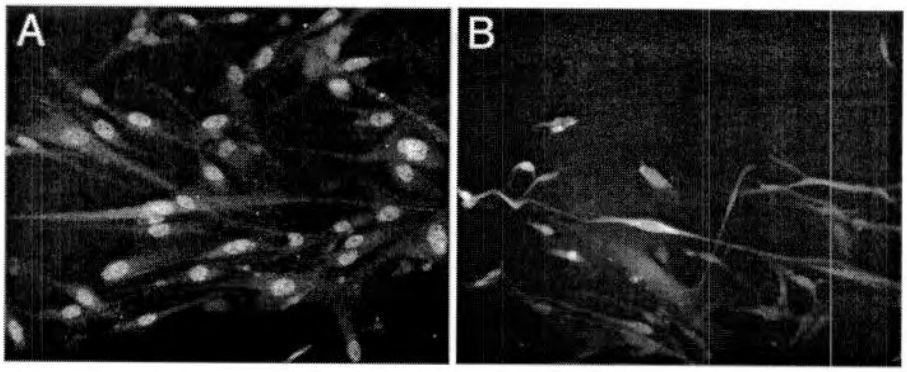

Fig. 1. sNF94.3 cells have a Schwann-like phenotype. sNF94.3 cultures were examined for the immuno expression of two Schwann cell markers, S-100 (**A**) and p75 (**B**) by fluorescent immunocytochemistry. p75 was easily detected on the surface of sNF94.3 cells and cytoplasmic labeling for S-100 was observed. Original magnifications: 400×.

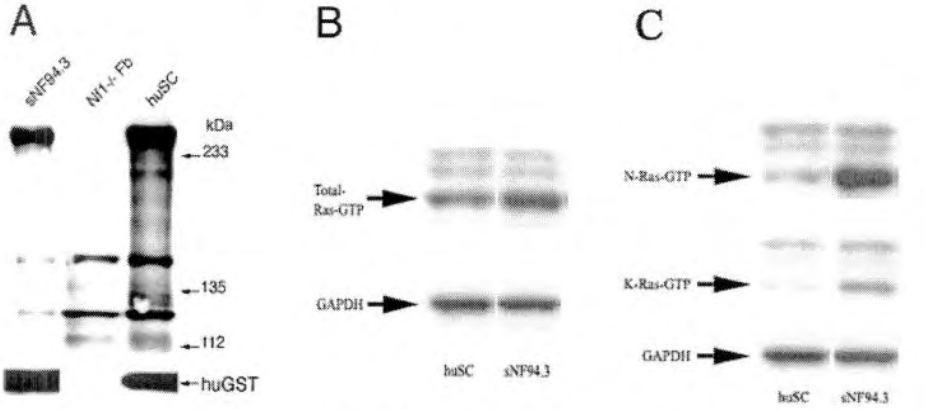

Fig. 2. sNF94.3 cells express apparently full-length but non-functional neurofibromin. **A:** Extracts from sNF94.3 cultures, fibroblast cultures derived from embryonic *Nf1−/−* knockout mice, and normal human Schwann cell cultures were analyzed for neurofibromin expression by Western immunoblotting. Full-length neurofibromin appeared as a ≈250 kDa band in the normal human Schwann cell sample. An equal amount of total protein was loaded for each sample. **B:** Increased activated Ras is seen in serum-starved sNF94.3 cells, as are increased levels of activated N-Ras and K-Ras isoforms (**C**).

≈250 kDa) by Western immunoblotting using several anti-neurofibromin antibodies (Fig. 2A). Full-length neurofibromin was not detected in extracts of fibroblast cultures derived from embryonic *Nf1−/−* knockout mice. As a positive control, normal human Schwann cell cultures showed a substantial band-pair corresponding to full-length neurofibromin. A secondary immunolabeling of the blot for huGST showed consistent loading for all of the human samples. Next, sNF94.3 cells and normal human Schwann cells were serum-starved and Ras activation was determined by Western immunoblotting. Total activated Ras-GTP was elevated in sNF94.3 cells when compared to normal human Schwann cell cultures (Fig. 2B). In addition, both of the specific N-Ras and K-Ras isoforms were activated in sNF94.3 cells (Fig. 2C). Similar results have been reported for other NF1-derived Schwann cells (Thomas, et al., 2006). Consistent with Ras activation, sNF94.3 cells proliferate rapidly and display vigorous growth in culture, on par with other human NF1 MPNST cell lines established in our lab.

sNF94.3 leukocyte DNA (from a polyclonal population of cells) was analyzed first for heterozygosity at the androgen receptor and *PGK* gene polymorphisms. This sample was heterozygous at the androgen receptor gene, warranting additional DNA analysis. The X-chromosome inactivation pattern for sNF94.3 at the androgen receptor locus was consistent with that of a clonally derived tumor sample ($P = 0.008$, data not shown).

The cytogenetic analysis showed a normal 46, xx karyotype, which is unusual for MPNSTs (Mertens et al., 2000). Sample sNF94.3 cells do not have p53 loss of heterozygosity but showed a constitutional *NF1* mutation, which is a microdeletion of the common 1.4 Mb type with breakpoints in the NFREPs and was detected using PCR (Dorschner et al., 2000; Lopez-

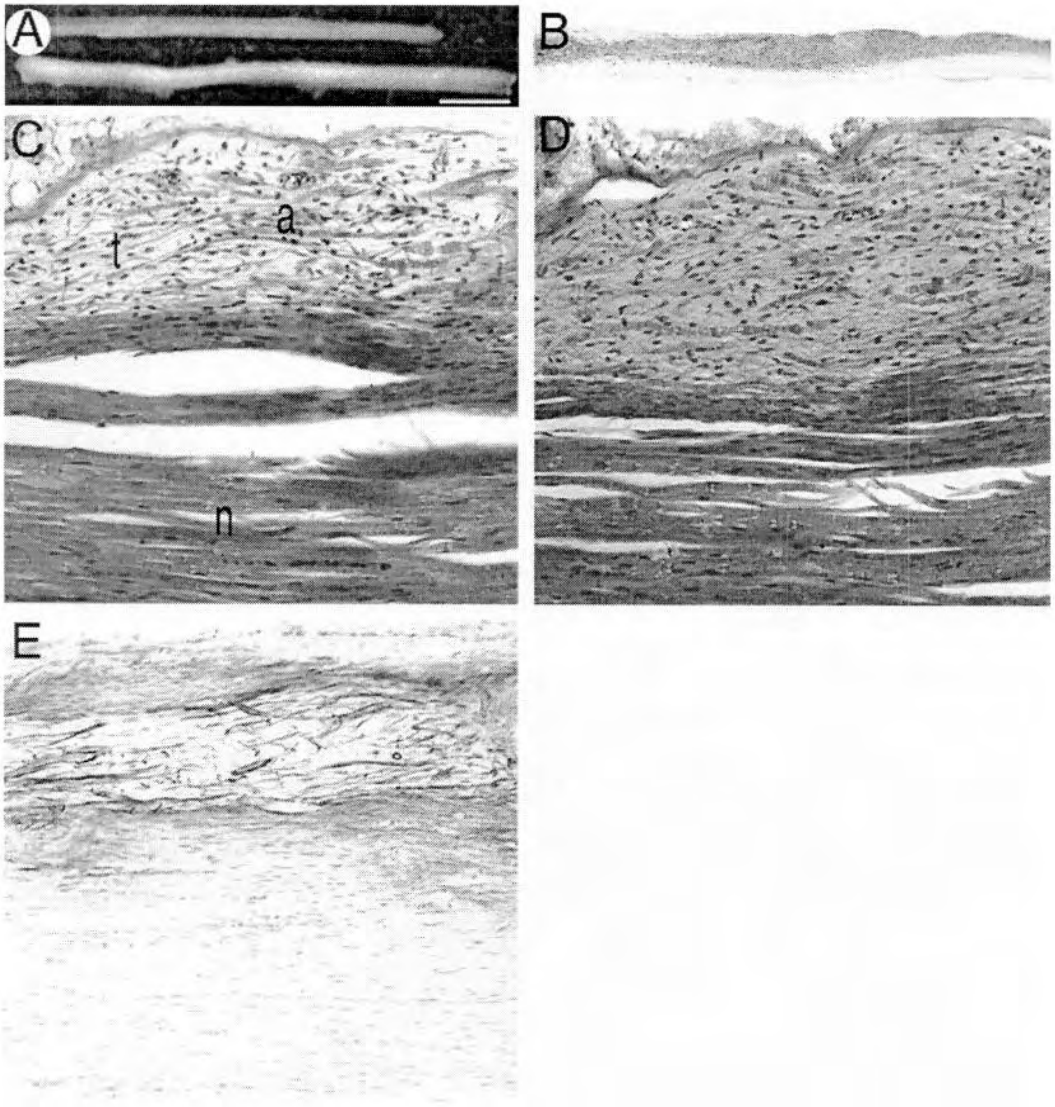

Fig. 3. sNF94.3 xenografts form hypocellular plexiform-like tumors. **A:** The normal mouse sciatic nerve (**upper**) is slender and symmetric whereas 8 weeks after implantation with sNF94.3 the nerve appears swollen and mildly deformed (**lower**) (scale bar = 2 mm). **B:** HuGST immunostaining readily identifies and traces the infiltration of human sNF94.3 cells throughout the xenografted host sciatic nerve. C: H&E stain shows tumor hypocellularity and nerve remodeling. Developing tumor (t), axons (a) displaced by infiltrating tumor and a small region with relatively normal nerve structure (n) are visible. **D:** A serial section stained with Alcian blue highlights the abundant deposition of extracellular mucopolysaccharide matrix associated with the hypocellular tumor. Immunostaining for human laminin (**E**) showed the presence of basal laminae. Original magnification: 100× (B); 200× (C–F).

Correa et al., 2001). The somatic mutation is not a large deletion and remains unknown despite analysis of numerous exons. This is consistent with the patient's heavy dermal tumor burden and occurrence of the MPNST (De Raedt et al., 2003). The NF1 mRNA is of the Type II isoform, which is due to inclusion of exon 23a (encoding 21 amino acids). This isoform is known to have reduced GAP activity, and is the predominant type expressed in normal peripheral nerve, brain tumors, and neurofibromas (Suzuki et al., 1991; Teinturier et al., 1992; Andersen et al., 1993). All exon and immediate flanking intron bases have been sequenced and are normal. There is no evidence for aberrant splicing at the RNA level, via reverse transcriptase (RT)-PCR polyacrylamide gel analysis, and sequencing. It is possible, however, that a mutation lies in an untranslated region or promoter region, affecting RNA transcription level or stability, or hemizygosity for the Type II isoform results in Ras-GAP activity reduced sufficiently to allow tumor progression.

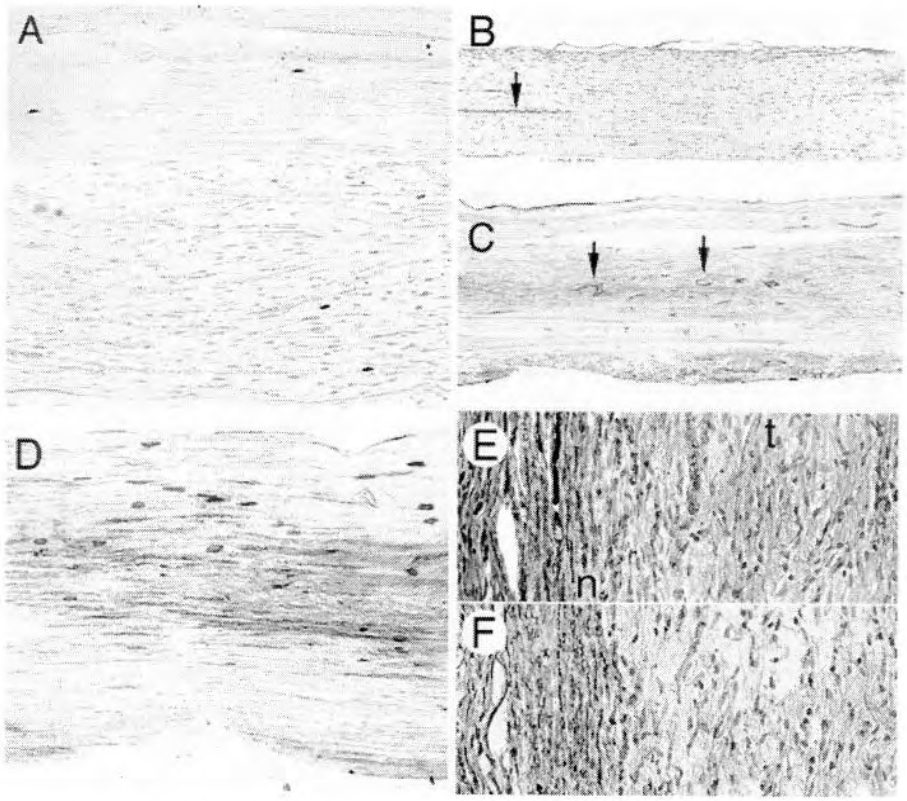

Fig. 4. sNF94.3 tumors proliferate slowly, are highly vascular, are infiltrated by mast cells and display Schwann cell markers. **A:** Eight weeks after xenograft, Ki67 immunostaining of an sNF94.3 tumor indicates a low rate of proliferation. **B:** Immunostaining for von Willebrand's Factor shows normal mouse nerve has scant and slender vasculature (arrow) aligned with the longitudinal axis. **C:** Increased vascularity (arrows) was associated with sNF94.3 xenograft tumors as early as two weeks. The blood vessels splay into the developing tumor indicative of angiogenic activity. **D:** Xenografted nerves were immunostained for huGST (brown) and counterstained for mast cells using acidic toluidine blue. Compared to normal nerve, there was an apparent increase in mast cell infiltration in the xenografted nerves closely associated with the expanding tumor. Nerves were also immunostained for two Schwann cell markers, S-100 (**E**) and p75 (**F**). Faint and variable immuno expression of these Schwann cell markers by sNF94.3 xenograft tumors was observed by immunoperoxidase methods (n, normal nerve; t, xenograft tumor). Original magnification: 200× (A,D–F); 100× (B,C).

Intraneural sNF94.3 Xenograft Tumors Resemble Plexiform Neurofibroma

Like cultures from neurofibromas, sNF94.3 failed to form subcutaneous tumors in *scid* mice. Nevertheless, sNF94.3 xenografts consistently formed slow growing, infiltrative tumors in the mouse nerve. Figure 3A shows the gross morphology of a normal mouse sciatic nerve and a representative sNF94.3 nerve xenograft 8 weeks after intraneural implantation. Thirty-nine sNF94.3 engraftments were carried out and examined at time points from 8 days to 1 year after initiation. Overall, 94.9% of the sNF94.3 xenografts were successful and resulted in established foci of huGST-immunopositive cells. Most sNF94.3 tumors caused a moderate enlargement of the host nerve. Eight weeks after implantation with sNF94.3, nerve diameters were on average 55% larger (0.472 mm ± 0.1469, n = 6) than normal, age-matched mouse sciatic nerves (0.304 mm ± 0.0392, n = 4). Vehicle injected mouse sciatic nerves were not increased in size compared to normal nerves (0.293 mm ± 0.0645, n = 2 vs. 0.304 mm ± 0.0392, n = 4, respectively), indicating the increase in nerve diameter did not result from surgically induced inflammation. In addition, xenograft of normal human Schwann cells resulted in only a slight, 9.7% increase in nerve diameter (0.334 mm ± 0.0643, n = 6 vs. 0.304 mm ± 0.0392, n = 4) after 8 weeks. This occurred despite only transient occupancy and limited survival as the normal Schwann cells were most often undetectable after 8 weeks in vivo. Xenografts of sNF94.3 grew slowly and were histopathologically similar to human NF1 plexiform neurofibromas. Immunostaining for the marker protein huGST identified the xenografted human tumor cells and their propensity to diffusely involve the nerve, mimicking the hypocellular growth pattern often found in plexiform neurofibromas (Fig. 3B). The engrafted tumor cells increased in number over time and eventually infiltrated the nerve far from the site of initial implantation.

Regardless of the extent of tumor growth, no overt signs indicating loss of nerve function were observed in any of the xenografted mice, also commonly the case with human NF1 plexiform neurofibromas. Growth of the sNF94.3 cell line in sciatic nerves of adult *scid* mice caused intraneural disruption and nerve remodeling (Fig. 3C). The hypocellular tumors were composed of diffusely distributed, spindle-shaped cells and were associated with deposition of a mucopolysaccharide-rich, collagenous extracellular matrix (Fig. 3D) and basal laminae (Fig. 3E), hallmarks of NF1 plexiform neurofibroma (Scheithauer et al., 1997). The basal laminae found in sNF94.3 xenografts was produced by the sNF94.3 cells themselves, not the host mouse cells, because the monoclonal antibody used for laminin immunolabeling is specific for human laminin only and does not immunostain mouse laminin (Engvall et al., 1986; Graham et al., 2007). This specificity for human laminin is further shown by the lack of laminin immunostaining in the unaffected portion of the mouse nerve (Fig. 3E). Mucopolysaccharide deposition, shown by Alcian blue staining, was observed as early as 2 weeks after sNF94.3 xenograft and increased over time, as did hypocellularity observed with H&E staining. Neither Alcian blue staining nor H&E hypocellularity was observed in xenografts of normal human Schwann cells after 8 weeks (n = 6) nor nerves injected with vehicle alone (n = 4). Furthermore, xenografts of another human NF1 cell line using the exact same procedures results in large hypercellular tumors with little mucopolysaccharide and laminin deposition (data not shown).

sNF94.3 xenografts were immunostained for Ki67 (a nuclear antigen found in proliferating cells) and von Willebrand Factor (vWF), an endothelial cell marker. Ki67-positive nuclei were found only within the tumor xenografts (huGST-immunopositive cells) and not in adjacent normal host nerve tissue. A low percentage of tumor cells labeled for Ki67 (Fig. 4A). Similar observations were made in xenografts after 8 days and 1 year, indicating slow but sustained proliferation by the sNF94.3 tumor cells, mimicking that of plexiform neurofibromas. Immunostaining for vWF showed scant blood vessels in normal mouse nerves arranged almost exclusively along the longitudinal nerve axis (Fig. 4B). Increased vascularity was evident in sNF94.3 xenografts as early as 2 weeks (Fig. 4C) and 8-week tumors showed a high degree of vascularity. A more centripetal pattern of blood vessels was observed indicating an angiogenic response to the developing neoplasm. Nearly identical results were obtained by labeling xenograft tumor tissue with antibodies to Flk-1, a high affinity receptor for vascular endothelial growth factor (VEGF) also found on blood vessels (not shown). These results indicate the induction of new blood vessels by the tumor xenograft and provide the opportunity to examine angiogenesis in this NF1 tumor model. Sections of sNF94.3 xenografts immunostained for huGST were counterstained with acidic toluidine blue to visualize mast cells. Although a few mast cells were found in normal mouse sciatic nerves, there was a conspicuous increase in mast cell number in the xenografted nerves (Fig. 4D). Given the fact that mast cells are known to release factors that influence tumor formation, these results may indicate a potential mast cell influence on intraneural sNF94.3 xenograft tumorigenicity. S-100 and p75 immunostaining of sNF94.3 xenograft tumors was faint and variable (Fig. 4E,F, respectively), similar to that of the originative tumor specimen.

TABLE I. Characteristics of sNF94.3 Xenograft Tumor and NF1 Benign Plexiform Neurofibroma

	sNF94.3 xenograft tumors[a]	NF1 plexiform neurofibroma[b]
Hypocellularity	+	+
Low proliferation	+	+
Spindle-shaped cells	+	+
S-100 immunoexpression	+	+
p75 immunoexpression	+	+
Diffusely infiltrative	+	+
Longitudinal spread	+	+
Invade basement membranes	+	+
Cells align along nerve axis	+	+
Abundant ECM	+	+
Possess basal laminae	+	+
Unencapsulated	+	+
Highly vascular	+	+
Intact nerve function	+	+
"Bag of worms" appearance	–	+
Severely deform tissue	–	+

[a]Eight week xenografts.
[b]Described by Scheithauer et al. (1997).

Table I summarizes the histologic observations and indicates similarities and differences between the sNF94.3 xenograft tumors and human NF1 plexiform neurofibroma. Based on these criteria and the findings presented we conclude that intraneural sNF94.3 xenografts show tumorigenic growth in the nerves of *scid* mice highly consistent with that of naturally-occurring human plexiform neurofibroma. Classifications for peripheral nerve sheath tumors arising in genetically engineered mouse (GEM) models have been devised because of some important differences between human and murine lesions (Stemmer-Rachamimov et al., 2004). In the same way it is difficult to apply the GEM classifications to tumors arising in xenografting models. Clearly, sNF94.3 xenograft tumors result from the proliferation of NF1-deficient Schwann cells and the admixture of various cell types from the mouse nerve including endothelial and mast cells. For the most part, sNF94.3 xenografts fit the Grade I GEM tumor classification because of low cellularity and no necrosis. They exceed that classification, however, due to their low to moderate proliferation (Ki67 positivity) and infiltration.

DISCUSSION

A variety of genetic strategies have been tested to determine the role of *Nf1*-deficiency in tumorigenesis and to induce peripheral nerve sheath tumors in animal

models. Genetic manipulations to generate *Nf1−/−* chimera and conditional knockout mice have provided valuable insights into the role of the *Nf1* gene in tumor pathogenesis (Cichowski et al., 1999; Zhu et al., 2002; Stemmer-Rachamimov et al., 2004). On the other hand, tumor xenografting is a time-tested approach with numerous advantages for testing anti-cancer therapies. Despite tumorigenic properties shown in vitro, neurofibroma cultures fail to form subcutaneous tumors in immunodeficient mice (Sheela et al., 1990; Muir et al., 2001). Early studies achieved limited growth by transplantation of human neurofibroma tissue or mixed cell preparations into mice (Appenzeller et al., 1986; Lee et al., 1992), yet reliable working xenograft models for NF1 tumors have been difficult to establish. In previous work we found that a subset of neurofibromin-negative Schwann cell cultures derived from neurofibromas did form slow growing tumors as intraneural xenografts (Muir et al., 2001). Although these xenografts provide a useful model of neurofibroma, several months are required to develop histologically detectable tumors for experimental therapeutics. In addition, cell lines derived from benign neurofibromas are not immortal and thus are a limited resource. Therefore, we investigated more advantageous xenograft models of NF1 tumorigenesis by implantation of rapidly growing NF1 MPNST cell lines into the mouse nerve.

We report a practical and reproducible NF1 tumor xenograft model by transplantation of an immortal human NF1 tumor-derived Schwann cell line, sNF94.3, into the peripheral nerve of *scid* mice. sNF94.3 is a stable and homogeneous cell line that provides a permanent and consistent cell source for xenograft initiation. sNF94.3 are Schwann-like cells that express S-100 and p75, as do the clonal element of most human NF1 plexiform neurofibromas. sNF94.3 cells have an apparently normal karyotype. The manifestation and severity of the originative patient's NF1 symptoms (including abundant dermal and plexiform neurofibromas and MPNST) are consistent with a germline ~1.4 megabase microdeletion of the *NF1* gene (De Raedt et al., 2003). The germline mutation completely deletes the *NF1* and surrounding genes, whereas the somatic *NF1* mutation(s) remain unknown. It is likely the somatic *NF1* mutation in sNF94.3 is subtle, such as a missense mutation, because this cell line produces apparently full-length neurofibromin protein as seen by Western blotting. Our studies show that these cells, however, have constitutively activated Ras indicating that the neurofibromin in sNF94.3 cells is not functional. This functional deficit is consistent with the phenotype of sNF94.3 cells in vitro and in vivo.

Although no animal model system can recapitulate every aspect of a complex human disease such as NF1, we conclude the sNF94.3 xenograft is a valid model of plexiform-like neurofibroma and provides a valuable tool in the study of NF1 tumorigenesis. Like human NF1 plexiform neurofibroma, intraneural sNF94.3 xenografts displayed hypocellularity with widely-spaced spindle-shaped cells, a low proliferative index, an extracellular matrix-rich stroma and basal laminae. Neurofibromas and MPNST have been shown previously to produce laminin (Chanoki et al., 1991). Schwann cells require the presence of other cell types, such as axons and fibroblasts, to produce basal laminae (Obremski et al., 1993). The fact that basal laminae are formed by sNF94.3 tumors suggests that these tumor cells interact with the surrounding host cells to form highly differentiated Schwann cell neoplasms (Leivo et al. 1989). Additionally, the tumors spread longitudinally in the nerve fascicles, intermingling with host axons while causing little or no impairment of nerve function, similar to human plexiform neurofibromas.

The increase of blood vessels observed in benign sNF94.3 xenograft tumors recapitulates another important feature of NF1 plexiform neurofibroma, which are angiogenic and highly vascularized (Arbiser et al., 1998). Angiogenesis has been suggested as a potentially important target for therapeutic treatment of many types of cancers (Folkman, 2003). As in human NF1 plexiform neurofibromas, the induction of angiogenesis points to the possible effectiveness of anti-angiogenic therapies to limit and control tumor growth. Therefore, the sNF94.3 xenograft model facilitates testing anti-angiogenic therapies for NF1 tumors. In addition, we have established *scid* mice with a heterozygous *Nf1* genotype, providing the opportunity to examine the interactions of xenografts with haplo-insufficient host cells. This may be particular interesting for further studies of angiogenesis given our recent observations of exaggerated neovascular responses in *Nf1* haplo-insufficient mice (Wu et al., 2006).

Xenografting requires the use of immunodeficient mice that can complicate the interpretation of host–implant cell interactions. *Scid* mice lack a functional adaptive immune system, yet they do possess a completely intact innate immune system, including mast cells (Dorshkind et al., 1984). Additionally, NF1 tumorigenic Schwann cells are known to produce stem cell factor, a potent mast cell mitogen (Ryan et al., 1994). It has been shown that murine innate immune cells can contribute to the inhibition of human tumor-cell engraftment in some human tumor-*scid* mouse models (Lozupone et al., 2000). Alternatively, this innate immune response may also contribute to tumor engraftment and growth. Previous studies have suggested that mast cells may induce or contribute to tumor formation in *Nf1* mutant mouse models (Zhu et al., 2002; Yang et al., 2003). It is interesting to speculate whether this mast cell infiltration and activation may be a relevant feature of slow-growing plexiform tumors, as suggested by our xenograft model and by others (Viskochil, 2003).

Although a number of NF1 mouse models have been developed in recent years (Gutmann and Giovannini, 2002; Stemmer-Rachamimov et al., 2004), ours is the first xenograft model allowing the properties of human NF1 tumor-derived cells to be examined in a relevant cellular environment. The sNF94.3 xenograft model closely recapitulates the natural history, pathobiol-

ogy, and biochemistry of human NF1 plexiform neurofibroma (Table I). This model is reproducible and consistent with a xenograft success rate of nearly 95%. Because the tumor cell injection is fully controlled by the investigator, a low tumor burden can be established precluding premature death from tumor overload. Also, tumors develop with a relatively short latency.

In summary, the plexiform-like sNF94.3 xenograft model offers several advantages. First, the sNF94.3 xenografts can be compared to the originative tumor specimen as well as other xenografts and cognate tumor specimens. Second, before implantation, sNF94.3 cultures can be examined for in vitro neoplastic properties, karyotype, and genetic abnormalities. Third, the investigator can precisely define the initiation of tumor xenografts by cell number, time, and location in a relevant cellular environment. Fourth, xenografts can be initiated in hosts with various genetic and phenotypic alterations and at various developmental stages. In addition, for future studies, we have also developed a strain of *scid* mice with an *Nf1+/−* background (Brannan et al., 1994; Jacks et al., 1994) to enhance the validity and relevance of tumor-host cell interactions. The plexiform-like sNF94.3 xenograft model recapitulates the main aspects of plexiform neurofibroma. These features, combined with high reproducibility and technical simplicity, will greatly facilitate preclinical testing of new therapeutic approaches for NF1 tumors.

ACKNOWLEDGMENTS

The authors thank D. Neubauer, E. Baldwin, and T. Lewis for their assistance in performing experiments, Dr. L. Zhang, Dr. H. Li, and F. Kweh for mouse breeding and colony maintenance and the University of Florida Cytogenetics Lab for cytogenetic analysis. This study was supported by the National Institutes of Health Training Grant T32-CA09126-27 (G.Q.P.), the U.S. Department of Defense grants DAMD 17-01-10707 (M.R.W.), and DAMD 17-03-1-0224 (D.M.).

REFERENCES

Abernathy CR, Rasmussen SA, Stalker HJ, Zori R, Driscoll DJ, Williams CA, Kousseff BG, Wallace MR. 1997. NF1 mutation analysis using a combined heteroduplex/SSCP approach. Hum Mutat 9:548–554.

Allen RC, Zoghbi HY, Moseley AB, Rosenblatt HM, Belmont JW. 1992. Methylation of HpaII and HhaI sites near the polymorphic CAG repeat in the human androgen-receptor gene correlates with X chromosome inactivation. Am J Hum Genet 51:1229–1239.

Andersen LB, Ballester R, Marchuk DA, Chang E, Gutmann DH, Saulino AM, Camonis J, Wigler M, Collins FS. 1993. A conserved alternative splice in the von Recklinghausen neurofibromatosis (NF1) gene produces two neurofibromin isoforms, both of which have GTPase-activating protein activity. Mol Cell Biol 13:487–495.

Appenzeller O, Kornfeld M, Atkinson R, Snyder RD. 1986. Neurofibromatosis xenografts. Contribution to pathogenesis. J Neurol Sci 74: 69–77.

Arbiser JL, Flynn E, Barnhill RL. 1998. Analysis of vascularity of human neurofibromas. J Am Acad Dermatol 38:950–954.

Blunt T, Gell D, Fox M, Taccioli GE, Lehmann AR, Jackson SP, Jeggo PA. 1996. Identification of a nonsense mutation in the carboxyl-terminal region of DNA-dependent protein kinase catalytic subunit in the scid mouse. Proc Natl Acad Sci U S A 93:10285–10290.

Brannan CI, Perkins AS, Vogel KS, Ratner N, Nordlund ML, Reid SW, Buchberg AM, Jenkins NA, Parada LF andCopeland NG. 1994. Targeted disruption of the neurofibromatosis type-1 gene leads to developmental abnormalities in heart and various neural crest-derived tissues. Genes Dev Rev 8:1019–1029.

Chanoki M, Ishii M, Fukai K, Kobayashi H, Hamada T, Muragaki Y, Ooshima A. 1991. Immunohistochemical localization of type I, III, IV, V, and VI collagens and laminin in neurofibroma and neurofibrosarcoma. Am J Dermatopathol 13:365–373.

Cichowski K, Shih TS, Schmitt E, Santiago S, Reilly K, McLaughlin ME, Bronson RT, Jacks T. 1999. Mouse models of tumor development in neurofibromatosis type 1. Science 286:2172–2176.

Colman SD, Williams CA, Wallace MR. 1995. Benign neurofibromas in type 1 neurofibromatosis (NF1) show somatic deletions of the NF1 gene. Nat Genet 11:90–92.

De Raedt T, Brems H, Wolkenstein P, Vidaud D, Pilotti S, Perrone F, Mautner V, Frahm S, Sciot R, Legius E. 2003. Elevated risk for MPNST in NF1 microdeletion patients. Am J Hum Genet 72:1288–1292.

Dorschner MO, Sybert VP, Weaver M, Pletcher BA, Stephens K. 2000. NF1 microdeletion breakpoints are clustered at flanking repetitive sequences. Hum Mol Genet 9:35–46.

Dorshkind K, Keller GM, Phillips RA, Miller RG, Bosma GC, O'Toole M, Bosma MJ. 1984. Functional status of cells from lymphoid and myeloid tissues in mice with severe combined immunodeficiency disease. J Immunol 132:1804–1808.

Enerback L, Miller HRP, Mayrhofer G. 1986. Methods for the identification and characterization of mast cells by light microscopy. In: Befus AD, Bienenstock J, Denburg JA, editors. Mast cell differentiation and heterogeneity. New York, NY: Raven Press. p 405–417.

Engvall E, Davis GE, Dickerson K, Ruoslahti E, Varon S andManthorpe M. 1986. Mapping of domains in human laminin using monoclonal antibodies: localization of the neurite-promoting site. J Cell Biol 103: 2457–2465.

Folkman J. 2003. Angiogenesis and apoptosis. Semin Cancer Biol 13: 159–167.

Graham JB, Neubauer D, Xue QS, Muir D. 2007. Chondroitinase applied to peripheral nerve repair averts retrograde axonal regeneration. Exp Neurol Jan; 203:185–195.

Gutmann DH, Wood DL, Collins FS. 1991. Identification of the neurofibromatosis type 1 gene product. Proc Natl Acad Sci USA 88:9658–9662.

Gutmann DH, Aynsworth A, Carey JC, Korf B, Marks J, Pyeritz RE, Rubenstein A, Viskochil D. 1997. The diagnostic evaluation and multidisciplinary management of neurofibromatosis 1 and neurofibromatosis 2. JAMA 278:51–57.

Gutmann DH, Giovannini M. 2002. Mouse models of Neurofibromatosis 1 and 2. Neoplasia 4:279–290.

Hirose T, Sano T, Hizawa K. 1986. Ultrastructural localization of S-100 protein in neurofibroma. Acta Neuropathol 69:103–110.

Jacks T, Shih TS, Schmitt EM, Bronson RT, Bernards A, Weinberg RA. 1994. Tumour predisposition in mice heterozygous for a targeted mutation in Nf1. Nat Genet 7:353–361.

Krone W, Mao R, Muhleck OS, Kling H, Fink T. 1986. Cell culture studies on neurofibromatosis (von Recklinghausen). Characterization of cells growing from neurofibromas. Ann NY Acad Sci 486:354–370.

Lee JK, Sobel RA, Chiocca EA, Kim TS, Martuza RL. 1992. Growth of human acoustic neuromas, neurofibromas and schwannomas in the sub renal capsule and sciatic nerve of the nude mouse. J Neurooncol 14:101–112.

Lee ST, McGlennen RC, Litz CE. 1994. Clonal determination by the fragile X (FMR1) and phosphoglycerate kinase (PGK) genes in hematological malignancies. Cancer Res 54:5212–5216.

Leivo I, Engvall E, Laurila P, Miettinen M. 1989. Distribution of myrosin, a laminin-related tissue-specific basement membrane protein, in human Schwann cell neoplasms. Lab Invest 61:426–432.

Li Y, Rao PK, Wen R, Song Y, Muir D, Wallace P, Van Horne SJ, Tennekoon GI, Kadesch T. 2004. Notch and Schwann cell transformation. Oncogene 23:1146–1152.

Lopez-Correa C, Dorschner M, Brems H, Lazaro C, Clementi M, Upadhyaya M, Dooijes D, Moog U, Kehrer-Sawatzki H, Rutkowski JL, Fryns JP, Marynen P, Stephens K, Legius E. 2001. Recombination hotspot in NF1 microdeletion patients. Hum Mol Genet 10:1387–1392.

Lozupone F, Luciani F, Venditti M, Rivoltini L, Pupa S, Parmiani G, Belardelli F, Fais S. 2000. Murine granulocytes control human tumor growth in SCID mice. Int J Cancer 87:569–573.

Mertens F, Dal Cin P, De Wever I, Fletcher CD, Mandahl N, Mitelman F, Rosai J, Rydholm A, Sciot R, Tallini G, van Den Berghe H, Vanni R, Willen H. 2000. Cytogenetic characterization of peripheral nerve sheath tumours: a report of the CHAMP study group. J Pathol 190:31–38.

Mirsky R, Jessen KR. 1999. The neurobiology of Schwann cells. Brain Pathol 9:293–311.

Muir D, Neubauer D, Lim IT, Yachnis AT, Wallace MR. 2001. Tumorigenic properties of neurofibromin-deficient neurofibroma Schwann cells. Am J Pathol 158:501–513.

Obremski VJ, Johnson MI, Bunge MB. 1993. Fibroblasts are required for Schwann cell basal lamina deposition and ensheathment of unmyelinated sympathetic neurites in culture. J Neurocytol 22:102–117.

Perrin GQ, Fishbien L, Thompson S, Wallace M, Hwang MS, Mareci T, Yachnis AT, Muir D. 2006. Malignant peripheral nerve sheath tumors developed in the mouse by xenograft of an NF1 tumor-derived Schwann cell line. Oncogene. Submitted.

Rasmussen SA, Colman SD, Ho VT, Abernathy CR, Arn PH, Weiss L, Schwartz C, Saul RA, Wallace MR. 1998. Constitutional and mosaic large NF1 gene deletions in neurofibromatosis type 1. J Med Genet 35: 468–471.

Ryan JJ, Klein KA, Neuberger TJ, Leftwich JA, Westin EH, Kauma S, Fletcher JA, DeVries GH, Huff TF. 1994. Role for the stem cell factor/KIT complex in Schwann cell neoplasia and mast cell proliferation associated with neurofibromatosis. J Neurosci Res 37:415–432.

Scheithauer BW, Woodruff JM, Erlandson RA. 1997. Tumors of the peripheral nervous system. In: Rosai J, Sobin LH, editors. Atlas of tumor pathology. Series 3. Fascicle 24. Washington, DC: Armed Forces Institute of Pathology. p 385–405.

Scott JE, Mowry RW. 1970. Alcian blue—a consumer's guide. J Histochem Cytochem 18:842.

Sheela S, Riccardi VM, Ratner N. 1990. Angiogenic and invasive properties of neurofibroma Schwann cells. J Cell Biol 111:645–653.

Singer-Sam J, LeBon JM, Tanguay RL, Riggs AD. 1990. A quantitative HpaII-PCR assay to measure methylation of DNA from a small number of cells. Nucleic Acids Res 18:687.

Stemmer-Rachamimov AO, Louis DN, Nielsen GP, Antonescu CR, Borowsky AD, Bronson RT, Burns DK, Cervera P, McLaughlin ME, Reifenberger G, Schmale MC, MacCollin M, Chao RC, Cichowski K, Kalamarides M, Messerli SM, McClatchey AI, Niwa-Kawakita M, Ratner N, Reilly KM, Zhu Y, Giovannini M. 2004. Comparative pathology of nerve sheath tumors in mouse models and humans. Cancer Res 64:3718–3724.

Suzuki Y, Suzuki H, Takamasa K, Yoshimoto T, Shibahara S. 1991. Brain tumors predominantly express the neurofibromatosis type 1 gene transcripts containing the 63 base insert in the region coding for GTPase activating protein-related domain. Biochem Biophys Res Commun 181:955–961.

Teinturier C, Danglot G, Slim R, Pruliere D, Launay JM, Bernhiem A. 1992. The neurofibromatosis 1 gene transcripts expressed in peripheral nerve and neurofibromas bear the additional exon located in the GAP domain. Biochem Biophys Res Commun 188:851–857.

Thomas SL, Deadwyler GD, Tang J, Stubbs EB, Muir D, Hiatt KK, Clapp DW, DeVries GH. 2006. Reconstitution of the *NF1 GAP*-related domain in NF1-deficient human Schwann cells. Biochem Biophys Res Comm 348:971–980.

Viskochil DH. 2003. It takes two to tango: mast cell and Schwann cell interactions in neurofibromas. J Clin Invest 112:1791–1793.

Wallace MR, Rasmussen SA, Lim IT, Gray BA, Zori RT, Muir D. 2000. Culture of cytogenetically abnormal Schwann cells from benign and malignant NF1 tumors. Genes Chromosomes Cancer 27:117–123.

Wu M, Wallace MR, Muir D. 2006. Nf1 haploinsufficiency augments angiogenesis. Oncogene 25:2297–2303.

Yang F-C, Ingram DA, Chen S, Hingtgen CM, Ratner N, Monk KR, Clegg T, White H, Mead L, Wenning MJ, Williams DA, Kapur R, Atkinson SJ, Clapp DW. 2003. Neurofibromin-deficient Schwann cells secrete potent migratory stimulus for Nf1 +/− mast cells. J Clin Invest 112:1851–1861.

Zhu Y, Ghosh P, Charnay P, Burns D, Parada LF. 2002. Neurofibromas in NF1: Schwann cell origin and role of tumor environment. Science 296:920–922.